Transient interactions between photosynthetic proteins

Hulsker, R.

Transient interactions
between photosynthetic proteins

Proefschrift

ter verkrijging van

de graad van Doctor aan de Universiteit Leiden,

op gezag van de Rector Magnificus Prof. Mr. P.F. van der Heijden,

volgens besluit van het College voor Promoties

te verdedigen op woensdag 21 mei 2008

klokke 15.00 uur

door

Rinske Hulsker

Geboren te Leidschendam in 1978

Promotiecommissie

Promotor: Prof. Dr. G. W. Canters

Co-promoter: Dr. M. Ubbink

Referent: Prof. Dr. C. Griesinger (Max Planck Institut für Biophysikalische Chemie, Göttingen)

Overige leden: Prof. Dr. J. Brouwer

Prof. Dr. J. P. Abrahams

Dr. J. A. R. Worrall (University of Essex)

Voor mijn moeder,

Aan Georg

Contents

Abbreviations

Amp	ampicillin
ATP	adenosine 5'-triphosphate
cytc_6	cytochrome c_6
cyt$f$	cytochrome f
$\Delta\delta_{avg}$	average chemical shift perturbation
$\Delta\delta_{bind}$	chemical shift perturbation caused by complex formation
$\Delta\delta_{max}$	fitted maximum of $\Delta\delta_{bind}$
HSQC	heteronuclear single quantum coherence
IPTG	isopropyl-β-D-thiogalactopyranoside
K_a	association constant
K_d	dissociation constant
k_{off}	dissociation rate constant
k_{on}	association rate constant
LB	Luria – Bertani broth
MTS	(1-acetyl-2,2,5,5-tetramethyl-3-pyrroline-3-methyl)-methanethiosulfonate
MTSL	(1-oxyl-2,2,5,5-tetramethyl-3-pyrroline-3-methyl)-methanethiosulfonate
NOESY	nuclear Overhauser enhancement spectroscopy
NMR	nuclear magnetic resonance
Pc	plastocyanin
PCd	cadmium-substituted plastocyanin
PCu	cuprous plastocyanin (oxidation state in Roman numerals)
PCS	pseudocontact shift
PMSF	phenylmethylsulphonyl fluoride
PRE	paramagnetic relaxation enhancement
PSI	photosystem I
PSII	photosystem II
rmsd	root mean square deviation
TOCSY	total correlation spectroscopy
wt	wild type

Chapter I

Introduction

Static or transient

The vast number of biological processes that occur in living systems are mediated mostly by protein-protein interactions. In the cell, genetically encoded information is translated into proteins, which are crucial to the majority of cellular functions. Protein-protein complexes show a great variety in properties, depending on the function they perform. One aspect to consider when studying these complexes is their affinity, which is directly related to the lifetime of the complex. Historically, because protein complexes with a high affinity have long lifetimes, they were the first to be characterised. These so-called static complexes are exemplified by two well-studied RNase-inhibitor complexes. The low dissociation constant (K_d) of 10^{-14} M of the barnase-barstar complex[1] is essential to ensure tight binding and thereby inhibition of the potentially harmful intracellular activity of barnase (an extracellular RNase from *Bacillus*). The same is true for the human angiogenin – ribonuclease inhibitor complex[2]. Angiogenin induces blood vessel formation and is involved in many types of cancer. The angiogenin - inhibitor complex has an even lower[3] K_d of $<10^{-15}$ M, again indicative of the strict control organisms hold over RNases. A typical feature of static complexes are the so called 'hot spots', which are areas of interface residues that can be found by alanine scanning mutagenesis and that energetically contribute most to binding[4-7].

At the other extreme of the scale of affinities in protein interactions, apart from aspecific interactions, we find the transient protein complexes. Their affinities are in the μM^{-1} – mM^{-1} range and the associated lifetimes are on the millisecond time-scale. Transient protein complexes exhibit high turn-over and comprise proteins that interact with multiple partners: signal transduction cascades and electron transfer chains in photosynthesis and respiration for example. The field of metallo-proteins produced the initial questions and insights into the properties of proteins in redox chains and was at the basis of much current knowledge on transient protein complexes[8,9].

Transient protein complex formation and interface

In order to sustain the high turn-over rates required in electron transfer chains and signal transduction cascades, the chain components need to interact transiently. This is achieved by a high dissociation rate constant ($k_{off} \geq 10^3$ s^{-1}). Considering the association rate constants in the range of 10^7-10^9 M^{-1} s^{-1} found experimentally for several electron transfer complexes[10-13], we can explain the weak binding of transient complexes, with association constants ($K_a = k_{on}/k_{off}$) in the μM^{-1} – mM^{-1} range[8].

High k_{off} rates and the need to interact with multiple partners account for the poorly packed complex interfaces which are typical for these complexes[14]. Dissociation can be more rapidly achieved when water has increased access to the poorly packed interface. Promiscuity is also facilitated by the lack of geometric complementarity of the interface. In static as well as transient complex interfaces charged residues are found, but in transient interfaces they are more often located at the perimeter. There, they are usually not involved in salt-bridges and hydrogen bonds. These observations can be rationalised by two considerations. First, the presence of opposite charges on the partner proteins can facilitate complex formation by increasing the chance of the proteins finding each other, which is also true for static complexes[15-18]. Second, the need for high turn-over dictates that the proteins need to release easily, which is reflected in the high k_{off} rates. Strong electrostatic interactions in the complex interface would inhibit the release, so by not matching the charges in the interface exactly, these high k_{off} rates can be achieved.

While long-range electrostatic interactions are mainly involved in the initial stages of transient protein-protein association, hydrophobic interactions are more important for the specificity and stability of the transient complex. In electron transfer complexes a patch of hydrophobic residues is often found on the surface, close to the active site. This is thought to facilitate electron transfer by providing an entry point for the electrons. In order to prevent complete desolvation, as can be seen in static complexes, these patches are often kept small and are surrounded by a ring of polar residues, which enhances dissociation of the complex.

The encounter complex, kinetic models of binding

The theoretical diffusion-limited association rate for two spherical proteins of 18 Å proteins, given by the Smoluchowski equation[19] is 7 x 10^9 M^{-1} s^{-1}. In reality however, a successful binding event requires the interface residues on the proteins to align. As the interface area comprises on average 10-15% of the total surface area[20] and considering the high steric specificity needed to align the interface areas properly, the association rate is expected to drop by at least three or four orders of magnitude[8,21-23]. However, some protein-protein complexes, such as cytochrome *c* – cytochrome *c* peroxidase[24] and cytochrome *c* - cytochrome b_5 [25], exhibit association constants of ~10^9 M^{-1} s^{-1}. This discrepancy raises the question of how some of these complexes can achieve such high association rates. Several models have been proposed to explain the experimental data available. From laser flash kinetics studies on the electron transfer from Pc and cytc_6 to PSI three models were proposed that could account for the observed electron transfer reaction rates[12,26]. The type I model is a simple collisional model without the formation of a transient complex. The type II model involves complex formation and electron transfer, without a transitional rearrangement step. This suggests that the preformed complex is either sufficiently oriented for electron transfer or that rearrangement is too fast to be detected. The most elaborate (type III) model includes the formation of an ensemble of pre-oriented complexes guided by electrostatic interactions. Intermolecular rearrangement then forms the active electron transfer complex. This mechanism is reminiscent of the earlier Velcro-model[27], which rejected the classical 'lock and key' concept, that is more appropriate to describe static complexes and enzymatic processes. Instead, it suggested that the recognition and binding of electron transfer proteins originate from charged and hydrophobic complementary patches that stick on contact like Velcro.

From a cross-linking study on the plant Pc - cyt*f* complex, which causes the inhibition of electron transfer, it can be concluded that the initial orientation of the complex is not productive[28]. NMR structural studies of plant Pc - cyt*f* complexes[29,30] indicated that a large rearrangement from the well-defined state was unlikely. These results lead to the proposition of a two-step model[29,31] in which an ensemble of orientations is formed based

on electrostatic interactions, followed by a well-defined complex which is capable of electron transfer. In the case of plant Pc - cyt*f* the equilibrium between these steps lies towards the well-defined state, but in other cases the equilibrium is more toward the ensemble of orientations. The cytochrome b_5 – myoglobin complex can mainly be found in this state, existing as a number of isoenergetic binding orientations, described by the term dynamic docking[32-34]. More recently the investigation of the dynamics in the cytochrome *c*- cytochrome *c* peroxidase complex refined the two-step model and defined a dynamic encounter state as a combination of all encounter complexes, followed by a single-orientation or well-defined state[31,35] (Fig. 1.1).
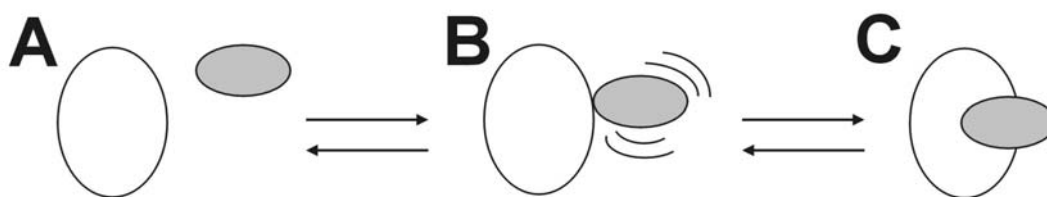
Figure 1.1. Model for the formation of a protein complex[29,31]. Free proteins (A) associate to form an encounter complex (B) consisting of an ensemble of protein orientations, which is in equilibrium with a single-orientation complex (C).

Dynamics in protein complexes studied by NMR spectroscopy

The term dynamics is used to describe movement in proteins and protein complexes on every timescale possible[36]. 'Dynamics' ranges from side chain and domain movements in proteins, to movement of proteins with respect to each other in protein complexes, but the term is also used for the turn-over of protein complexes on timescales that are involved in cellular processes. In this work, when the term dynamics is used it covers the movements of proteins in the (transient) protein complex. As mentioned above, these movements are thought to result in an ensemble of orientations, which together form the encounter state. The field of NMR spectroscopy has had a great impact on the understanding of transient complexes as well as on the dynamics involved. Several types of NMR experiments have been deployed to study them[37]. The chemical shift perturbation experiment, where a ^{15}N-labelled protein is monitored while being titrated with its partner protein, is used to

determine which residues experience a change in their magnetic environment caused by the presence of the other protein. Plotting these changes on a surface representation of the protein then provides a map of the interface. Furthermore, titration curves can be fitted to produce a binding constant[16]. Interestingly, the overall size of the chemical shift changes was found to be a qualitative measure of the dynamics in the complex[33,38]. The more dynamic the complex, the more the chemical shift changes average out. In its extreme form the chemical shift changes are indistinguishable from aspecific interactions, as is the case for the myoglobin-cytochrome b_5 complex. Complex formation could be inferred from an increase in overall correlation time and the fact that the chemical shift perturbations titrate[33]. These NMR studies indicated that transient complexes cover a full range from single-orientation to fully dynamic.

Recently, paramagnetic spin labels have been utilised in attempts to quantify the dynamics in protein-protein complexes[31,39]. The paramagnetic properties of metals in electron transfer proteins were recognised earlier to be useful in structural studies of transient complexes[29,30,40-42]. This is being extended to proteins that do not naturally contain metals, by the attachment of metal-chelating tags[43-49] and nitroxide spin-labels[50-54] to the protein surface. Chemical shift perturbations give information on the proximity of the partner protein, but not to which specific nuclei of the partner protein is close to a particular nucleus in the ^{15}N-labelled protein. Paramagnetic effects on the other hand, give information on the distance of a nucleus to the paramagnetic centre, with the added advantage in the case of pseudocontact shifts that they also provide angular information. This is due to the anisotropic nature of the paramagnetic centre used to induce pseudocontact shifts. Both forms of information can be converted to distance and angular restraints and used in docking calculations to determine the structure of complexes. The use of paramagnetic relaxation enhancement has recently been discovered to be useful as a tool for investigating dynamics[31,39,55].

Photosynthesis

The proteins studied in this thesis transfer electrons as part of oxygenic photosynthesis. For recent reviews on the structural and mechanistical aspects of photosynthesis and photosynthesis as the inspiration for designing solar powered biotechnologies see references[56-59]. Oxygenic photosynthesis, performed by plants, green algae and cyanobacteria, converts sunlight into chemical energy (Fig. 1.2).
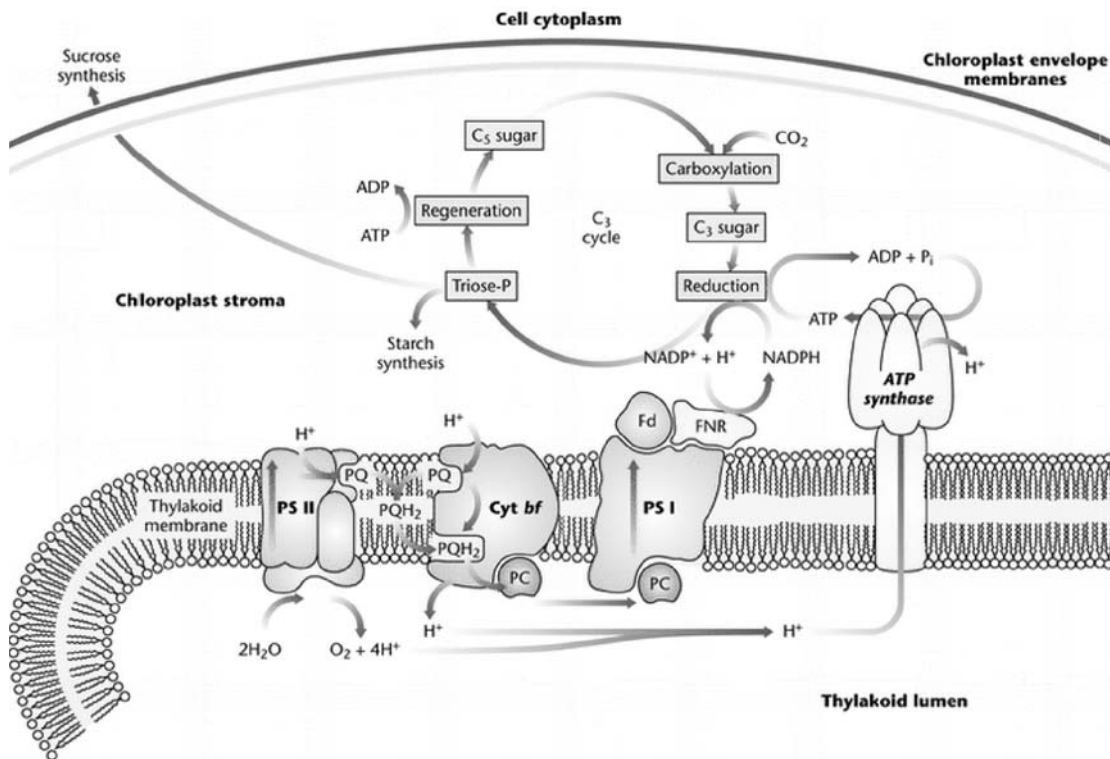
Figure 1.2. Schematic representation of oxygenic photosynthesis in plant chloroplasts[60].

The production of oxygen as a side product and the assimilation of carbon dioxide into organic matter are essential to all life forms. Photosynthesis in plants takes place in specialised organelles called chloroplasts, which are compartmentalised by stacked thylakoid membranes. These separate the lumen from the stroma, and facilitate formation of a proton gradient (also called proton motive force or pmf), which is the direct result of the light reactions. This starts with the splitting of water by PSII, providing the electrons

and producing O_2. The electrons are translocated across the membrane, initialised by the excitation of the reaction centres. This is achieved by light harvested by chlorophyll and other pigments that funnel the energy to specialised reaction centre chlorophylls in PSII. The electrons are then taken up by a quinone pool in the thylakoid membrane and shuttled to the cytochrome b_6f membrane complex where the redox energy is converted into the proton gradient. The proton gradient is used by an ATP synthase to form ATP. At the same time the electrons are shuttled by Pc to PSI, which produces reduced ferrodoxin at the stromal side of the membrane. Reduced ferrodoxin can be used for NADPH production, but also for other processes that need reductive power.

The proteins:
Plastocyanin

Plastocyanin (Pc) was first discovered in 1960 by Sakae Katoh[61], as a copper containing redox protein with an absorption maximum at 597 nm. It had been isolated from the green alga *Chlorella ellipsoidea* and was named plastocyanin[62] in 1961. The experiment that settled the discussion on whether Pc interacts with PSII or PSI was essential in determining the order of electron flow in the light reaction of photosynthesis[63]. It is now well established that Pc transports electrons from the cytochrome b_6f complex to PSI in green algae, cyanobacteria and plants. The divergent sequence of the *petE* gene coding for Pc is known for more than forty organisms. It codes for 97 to 105 amino acids and is usually longer in cyanobacteria. Crystal and solution structures are available for Pc from fifteen sources[65-81]. Despite its sequence divergence the structure of the ~11 kDa protein (Fig. 1.3) is conserved and forms a β-sandwich consisting of seven β-strands and an irregular strand that contains a small helix in the longer Pc's. An invariable feature is the type I 'blue' copper site, which is characterised by an intense blue colour at ~600 nm, an unusually narrow hyperfine coupling ($A_\parallel$ values of 0.0035-0.0063 cm^{-1}) in the EPR spectrum due to assymmetry at the metal and a high midpoint-potential (>350 mV at pH 7 for Pc's) as compared to the aqua Cu(II/I) couple[82]. Type II proteins also have a single copper atom, but are not characterised by an intense colour or unusual EPR spectrum.

Type 3 proteins are binuclear and therefore not EPR active. More types of copper sites have recently been discovered, but these will not be discussed here.

Figure 1.3. Three-dimensional representation of Pc. Pc is shown as a blue ribbon, with the Cu ion as a magenta sphere. The four copper ligands, a cysteine, methionine and two histidines, are shown as sticks. The molecular coordinates were taken from the crystal structure of reduced fern Pc (PDB entry 1KDI). This figure and Figures 1.4, 3.3, 3.5, 3.8, 4.1, 4.4, 4.6 and 5.3 were made in PyMOL v0.98 [64].

The copper ion in Pc is coordinated by a S_γ of a Cys, S_δ of a Met and two N_δ of two His side chains in a trigonal pyramid [83,84]. The colour of PCu(II) is caused by the Cys S_γ – Cu(II) charge transfer, which has a maximum at ~600 nm. The C-terminal histidine is the point of entry of the electron and becomes protonated in the reduced protein when the pH is lowered to <5. The only exception to that rule has been reported for Pc from Japanese fern[77,85] (but see Chapter II and reference [86]). This active site histidine is located at the so called 'north' end of the protein in a hydrophobic patch. Pc from the cyanobacterium *P. hollandica* contains two unique residues in this patch (Tyr12 and Pro14), that have not been found in other Pc's. When converted back to the otherwise conserved residues the complex with cyt*f* appears to show increased dynamics[87]. Another site of interest is the 'eastern' or acidic patch. It is usually located at the irregular strand 5 and includes residues 42-65. It was thought to be directly involved in electron transfer from cyt*f*, as deduced from studies with inorganic compounds[88-97], but this could be disproved once the first structure of the Pc - cyt*f* complex was determined[29]. The electrostatic interaction of this patch with oppositely charged residues that are located in and near the small domain of plant cyt*f* contribute to complex formation as discussed above. Curiously, the charges

on Pc and cyt*f* are reverted in the Pc - cyt*f* complex from cyanobacterium *Nostoc* sp. PCC 7119, with a basic patch on Pc interacting with acidic side chains of cyt*f*[41,98].

Cytochrome f

Figure 1.4. Three dimensional representation of cyt*f*. Cyt*f* is shown as a red ribbon, the haem in sticks and the Fe ion as a red sphere. The molecular coordinates were taken from a homology model[109] of *Nostoc* sp. PCC 7119 cyt*f* (see Chapter IV), based on the crystal structure of *Brassica rapa* (PDB entries 1CTM and 1HCZ).

Cytochrome *f* (cyt*f*) is a protein with a unique structure, which makes it the only member of a family and superfamily of protein structures[99]. It was discovered in the 1930s and first characterised in the 1950s by Robert Hill[100]. The discovery of its natural proteolysis in *Brassica* spp. in 1975, promoted by the presence of organic solvent, was an important step for the isolation of this membrane anchored protein[101]. The method was later perfected and extended to other plants by John Gray[102]. Cyt*f* is part of the membrane complex cytochrome b_6f, which was independently crystallised from two sources in 2003 [103,104]. This complex takes up two electrons from a quinone bound at the lumenal Q_0 site, which results in the release of two protons to the aqueous lumen. Cyt*f* is anchored in the thylakoid membrane by a stretch of thirty hydrophobic, C-terminal residues. The truncated soluble part (Fig. 1.4) is ~28 kDa and the crystal structure of cyt*f* from only three sources has been determined, one each from plant, green algae and cyanobacteria[105-108]. As for Pc, the sequence of cyt*f* shows diversity between plants, green algea and cyanobacteria, while the structure is much conserved. The differences in sequence reflect the differences at the surface and are linked with the surface properties of its partner Pc. The first crystal structure of cyt*f* [105]

revealed a few unique features of this protein that was classified as a *c*-type cytochrome, characterised by the haem co-factor that is covalently linked by two thioether bonds to two cysteine residues, which are part of a conserved CXXCH motif[110]. The histidine acts as the fifth ligand to the iron, but unlike the Met or His residue that is usually found as sixth ligand in *c*-type cytochromes, the N-terminal amino group of residue Tyr1 is the sixth ligand in cyt*f*. The structure of cyt*f* has a curious elongated shape and is mainly made up from β-sheets. It is composed of a small and large domain, the latter of which contains the active site haem.

Cytochrome c₆

Confused with cyt*f* in early literature[99] and also called cytochrome *c*-552 or *c*-553, this protein is a soluble *c*-type cytochrome, that performs the same functions as Pc in certain cyanobacteria and green algae. Other photosynthetic organisms can adapt to the copper availability in their environment by expressing either Pc or cytc_6[111]. Cytc_6 from green alga *Euglena gracilis,* was first characterised in 1959 as a *c*-type cytochrome with an α-band at 552 nm[112]. Recently, a homologous protein in plants was found, cytochrome c_{6A}, which has a lower midpoint potential[113,114] and is probably not involved in photosynthesis[115-117]. From the structure of *Ph. laminosum* cytochrome c_6 it was concluded that the replacement of a conserved Gln with Val in cytochrome c_{6A} caused its ~200 mV lower midpoint potential[114].

The structure of cytc_6 from eight different cyanobacteria or algae has been determined[114,118-126]. As mentioned before, in all class I cytochromes the haem is bound near the N-terminus by a CXXCH motif, of which the His is the fifth iron ligand. In cytc_6 a Met is the sixth ligand[127]. Contrary to plastocyanin the protein fold consist mainly of α-helices, typical of a cytochrome *c*.

When both proteins are available in one organism, they exhibit similar features. For instance, cytc_6 and plastocyanin share properties such as midpoint potential (~350 mV at pH 7) and isoelectric point. The isoelectric point is similar for both proteins within the same organism, but varies from one organism to another. It is believed the proteins underwent parallel surface mutations throughout evolution due to common

functionality[128,129]. Furthermore, cytc_6 is thought to have been replaced by plastocyanin when the character of the earth's atmosphere went from reducing to oxidative[129], because Cu^{II} is more readily available then Cu^{I} and the opposite is true for Fe^{III} and Fe^{II}.

The complexes of Pc and cytc$_6$ with cytf

The transient nature of the Pc - cyt$f$ and cytc_6 - cyt$f$ complexes makes it difficult to co-crystallise them. For this reason NMR has been the method of choice for structural studies of these complexes. Before this was possible kinetics studies of the plant Pc - cyt$f$ complex had already revealed the effect of ionic strength on the reaction rate[130] and electron transfer rate[16] showing the importance of electrostatics in the first step of association. For the determination of the first structure of the plant Pc - cyt$f$ complex, pseudocontact shifts caused by the Fe^{III} in cyt$f$ were used[29]. The copper in plastocyanin was replaced with cadmium to prevent reduction of cyt$f$. The structure revealed a so called 'side-on' orientation caused by the interaction of cyt$f$ with the 'northern' hydrophobic patch and the eastern acidic patch on Pc as described above. When the same approach was used on the cyanobacterial, thermophilic *Ph. laminosum* Pc - cyt$f$ [40], the structure showed an orientation of Pc which was 'head-on' instead, due to the lack of interactions with the eastern patch on Pc. The complex was found to be more dynamic, which is probably related to the fact that hydrophobic interactions seem to dominate in this complex, a view that is supported by results from kinetic studies[13,131]. The structure of the cyanobacterial *Nostoc* sp. PCC 7119 Pc - cyt$f$ complex[109] revealed an orientation similar to the plant complex, but curiously the charges on Pc and cyt$f$ are reversed. The differences between the Pc - cyt$f$ complexes from different organisms can be attributed to differences of the surface properties of the proteins[41]. Theoretical studies, which often use Brownian dynamics, support the view from experimental work on the role of electrostatics and the ensemble of orientation formed in the initial association step[132-134]. The complex of cytc_6 - cyt$f$ has received much less attention than the Pc - cyt$f$ complex. The only reported structure is a docking model based on chemical shift perturbation data for the physiological cytc_6 - cyt$f$ complex[135]. Despite the structural differences between Pc and cytc_6 the interaction with cyt$f$ was found to be similar[136,137].

Outline of thesis

The aim of this thesis was to study several aspects that influence the transient interaction of Pc and cytc_6 with cyt$f$. In Chapter II the protonation of a copper histidine ligand of reduced fern Pc at low pH is investigated. This inactivation of Pc has been suggested as a way to down regulate photosynthesis. Protonation of the histidine ligand was reported for other Pc's but in fern Pc it seemed to be prevented by $\pi-\pi$ stacking with nearby phenyl ring. This is investigated by NMR spectroscopy, X-ray crystallography and cyclic voltammetry for wt and mutant fern Pc. In Chapter III the complex of *P. hollandica* Pc - cyt$f$ is structurally characterised by NMR spectroscopy. The structure of the physiological wt complex, determined by docking with NMR restraints, is presented. The mutation of two otherwise conserved residues in the hydrophobic patch of *P. hollandica* Pc is used to study the dynamics of this complex, which is balanced between well-defined and encounter state. The dynamics in the complex of *Nostoc* sp. PCC 7119 cytc_6 - cyt$f$ are investigated in Chapter IV. Both pseudocontact shifts and PRE from five differently positioned spin labels on cyt$f$ are used as distance restraints in docking calculations. In Chapter V the interaction of charged peptides with *S. pratensis* Pc is examined by NMR. These peptides have been shown to inhibit the electron transfer between Pc and cyt$f$. By addition of hydrophobic residues to the peptide, the effect of hydrophobics on the interaction is also investigated. In Chapter VI the effect of molecular crowding on the transient Pc - cyt$f$ complex is investigated by NMR. The effects of addition of high molecular weight crowders on the binding constant and binding map of the complex are presented. Finally, in the concluding remarks the results from these chapters are put into a broader perspective and are discussed in relation with each other.

Chapter II

Protonation of a histidine copper ligand in fern plastocyanin

Abstract

Plastocyanin is a small (~11 kDa) blue copper protein that shuttles electrons as part of the photosynthetic redox chain. Its redox behavior is changed at low pH as a result of protonation of the solvent exposed copper coordinating histidine. Protonation and subsequent redox inactivation could have a role in the down regulation of photosynthesis. As opposed to plastocyanin from other sources, in fern plastocyanin His90 protonation at low pH has been reported not to occur. Two possible reasons for that have been proposed: $\pi-\pi$ stacking between Phe12 and His90 and lack of a hydrogen bond with the backbone oxygen of Gly36. We have produced this fern plastocyanin recombinantly and examined the properties of wt protein and mutants Phe12Leu, Gly36Pro and the double mutant with NMR spectroscopy, X-ray crystallography and cyclic voltammetry. The results demonstrate that, contrary to earlier reports, protonation of His90 in the wt protein does occur in solution with a pK_a of 4.4 ($\pm$ 0.1). Neither the single mutants nor the double mutant exhibit a change in protonation behavior, indicating that the suggested interactions have no influence. The crystal structure at low pH of the Gly36Pro variant does not show His90 protonation, similar to what was found for the wt protein. The structure suggests that movement of the imidazole ring is hindered by crystal contacts. This study illustrates a significant difference between results obtained in solution by NMR and by crystallography.

Introduction

Plastocyanin (Pc) is a small (~11 kDa) blue copper protein, which shuttles electrons from cyt*f* in the cytochrome b_6f complex to P700$^+$ of photosystem I (PSI) in oxygenic photosynthesis[138]. The copper in the type I site is coordinated by the N_δ atoms of two histidines, the thiolate sulphur of a cysteine and weakly by the thioether of a methionine[139]. Apart from one histidine the copper ligands are located in a C-terminal loop. The geometry and nature of the copper ligands are important determinants of the redox potential of blue copper proteins[140,141]. The histidine ligand that is solvent exposed is located in the hydrophobic 'northern' patch, which is important in electron transfer to both cyt *f* and PSI[29,30,40,142-144].

In several blue copper proteins the solvent exposed histidine ligand can be protonated in the reduced protein. The accompanying pK_a values vary between proteins and species. For instance, Pc's show a species dependent pK_a range, from 4.7 for French bean Pc to 5.7 for parsley Pc[85,139,145] and values of ~5 have been reported for pseudoazurin[146-148]. Amicyanin shows the highest pK_a value, ranging from a pK_a of 7.2 for *Thiobacillus* (now *Paracoccus*) *versutus*[149] to 7.5 for *Paracoccus denitrificans*[150]. For azurin and rusticyanin the transition is not observed down to a pH of 2-3 [151-153]. Several studies revealed the structural effects of the protonation[154-156]. Crystal structures of poplar Pc at six pH values showed that upon protonation the imidazole ring moves away from the copper and turns 180° around the C_β-C_γ bond[157]. The new position of the histidine is stabilised by a hydrogen bond with the backbone oxygen of Pro36. As a result of the protonation and 'flip' of the imidazole ring, the copper sinks into the plane of the other three ligands. Consequently, the reduction potential rises and the protein becomes redox inactive[158]. It is not entirely clear whether this serves a physiological purpose, but it is known that the lumen acidifies as a result of the light reaction in photosynthesis[159]. Acidification is thought to be involved in the down regulation of the light reaction. Possibly, protonation and subsequent inactivation of Pc plays a role in this process.

 To account for differences in reduction potential and protonation behavior between blue copper proteins several factors have been suggested. Among them are the length of the C-terminal ligand loop[160-162], the hydrogen bond network surrounding the metal site[163],

solvent accessibility of the metal site[164] and $\pi-\pi$ stacking interactions with the histidine ligand[77,147]. Stacking interactions have been found in an unusual Pc from *Dryopteris crassirhizoma* (a fern), which is the only Pc reported not to undergo histidine protonation[77]. Studies of this fern Pc, which shows only 33-38% sequence conservation with seed plant sequences, led to the conclusion that $\pi-\pi$ stacking interaction between Phe12 and the solvent exposed His90 prevented the histidine ligand from being protonated at low pH[77,85].

We have studied the histidine protonation behavior of *D. crassirhizoma* Pc by site directed mutagenesis, two-dimensional NMR, crystallography and cyclic voltammetry. We found that the protein does show protonation although at a pK_a lower than found for other Pc's. No significant differences are observed between wt Pc and the F12L, G36P and F12L/G36P mutants. It indicates that stacking interactions in fern Pc play no role in determining the protonation behavior. The results are discussed in relation to earlier studies on stacking interactions and histidine protonation in cupredoxins.

Materials and Methods

Gene synthesis and mutagenesis

The gene encoding *D. crassirhizoma* Pc was synthesised by Annabelle Mery and Dr. Martin Ph. Verbeet on the basis of back translation of the amino acid sequence[77], using frequent *Escherichia coli* codons (Wisconsin Package Version 10.0 Genetics Computer Group, Madison, WI). The DNA sequence of fern Pc was divided over four pairs of oligonucleotides (Table 2.1). Gene synthesis was performed in four successive steps. In step 1 oligonucleotides dryoa1 (coding) and dryob1 (non-coding) were used in a PCR reaction without template, consisting of one cycle of 5 minutes denaturation at 95°C, 2 minutes of hybridisation at 60°C and 20 minutes of elongation at 70°C. In step 2 primers dryoa2 (coding) and dryob2 (non-coding) hybridised with the product of step 1 in a PCR reaction consisting of 5 minutes denaturation at 95°C, 30 cycles of 1 minute of hybridization at 40°C, 1 minute of elongation at 70°C, 1 minute of denaturation at 95°C, 1 minute of hybridization at 40°C and finally 10 minutes of elongation at 70°C. Step 3

and 4 were identical to step 2 except that the products of step 2 and step 3, were used as template and dryoa3 / b3 and dryoa4 / b4 as primers, respectively. The introduced NcoI and BamHI sites were used to clone the fragment into the pET28c vector (Novagen). The resulting plasmid was transformed to *E. coli* JM109 cells and all clones were checked for the presence of the insert by SmaI digestion. Sequencing of the resulting pETDPc showed no alterations to the back translated sequence. Mutations F12L and G36P were introduced by site-directed mutagenesis following a procedure based on reference [165] and using oligonucleotides shown in Table 2.1 and T7 primers (Isogen Life Science). The presence of the mutations was confirmed by sequencing.

Table 2.1. Oligonucleotides used for gene synthesis and site directed mutagenesis

Oligonucleotide	Sequence
dryoa1	5'-GTGAAACCGGTCACAACATCGTTTTCGACATCCCGGCTGGTGCTCCGGGTACCGTTG-3'
dryob1	5'-GCAGGTCGTTTTCGTCCATAGAAGCAGCTTTCAGTTCGGAAGCAACGGTACCCGGAGCACCAG-3'
dryoa2	5'-GTTTCCGCTGGTGAAGCTGTTGAATTCACCCTGGTTGGTGAAACCGGTCACAAC-3'
dryob2	5'-G**CCCGGG**GTGGAAACTTTAGCTTTGAAGGACGGTTCGTCTTCGGACAGCAGGTCGTTTTCGTC-3'
dryoa3	5'-GGTAACTTCAAATTCTACCCGGACTCCATCACCGTTTCCGCTGGTGAAG-3'
dryob3	5'-CATGTTAGCGGATTTGTGCGGGGTGCAGTAGAAGGTGTAGGTG**CCCGGG**GTGGAAAC-3'
dryoa4	5'-ggtata**ccatgg**CTAAAGTTGAAGTTGGTGACGAAGTTGGTAACTTCAAATTC-3'
dryob4	5'-ctggctcga**ggatcc**tcaTTTAACGGTCAGAGTACCTTTCATGTTAGCGGATTTGTG-3'
dryof12l	5'-GGTATACCATGGCTAAAGTTGAAGTTGGTGACGAAGTTGGTAACCTCAAATTCTACC-3'
dryog36pfor	5'-GGTTGGTGAAACCCCTCACAACATCG-3'
dryog36prev	5'-CGATGTTGTGAGGGGTTTCACCAACC-3'

Capital letters: protein encoding sequence
Small letters: extra nucleotides
Bold: restriction sites NcoI, BamHI and SmaI
Underlined: overlapping regions

Protein expression and purification

Native *D. crassirhizoma* Pc was kindly provided by Prof. Takamitsu Kohzuma (Mito, Japan). It was isolated and purified as described before[77]. Recombinant Pc was produced in *E. coli* BL21(DE3) cells. A single colony of bacteria freshly transformed with pETDPc was incubated in 10 mL LB / kanamycin (50 mg/L) and inoculated at 37° overnight. A 100x dilution was made in 0.5 L 2xYT / kanamycin (50 mg/L) with 0.1 mM copper citrate and incubated at 37°, 250 rpm until the OD_{600} reached 0.7. Expression was induced with 1 mM IPTG and incubation was continued at 30° for 4 hours. Cells were harvested by centrifugation and lyzed with a French pressure cell in presence of 1 mM PMSF and 100 μM $CuNO_3$. Cell debris was removed by centrifugation. Reduced protein was purified using ion-exchange column chromatography with DEAE Sepharose (Amersham Biosciences) in 10 mM sodium phosphate, pH 7.0. The protein was eluted with a gradient of 0-250 mM NaCl. Fractions containing Pc were concentrated and salt was removed by ultra filtration. The chromatography was repeated with Pc in the oxidised state. Then, size exclusion chromatography with Superdex G-75 (Amersham Pharmacia Biotech) was performed in 10 mM sodium phosphate, pH 7.0, 100 mM NaCl. The protein was oxidised with potassium ferricyanide and reduced with sodium ascorbate. Pc concentrations were determined using $\varepsilon_{590} = 4.7$ cm^{-1} mM^{-1} [77] for recombinant wt Pc as well as the mutants. The yield of pure protein was 70 mg/L of culture. Pc was considered pure when the ratio $A_{278}/A_{590} \leq 1.3$ and the protein migrated as a single band on Coomassie stained SDS-gel. ^{15}N-labelled recombinant proteins were produced in M9 minimal medium supplemented with 0.3 g/L $^{15}NH_4Cl$. A single colony of freshly transformed *E. coli* BL21(DE3) was incubated in 10 mL LB / kanamycin (50 mg/L) and inoculated at 37° until the OD_{600} reached 0.6. This preculture was diluted 100x into 0.5 L minimal medium / kanamycin (50 mg/L) and incubated at 37°, 250 rpm until the OD_{600} reached 0.6. Expression was induced with 1 mM IPTG and incubation was continued at 30° overnight. Isolation and purification was done as above, yielding 5 mg of pure protein per litre of culture. For additional ^{13}C labelling the minimal medium was supplemented with 2 g/L ^{13}C-glucose.

Stopped flow kinetics

Stopped-flow experiments were performed using a computer-controlled Applied-Photophysics SX18MV stopped-flow system equipped with a PBP 05-109 Spectrakinetic monochromator. Electron transfer rates were determined in 10 mM sodium phosphate, pH 6 at 50 and 100 mM ionic strength (40/90 mM NaCl). For these measurements horse heart cytochrome *c* was reduced with sodium dithionite and kept under argon to prevent oxidation. Recombinant Pc was oxidised with excess ferricyanide. Excess reductant or oxidant was removed by use of a G25 Sephadex column. The experiment was carried out under pseudo first order conditions. The reaction rate was followed by measuring absorption at 420 nm.

Zn-substitution recombinant Pc

Zn-substitution of recombinant Pc was essentially done as described[166] with the following modifications. Of a 200 mM KCN, 500 mM Tris/HCl, pH 7.0 solution 0.5 mL was added to 0.5 mL 1 mM oxidised Pc. The sample was then loaded on a G25 Sephadex column pre-equilibrated with 1 mM $ZnCl_2$, 50 mM MOPS, pH 7.0. Fractions containing protein were washed with water and 10 mM sodium phosphate, pH 6.5.

NMR sample preparation

For ^{1}H NMR Pc Cu(II) and Zn-substituted Pc were concentrated to 1 mM in 10 mM sodium phosphate, pH 6.5. The copper protein was reduced with 2 mM ascorbate and 0.3 mM trimethylsilyl-d4-propionate (TSP) was added. For the pH titration followed by ^{1}H NMR the H_2O in the protein solutions was exchanged to D_2O and protein was reduced with 2 mM ascorbate. The pD was adjusted with μL aliquots of 0.1/0.5 M DCl. The sample for assignment of the backbone amide resonances consisted of ^{13}C/^{15}N labelled protein in 10 mM sodium phosphate, pH 6.5. Samples for 2D NMR pH titrations contained 1 mM ^{15}N labelled Pc in 50 mM potassium phosphate, pH 8.0 and 2 mM

ascorbate. The pH was adjusted with μL aliquots of 0.1/0.5 M HCl. Argon was flushed through all NMR samples to prevent reoxidation.

NMR spectroscopy

All NMR spectra were recorded at 600 MHz on a Bruker DMX spectrometer at 300 K. The ^{1}H spectra used for the assignment of active site histidine protons were recorded as described in[155,167]. Resonances in the heteronuclear single quantum coherence (HSQC) spectrum of Pc were assigned using 3D HNCACB and HN(CA)CO experiments[168-171]. The assigned resonances were submitted to the Biological Magnetic Resonance Data Bank (BMRB) under accession code 7370. The ^{2}J experiments for the detection of the imidazole ring ^{15}N nuclei[172] was performed using a standard ^{15}N,^{1}H HSQC experiment with 1/(2J) = 36 ms, an offset of 144 ppm and a spectral width of 172 ppm for the ^{15}N dimension. No ^{15}N decoupling was performed during ^{1}H detection, producing a cleaner background in the spectrum. The number of complex points in the indirect dimension was 256. Chemical shifts acquired in pH titration experiments were fitted to a model which describes a single protonation event: $\delta = (K_a\, \delta_H + [H^+]\, \delta_L) / (K_a + [H^+])$, where δ_H and δ_L are chemical shifts at high and low pH, respectively.

Electrochemical measurements

Electrochemical measurements and analysis were performed by Dr. Antonio Ranieri and Prof. Marco Sola (Modena, Italy). Cyclic voltammetry (CV) experiments and square-wave voltammetry experiments (SWV, using a frequency 5 Hz and a pulse amplitude of 0.025 V) were performed with a Potentiostat/Galvanostat EG&G PAR model 273 A. A 1 mm-diameter pyrolitic graphite disc (PGE) was used as working electrode, and a saturated calomel electrode (SCE) and a Pt ring as a reference and counter electrode, respectively. Potentials were calibrated against the MV^{2+}/MV^+ couple (E°'= -0.446 V vs. SHE)(MV = methyl viologen). All the redox potentials reported are referred to the standard hydrogen electrode (SHE). The electric contact between the reference electrode and the working solution was obtained with a Vycor® (PAR) junction. All measurements

were carried out under argon using a cell for small volume samples (V = 0.5 ml) under thermostatic control at 25±0.1 °C. Scan rates varied from 0.02 to 0.2 V s^{-1}. The cleaning procedure of the working electrode is crucial to the voltammetric response. The PGE was first treated with anhydrous ethanol for 5 min, and then polished with alumina (BDH, particle size of about 0.015 μm) water slurry on cotton rug for 3 min; finally the electrode was treated in an ultrasonic pool for about 5 min and used without further treatment. Modification of the electrode surface was performed by dipping the polished electrode into a 1 mM solution of polylysine and morpholine for 30 s, then rinsing it with nanopure water. 15 mM HEPES and 40 mM NaCl were used as base electrolytes. Protein samples were freshly prepared before use and their concentration, in general about 0.1 mM, was checked spectrophotometrically. The pH was changed by adding small amounts of concentrated NaOH or HCl under fast stirring. The experiments were performed several times and the reduction potentials were found to be reproducible within ± 3 mV.

Crystallisation

For crystallisation of the G36P Pc essentially the same conditions were used as for the wt protein[77]. The sitting-drop method was used with ammonium sulphate as precipitant. A drop of 4 μL containing 2.6 M ammonium sulphate, 0.1 M sodium acetate pH 4.5 and oxidised G36P in a final concentration of 0.5 mM was placed above a 1000 μL reservoir containing the same buffer. Single crystals were obtained at 20º C. To reduce the protein, a crystal was placed in mother liquid containing 10 mM sodium ascorbate. The distinct blue colour disappeared after 10 minutes. Data collection and processing as well as analysis of the crystallographic data were performed by Dr. Ellen Thomassen (Leiden, the Netherlands). Data were collected under cryo conditions in 12% glycerol on beam-line BM 14 at a wavelength of 0.95372 Å at the European Synchrotron Facility (ESRF). Data-collection and processing parameters as well as refinement statistics are listed in Table 2.2 and 2.3. The crystal structures were submitted to the Protein Data Bank (codes 2bz7 and 2bzc).

Table 2.2. Data-collection and processing parameters

Data collection	Oxidised (2BZ7)	Reduced (2BZC)
Crystal dimensions (mm)	0.1 x 0.1 x 0.05	0.1 x 0.1 x 0.05
Wavelength (Å)	0.95372	0.95372
Resolution range (Å)	21.57-1.76	23.90 – 1.79
Crystal system	Hexagonal	hexagonal
Space group	$P6_1$	$P6_1$
Unit cell parameters (Å)	a = 72.92, b = 72.92, c = 29.53	a = 72.98, b = 72.98, c = 29.70
Total No. reflections	99038	187009
No. unique reflections	9095	8720
multiplicity	10.89 (10.98) [a]	21.45 (21.22) [b]
Rsym[c]	0.053 (0.16)	0.059 (0.23)
Completeness (%)	99.8 (100)	100 (100)
Average I/σ (I)	7.62 (4.30)	7.43 (3.25)
solvent content (%)	40.1	40.6
V_M (Å^3 / Da)	2.1	2.1

[a] Data statistics of the outer resolution shell (1.86 – 1.76 Å) are given in parentheses, where applicable.
[b] Data statistics of the outer resolution shell (1.89 – 1.79 Å) are given in parentheses, where applicable.
[c] $Rsym = \Sigma_h \Sigma_i |I_{hi} - <I_h>| / \Sigma_h \Sigma_i |I_{hi}|$, where I_{hi} is the intensity of the ith measurement of the same reflection and $<I_h>$ is the mean observed intensity for that reflection.

Table 2.3. Refinement statistics

Refinement	Oxidised (2BZ7)	Reduced (2BZC)
Resolution range (Å)	21.57 – 1.76	23.90 – 1.79
number of reflections	8652 (428)[a]	8704 (413)[a]
Rfactor[b]	0.19 (0.24)	0.19 (0.25)
protein atoms / water molecules	761 / 87	761 / 87
r.m.s. deviations bonds (Å)	0.013	0.014
r.m.s. deviations angles (°)	1.505	1.539
Average B value protein / solvent (Å^2)	30.15 / 45.89	28.98 / 40.82
Average B value Cu (Å^2)	26.9	23.7
Ramachandran statistics[c] (%)	91.8 / 8.2 / 0 / 0	91.8 / 8.2 / 0 / 0
ESU[d] based on R value (Å)	0.137 (0.135)	0.142 (0.145)

[a] Data statistics of Rfree are given in parentheses, where applicable.
[b] $R = \Sigma||F_{obs} (hkl)| - |F_{calc}(hkl)|| / \Sigma |F_{obs}(hkl)|$
[c] According to the program PROCHECK [173]. The percentages are indicated of residues in the most favoured, additionally allowed, generously allowed and disallowed regions of the Ramachandran plot, respectively.
[d] Estimated overall coordinate error.

Results

Characterisation of recombinant wild type fern Pc

To obtain sufficient amounts of protein and enable mutagenesis a gene encoding *D. crassirhizoma* Pc was synthesised. The nucleotide sequence was obtained by back translation of the amino acid sequence[77] and divided over 4 sets of oligonucleotides (Table 2.1). The gene was then synthesised by polymerase chain reaction (PCR) in 4 subsequent steps. The product was cloned into the pET28c vector and the recombinant Pc was produced in *E. coli*, purified and characterised by mass spectrometry, UV-visible and NMR spectroscopy and stopped flow kinetics. The mass of both native and recombinant Pc is 10774 ± 1 Da. This is close to the theoretical mass of apo fern Pc, of which Met-1 is removed (10776.02 Da). The UV-visible spectrum of recombinant Pc shows the same maxima as the spectrum of native Pc. Reduction by horse heart cytochrome *c* was measured by stopped flow kinetics under pseudo first order conditions. The reduction rate constant at pH 6.0 is 1.3 ($\pm$ 0.1) $\times 10^7$ M^{-1} s^{-1} at 50 mM ionic strength and 3.9 ($\pm$ 0.1) $\times$ 10^6 M^{-1} s^{-1} and 100 mM ionic strength. The reduction rate constants are comparable to the rate of 4.1×10^7 M^{-1} s^{-1}, reported at pH 7.0, ~30 mM ionic strength[174]. They are also similar to those reported for angiosperm Pc. For instance, a reduction rate constant of 3.6 $\times$ 10^6 M^{-1} s^{-1} has been reported[175] at 100 mM ionic strength, pH 6.0. The ^{1}H NMR spectrum of recombinant Pc is essentially identical to the native counterpart (Fig. 2.1A).
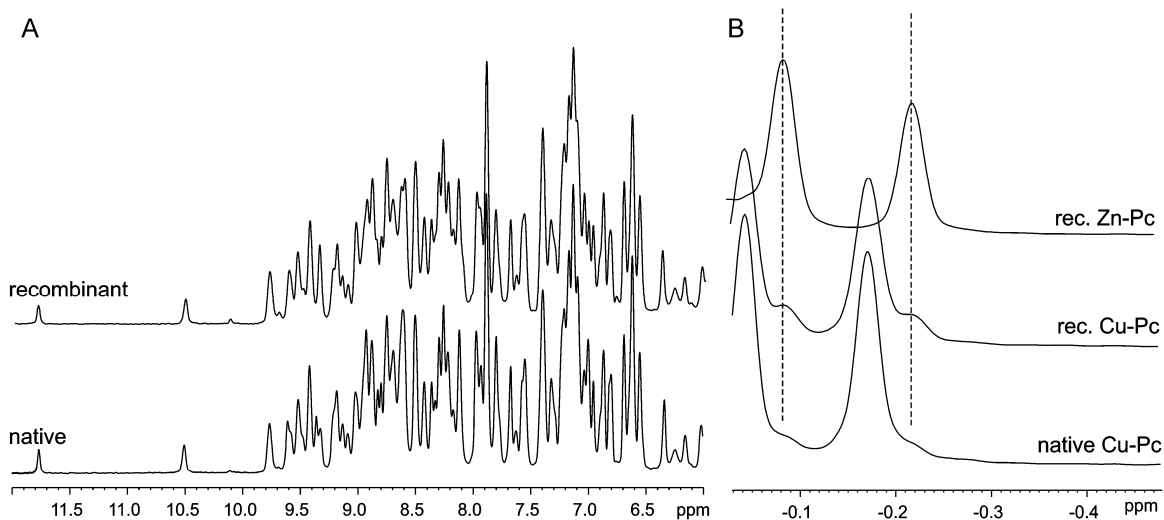
Figure 2.1. A) Amide region of the ^{1}H NMR spectra of native and recombinant Cu(I)-Pc. B) Comparison of upfield part of ^{1}H NMR spectra of native Cu(I)-Pc, recombinant Cu(I)-Pc and recombinant Zn(II)-Pc.

Some low intensity peaks were observed in both native and recombinant spectra, but more strongly for the recombinant species (Fig.2.1B). After comparison with the ^{1}H spectrum of Zn-substituted fern Pc these peaks were identified as corresponding to Zn-substituted Pc. It can be concluded that expression of recombinant Pc in *E. coli* results in the presence of a small fraction of Zn-substituted Pc (5-10%). Zn-Pc is apparently also present in native Pc but in smaller amounts (1-3%). The presence of zinc in blue copper proteins is a well-known phenomenon[176]. It is unclear whether the Zn-Pc is produced in the fern or is a consequence of the purification procedure.

Protonation behavior of His90 ring protons studied by ^{1}H NMR

In order to study the protonation behavior of His90 in fern Pc, mutations were made at Phe12 and Gly36, which were changed to Leu12 and Pro36, the residues most widely found at these positions in Pc's. ^{1}H NMR spectra of wt Pc and the F12L, G36P and F12L/G36P Pc mutants in D_2O were acquired. The singlet signals of histidine ring protons were identified by Hartman Hahn and CPMG experiments[155,167]. We could identify four signals of His37 and His90 protons (see below) in the recombinant wt Pc

spectrum (Fig. 2.2), in agreement with similar experiments done on native fern Pc[85]. As the pD is lowered to 5.8 signals of the His37 ring protons shift no more than 0.02 ppm, while the largest shift of the His90 protons is only 0.05 ppm. However, the resonances of the His90 protons (B and D) show significant broadening at pD 5.8, in line with exchange broadening due to protonation as observed in two-dimensional experiment (see below). At pD=5.4 and below, fern Pc shows significant aggregation, which impairs further ^{1}H NMR experiments.
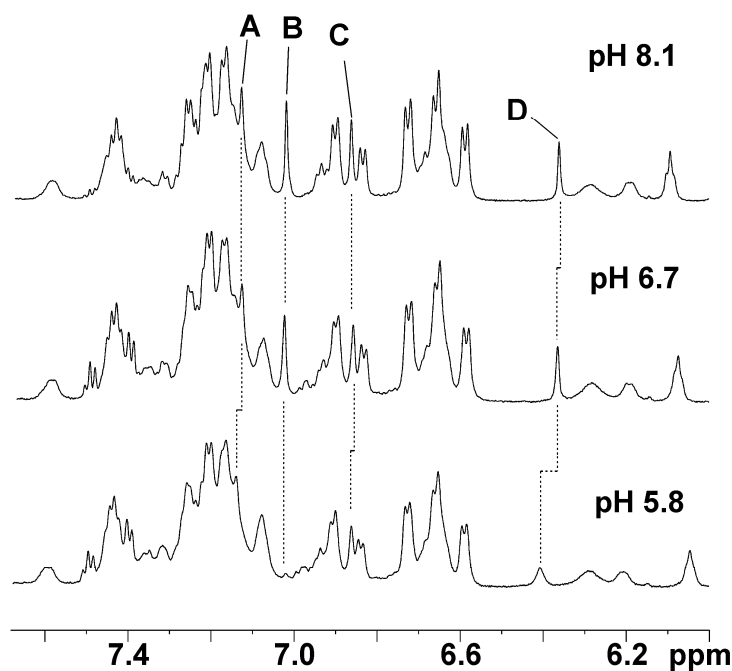
Figure 2.2. Part of ^{1}H NMR spectra of wild type Cu(I)-Pc in D_2O at pD 8.1, 6.7 and 5.8. Histidine peaks are assigned to A: $H_{\varepsilon1}$(His37), B: $H_{\varepsilon1}$(His90), C: $H_{\delta2}$(His37), D: $H_{\delta2}$(His90).

The histidine ring proton signals in the G36P mutant are all at similar positions as in the wt spectrum (Fig. 2.3). The two signals of His90 show a downfield shift of about 0.4 ppm in the F12L and F12L/G36P mutants (Fig. 2.3). The ring current shift caused by the aromatic ring of Phe12 is not present in these mutants. This confirms that the signals can be assigned to the ring protons of His90, which will be influenced most by the presence of the phenyl ring. Upon lowering of the pH the shifts of the histidine ring protons in the mutants are not significantly different from the wt shifts. This suggests a pH behavior of the mutants that is similar to that of the wt protein.
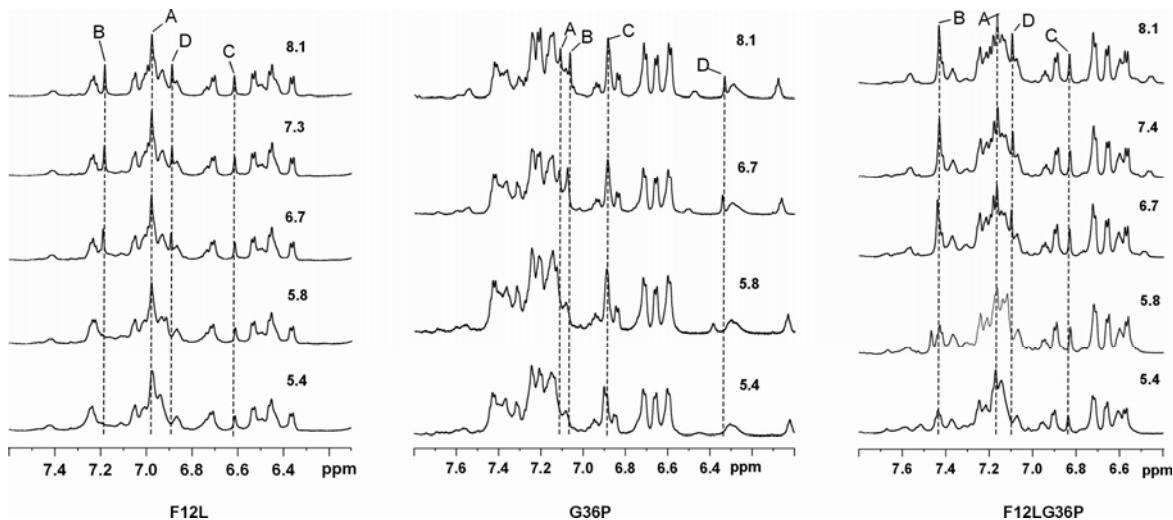
Figure 2.3. ^{1}H NMR spectra of Cu(I)-Pc mutants in D$_2$O. The numbers next to the spectra are the pD values at which the spectra were obtained. Histidine peaks could be assigned to A: H$_{\varepsilon 1}$ (His37), B: H$_{\varepsilon 1}$ (His90), C: H$_{\delta 2}$ (His37), D: H$_{\delta 2}$ (His90).

His90 backbone amide protonation

To gain a more detailed view of the protonation behavior a pH titration was performed with ^{15}N-labelled fern Pc. The resonances in the ^{15}N, ^{1}H HSQC spectrum were assigned on the basis of HNCACB and HN(CA)CO experiments done on a ^{15}N, ^{13}C-labelled Pc sample. During the pH titration, aggregation, which is a slow process on the NMR time scale, led to loss of peak intensities of the folded form and appearance of new peaks of the denatured form. Because of the high signal-noise ratio acquired by the HSQC experiment, we were able to record spectra of soluble, folded protein down to a pH of 4.0. Residues in the wt Pc spectrum that experience a change in chemical shift were identified. Nearly 73% of the resonances in the spectrum shift significantly upon lowering of the pH. Their chemical shifts in ^{1}H and ^{15}N dimensions were fitted to a pK$_a$. Surprisingly, the chemical shift of the backbone amide of His90 experiences a large ^{15}N chemical shift change which could be fitted to a pK$_a$ of 4.5 ($\pm$ 0.1) at 300 K, 50 mM ionic strength (Fig. 2.4A). The chemical shift change in the ^{1}H direction could be fitted to a pK$_a$ of 4.4 ($\pm$ 0.1). The amide resonances of the other copper ligands and several neighboring residues also experience chemical shift changes with pH. A global fit of these perturbations yields a pK$_a$ of 4.4 ($\pm$ 0.1) (Fig. 2.4B). This suggests that His90

indeed undergoes protonation and the effect is propagated towards other backbone amides in the vicinity as observed in other cases[148,177,178]. To investigate the effect of removing the phenyl ring that is close enough to have a $\pi-\pi$ stacking interaction with His90, spectra were acquired during a pH titration of the F12L mutant. The chemical shift changes of the His90 backbone amide resonance of F12L could be fitted to a pK_a of 4.4 ($\pm$ 0.1), which is equal to the value derived from a global fit (Fig. 2.4C). It can be concluded that the F12L mutation does not influence the pK_a of His90. The G36P mutation does have a small effect on the pK_a. The value derived from chemical shift changes in the amide backbone of His90 and from a global fit (Fig. 2.4D) is 4.7 ($\pm$ 0.1). Finally, this small effect is not observed in the double mutant, F12LG36P, where His90 has a pK_a of 4.4 ($\pm$ 0.1) (Fig. 2.4E).
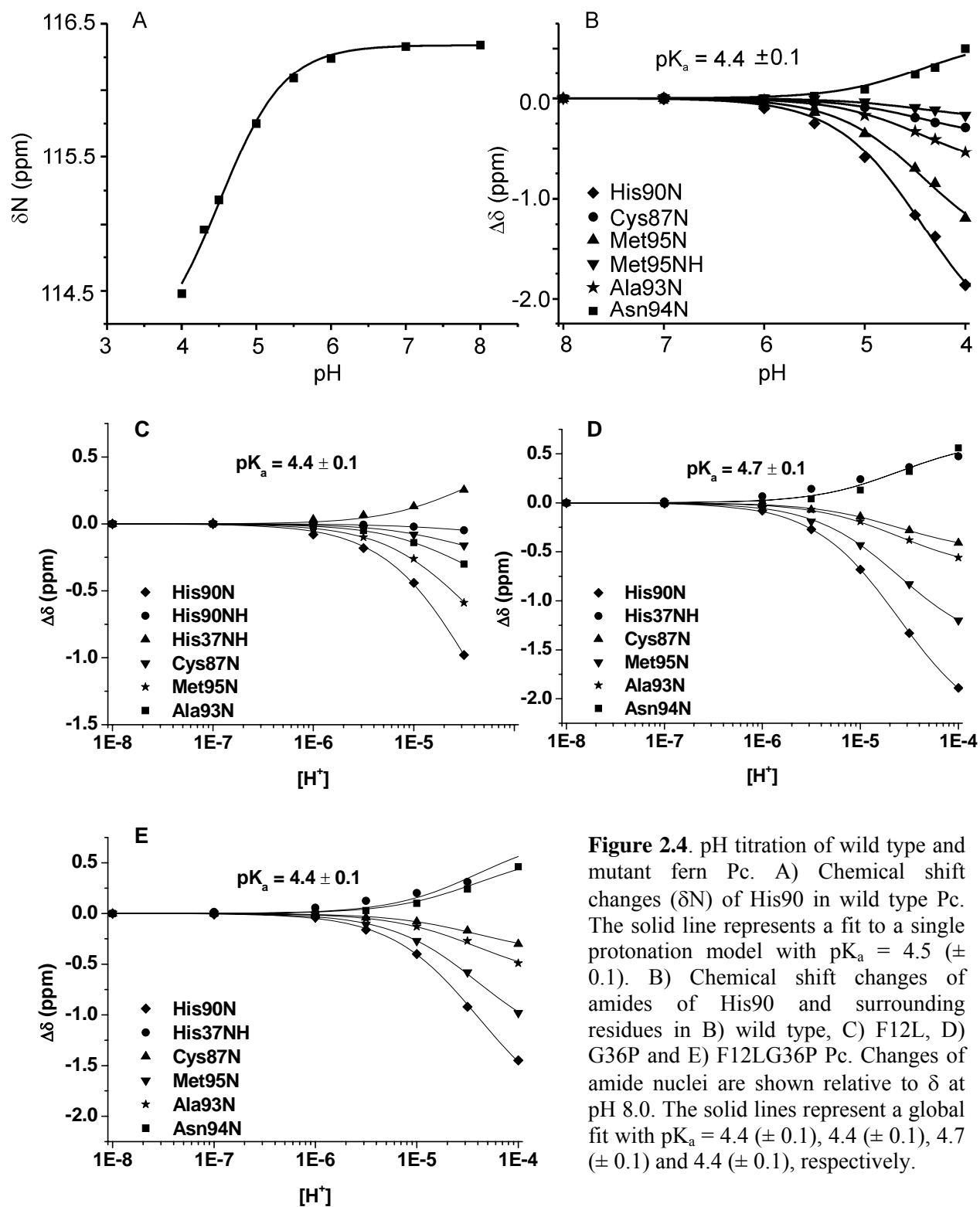
Figure 2.4. pH titration of wild type and mutant fern Pc. A) Chemical shift changes (δN) of His90 in wild type Pc. The solid line represents a fit to a single protonation model with $pK_a = 4.5$ ($\pm$ 0.1). B) Chemical shift changes of amides of His90 and surrounding residues in B) wild type, C) F12L, D) G36P and E) F12LG36P Pc. Changes of amide nuclei are shown relative to δ at pH 8.0. The solid lines represent a global fit with $pK_a = 4.4$ ($\pm$ 0.1), 4.4 ($\pm$ 0.1), 4.7 ($\pm$ 0.1) and 4.4 ($\pm$ 0.1), respectively.

Protonation behavior of His90 ring protons studied by 2D NMR

It is possible that the arc of acidic side chains, including Glu8, Glu34, Glu68, Asp69 and Glu70 in the proximity of the active site could cause the pK_a of 4.4 for the amide of His90, which is lower than found for other Pc's. To confirm that the imidazole ring of His90 becomes protonated, we performed [2]J coupled 2D NMR experiments on the same samples used for the HSQC experiments. The [2]J coupled experiment allows direct detection of the $N_{\delta1}$ and $N_{\epsilon2}$ nuclei of His residues, via coupling to the $H_{\delta2}$ and $H_{\epsilon1}$. Upon protonation the histidine $N_{\delta1}$ resonance shifts approximately -56 ppm, while the $N_{\epsilon2}$ resonance shift is smaller[172].

The histidines that coordinate the copper are the only histidines present in fern Pc. The resonances of their ring protons could be assigned in the wt and mutant [2]J spectra (Fig. 2.5A). Note that an $H_{\epsilon2}$ resonance is also observed in this experiment at 11.62 ppm. The resonance is split by [1]J-coupling in the ^{1}H dimension because the spectra were acquired without ^{15}N decoupling. In other blue copper proteins, the analogous resonance has been assigned to the $H_{\epsilon2}$ of the N-terminal His of the copper ligands, because this proton always forms a strong internal hydrogen bond, for instance to Thr35 in poplar Pc[179]. Analogously, this resonance can be assigned to His37 of fern Pc. In the crystal structure this $H_{\epsilon2}$ is hydrogen bonded to a buried water molecule, which would prevent its fast exchange with the solvent in solution. This leads to the assignment of the other His37 ring protons and consequently, those of His90. The assignments agree with the resonances found in the 1D experiments. Upon lowering of the pH, the signals of the His37 ligand ring protons shift slightly in both proton and nitrogen dimensions. This suggests that His37 does not become protonated, but experiences a protonation event in the neighborhood. The signals of the His90 ring protons, however, behave differently. Below pH 5.5 the signals of $H_{\epsilon1}$ and $H_{\delta2}$ coupled to $N_{\epsilon2}$ (~165 ppm) can no longer be detected, in accordance with the broadening observed in the 1D spectra (Fig. 2.2). The signal of $H_{\epsilon1}$ coupled to $N_{\delta1}$ (~237 ppm) disappears from the spectrum at pH 6.0. This behavior is the same as observed for pseudoazurin (kindly provided by Dr. Antoinetta Impagliazzo and Dr. Monica Vlasie), upon titration of its exposed histidine ligand (Fig. 2.6). The large chemical shift change for the ^{15}N ring nuclei results in exchange broadening, most strongly for $N_{\delta1}$.
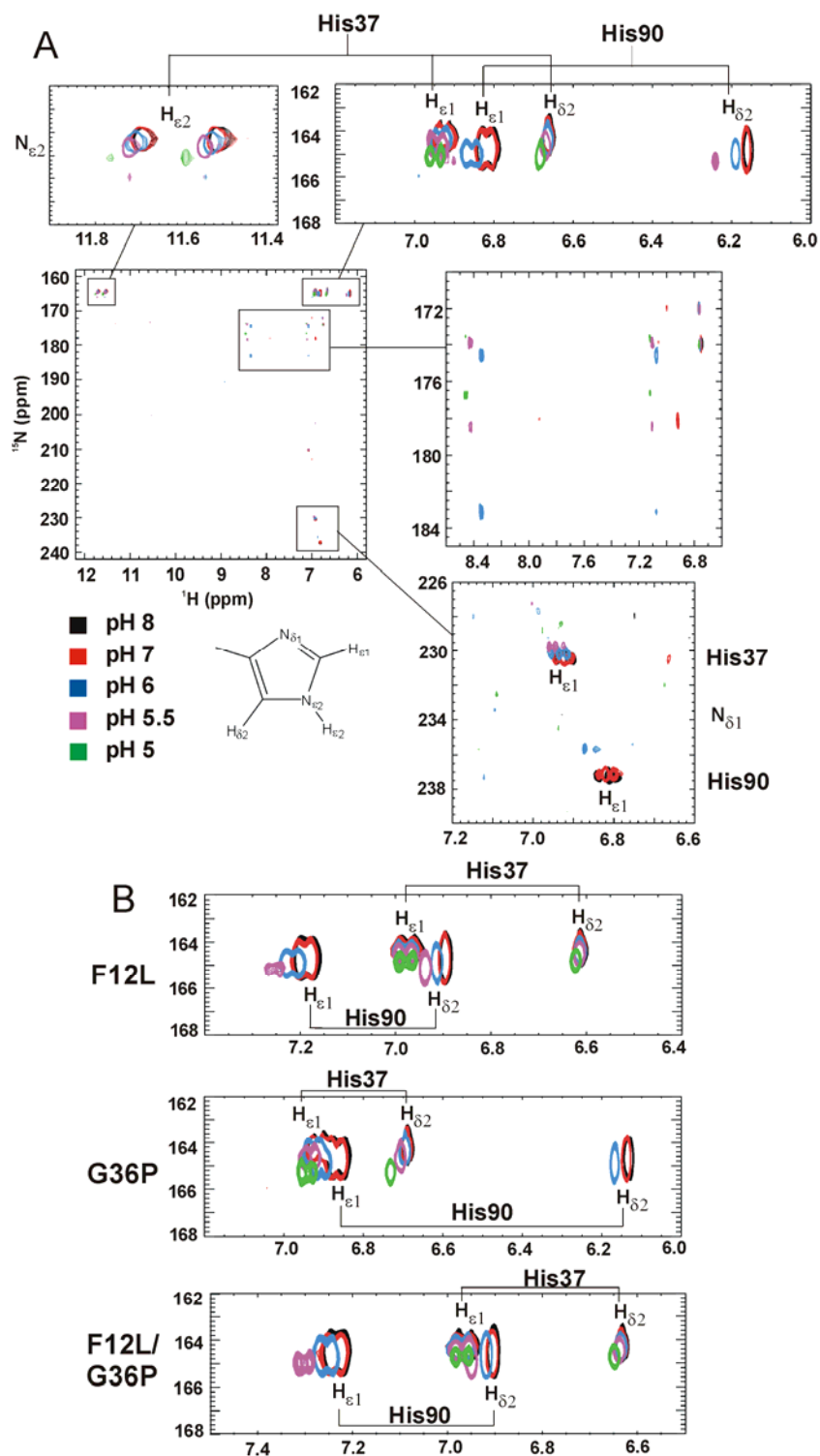
Figure 2.5. Histidine ring protonation. Overlay of ^2J coupled NMR spectra of wild type Pc (A) and F12L, G36P and F12LG36P Pc (B) at pH 8 (black), pH 7 (red), pH 6 (blue), pH 5.5 (magenta), pH 5 (green). Resonances of histidine protons are labelled. Areas of interest are enlarged for clarity.
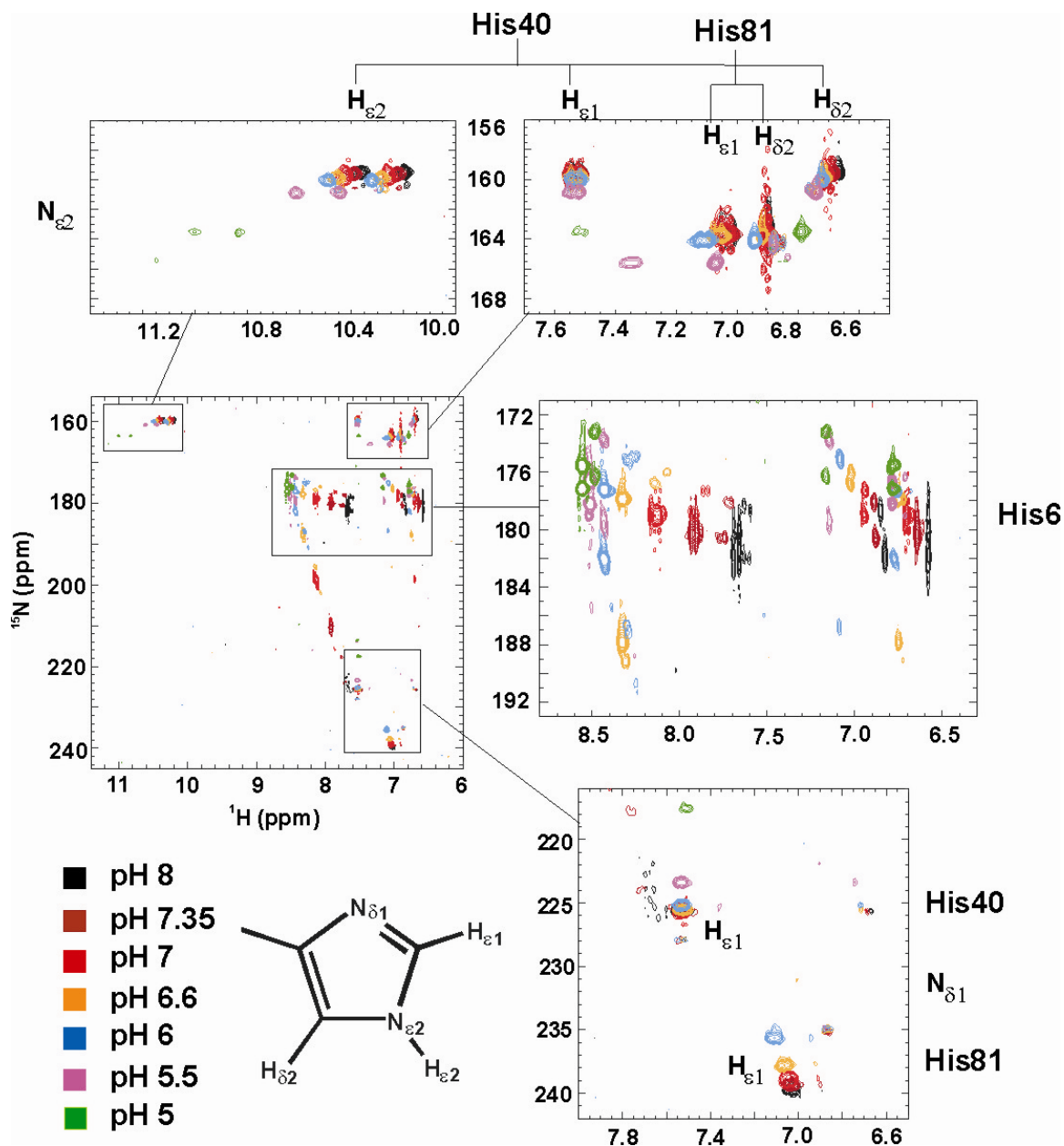
Figure 2.6. Overlay of ^{2}J coupled NMR spectra of wild type pseudoazurin, at pH 8 (black), pH 7.35 (brown), pH 7 (red), pH 6.6 (orange), pH 6.0 (blue), pH 5.5 (magenta), pH 5 (green). Resonances of histidine protons are labelled. Area's of interest are enlarged for clarity.

pH dependence of the reduction potential of fern Pc

Fern Pc shows a CV signal in the pH range of 7-2.5 at 25 °C, due to an electrochemically quasi-reversible monoelectronic reduction/oxidation of the Cu ion. Peak-to-peak separations vary between 60 to 90 mV within the range of scan rates investigated. Anodic and cathodic peak currents were found to be identical, and both were proportional to protein concentration and $v^{1/2}$ ($v=$ scan rate), indicating a diffusion controlled electrochemical process. Under these conditions, the $E_{1/2}$ values can be assumed to represent the E°' values. Potential values (E°') of +376 mV, +363 mV, +364 mV and +352 mV (± 3mV) have been determined at pH 7 for the wt, G36P, F12L and F12LG36P species, respectively. These values are in the range expected for blue copper proteins[82,164,180,181]. The reduction potential of recombinant wt fern Pc is similar to that for the native protein[85] (+376 vs. +382 mV). The small decrease in E°' for the F12L and G36P mutations of 10 mV appears to be additive as the change is 20 mV in the double mutant. When the pH is lowered below 7, the reduction potential increases (Fig. 2.7). This behavior has been observed elsewhere for Pc's[82,85,146,182], and other blue copper proteins[183], and has been attributed to a coupling of copper(II) reduction to histidine ligand protonation and detachment from the metal. Down to pH 4.5, the change in E°' of the wt protein is consistent with the behavior observed previously for native fern Pc[85]. At lower pH values, a pronounced potential increase is observed. The slope of the E°'/pH profile is 27 mV/pH, lower than the theoretical value of 59 mV/pH. This could be the result of protein unfolding occurring at these low pH values. The slope is similar for the F12L and G36P mutant, but smaller (15 mV/pH) for the double mutant. This could be due to more pronounced unfolding at low pH values.
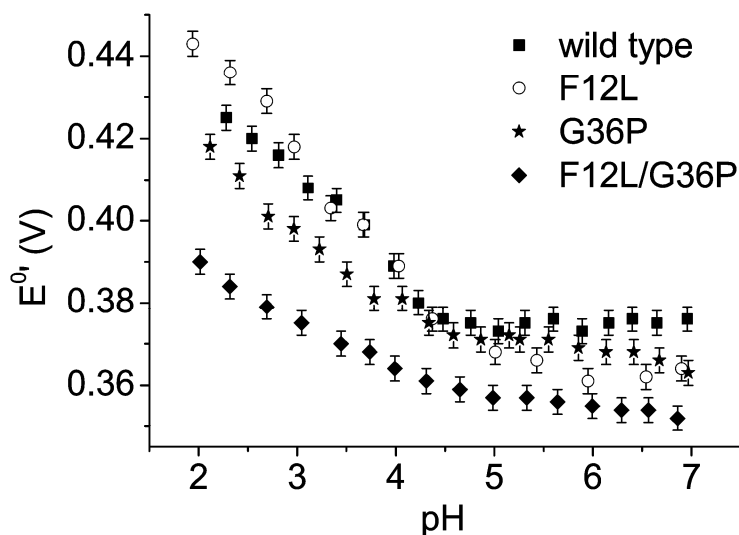
Figure 2.7. pH dependence of the reduction potential for wild type and mutant fern Pc.

Crystal structure of G36P plastocyanin

Crystals of the G36P mutant were grown at pH 4.5 and diffracted to a resolution of 1.7 and 1.8 Å for the oxidised and reduced protein, respectively. It was not possible to grow crystals of F12L or F12LG36P mutants even after extensive screening. The structure of the G36P protein was determined by molecular replacement with MOLREP[184], using the oxidised and reduced wt structures as models[185]. The average root-mean-square deviation (rmsd) between the wt and G36P Pc structures is 0.37 Å and between oxidised and reduced G36P Pc 0.24 Å. The differences observed between oxidised and reduced G36P Pc have also been reported for the oxidised and reduced wt Pc[185]. As in the reduced wt Pc at this pH, His90 in the G36P mutant does not flip and move away from the copper. The distances from the copper to all four ligands do not change significantly between the oxidised and reduced structures (Table 2.4) or from the wt structure. The apparent discrepancy between NMR and crystallographic data may be explained by the presence of crystal contacts around His90. Glu4 of the neighboring unit and a water molecule are found close to His90 (Fig. 2.8). The distance between the $O_{\varepsilon 1}$ of Glu4 and the water is 2.69 Å and that between $N_{\varepsilon 2}$(His90) and the water molecule is 2.92 Å. Apparently, the proximity of the neighboring asymmetric unit favors crystallization of the deprotonated fern Pc.

Table 2.4. Dimensions of the copper site in oxidised and reduced G36P fern Pc at pH 4.5.

	Oxidised Pc[a]	**Reduced Pc[a]**
Bond lengths (Å)		
Cu-N (His 37)	2.09	2.02
Cu-N (His 90)	2.14	2.14
Cu-S (Cys 87)	2.20	2.23
Cu-S (Met 95)	2.89	2.93
Bond angles (degrees)		
N (His 37)-Cu-N (His 90)	100.8	102.7
N (His 37)-Cu-S (Cys 87)	130.1	130.4
N (His 37)-Cu-S (Met 95)	81.7	81.2
N (His 90)-Cu-S (Cys 87)	123.2	121.8
N (His 90)-Cu-S (Met 95)	105.7	106.2
S (Cys 87)-Cu-S (Met 95)	104.8	104.2

[a] The ESU (estimated overall coordinate error) value for both structures is 0.14 Å.
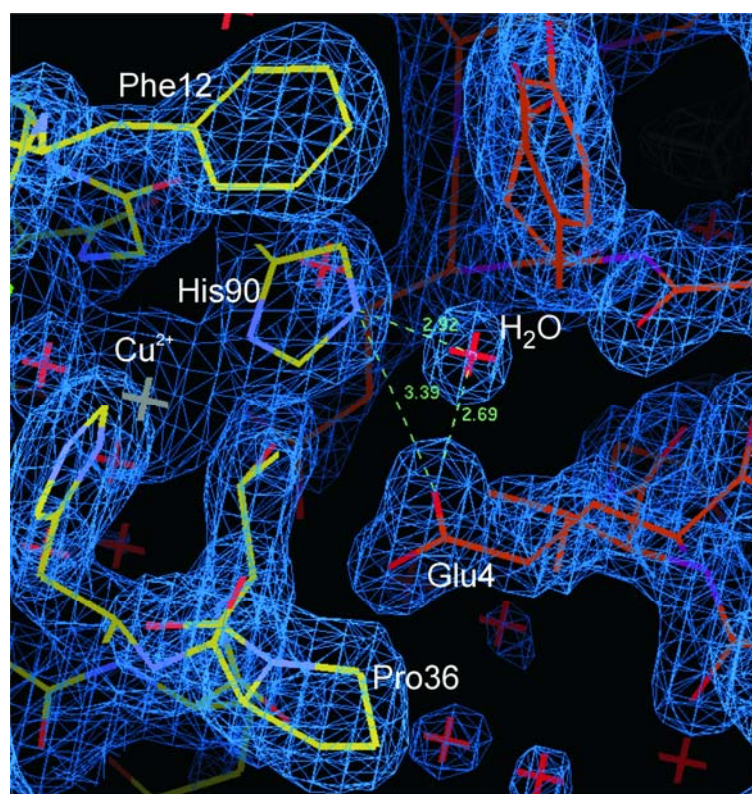
Figure 2.8. His90 in the crystal structure. $2F_0$ -F_c electron density map contoured at 1.5 σ of the area around the Cu-site of reduced G36P fern Pc (yellow), with nitrogen atoms in blue and oxygen atoms in red. Distances (Å) between $N_{\varepsilon2}$ of His90, crystalline water and $O_{\varepsilon1}$ of Glu4 in the neighbouring asymmetric unit (red and purple) are shown in green.

Discussion

Recombinant fern Pc was used to study the reported unusual pH dependent behavior of the solvent exposed histidine Cu-ligand. From our spectroscopic and mass spectrometry characterization as well as from comparison of the 1D ^{1}H NMR experiments[85] it can be concluded that the native and recombinant proteins are the same. These experiments show small chemical shift changes of the histidine ring protons in the ^{1}H dimension (Fig. 2.2) down to pH 5.4. At lower pH, aggregation impairs further experiments. This problem is less pronounced in the 2D HSQC experiments, because these are more sensitive. Another advantage is that more residues can be observed, gaining a more detailed picture. Chemical shift changes in the backbone amide of His90 of the wt protein could be fitted to a pK_a of 4.5 (± 0.1) (Fig. 2.4A). This corresponds well to the value 4.4 (± 0.1) from a global fit of chemical shift changes in the other copper ligands and surrounding amides (Fig. 2.4B). The ^{2}J coupled experiment shows that indeed the imidazole ring of His90 is protonated. Therefore it can be concluded that, contrary to previous reports, protonation of His90 in fern Pc does occur.

The relatively low pK_a value in combination with aggregation at low pH explains why it was difficult to determine this value before. 1D ^{1}H NMR experiments can only be done down to pH 5.4, which explains why protonation in fern Pc is difficult to detect with that method. Furthermore, it is well established that protonation in Pc is accompanied by a large increase in the midpoint potential[158,186]. As reported previously[85] the reduction potential for fern Pc does increase at lower pH, consistent with protonation. Although potentials could be measured at pH values below 4.3, it is not possible to fit this increase to a single acid-base equilibrium equation, probably due to the presence of unfolded protein.

Crystal structures have been a crucial method in studying the protonation behavior of blue copper proteins. The 'flipping' histidine was first shown in poplar Pc[187] and later for *A. faecalis* pseudoazurin[156]. Also, it was shown that histidine protonation is prevented in amicyanin when bound to MADH[150]. The crystals of poplar Pc showing a flipped histidine ligand have a space group different from that of fern Pc, leaving ample space for the histidine to make a 180º rotation. In the case of fern Pc, crystal packing forces appear

to favor the crystallization of the deprotonated form. Our work shows that sometimes differences can be found between results obtained in the solution and the crystalline states.

Mutations were made around the active site to test whether $\pi-\pi$ stacking with Phe12 or hydrogen bond formation with the backbone oxygen of Gly36 influences the protonation behavior. The G36P crystal structure at pH 4.5 does not show significant differences from the wt structure. No crystals could be obtained for either of the Phe12 mutants, so it cannot be excluded that this mutation has a subtle effect on the structure. The NMR spectra indicate that no major change occurs. To our surprise both the F12L and G36P mutations and the double mutation do not cause a large change in the pK_a of His90. This suggests that Phe12 and Gly36 do not contribute significantly to the protonation behavior of the His90 copper ligand in fern Pc, contrary to what has been reported for pseudoazurin. An increased reduction potential and decreased pK_a were observed in a pseudoazurin mutant in which a $\pi-\pi$ interaction was introduced[147].

The explanation for the relatively low pK_a value found for fern Pc remains as yet unclear. It may be related to the unique position of the acidic patch surrounding the hydrophobic patch in fern Pc, which will create an electrostatic environment different from that in other Pc's.

Dynamics in the transient complex of plastocyanin-cytochrome *f* from *Prochlorothrix hollandica*

Abstract

The nature of transient protein complexes can range from a highly dynamic ensemble of orientations to a single well-defined state. This represents variation in the equilibrium between the encounter and final, functional state. The transient complex between Pc and cyt*f* of the cyanobacterium *P. hollandica* was characterised by NMR spectroscopy. Intermolecular pseudocontact shifts (PCS) and chemical shift perturbations were used as restraints in docking calculations to determine the structure of the wt Pc - cyt*f* complex. The orientation of Pc is similar to orientations found in Pc - cyt*f* complexes from other sources. Electrostatics seems to play a modest role in complex formation. A large variability in the ensemble of lowest energy structures indicates a dynamic nature of the complex. Two unusual hydrophobic patch residues in Pc have been mutated to the residues found in other plastocyanins (Y12G/P14L). The binding constants are similar for the complexes of cyt*f* with wt Pc and mutant Pc, but the chemical shift perturbations are smaller for the complex with mutant Pc. Docking calculations for the Y12G/P14L Pc - cyt*f* complex did not produce a converged ensemble of structures as for the wt complex. Simulations of the dynamics were performed using the observed averaged NMR parameters as input. The results indicate a surprisingly large amplitude of mobility of Y12G/P14L Pc within the complex. It is concluded that the double mutation shifts the complex further from the well-defined towards the encounter state.

Introduction

Recent studies have shown the existence of dynamic encounter complexes in transient protein-protein and protein-DNA interactions[31,39,188]. The encounter state (or encounter complex) is thought to precede the well-defined (or single-orientation) complex as illustrated in a two-step model for protein complex formation (Fig. 1.1). In earlier studies, transient protein complexes were found to range from entirely dynamic to mostly well-defined[29,32-34,38,40,189-191]. The complex of Pc and cyt*f* is an interesting example in this respect, because comparative studies have shown that the degree of dynamics within the complex varies strongly between species.

The soluble Pc transfers electrons in oxygenic photosynthesis between the membrane-bound cytochrome b_6f and photosystem I complexes[56,142]. Pc is a small (~11 kDa) blue copper protein, which contains a type I copper site for electron transfer[139,192]. Cyt*f* is a *c*-type haem containing cytochrome, of which the truncated N-terminal soluble part (~28 kDa) is used for *in vitro* experiments ([99,193,194] and references therein). Because of the transient nature of the complex all structures of Pc - cyt*f* complexes determined so far have been determined by NMR spectroscopy[29,30,40,109] . The first structure of the plant complex revealed an electron transfer pathway between the hydrophobic patch surrounding the copper site of Pc and haem ligand Tyr1 in cyt*f* [29]. Kinetic studies *in vitro*[16,130,142,195-198] have shown that electrostatics play an important role in complex formation. *In vivo* studies suggest, however, that charged residues are not relevant for fast electron transfer reactions[199,200]. Nonetheless, the structure of the plant complex showed that the acidic 'eastern' patch on Pc interacts with a set of basic residues in the small domain of cyt*f*. The results suggested that this complex is mostly in a well-defined state. The structure of the complex from cyanobacterium *Nostoc* sp. PCC 7119 (former *A. variabilis*) is similar to that from plants, yet the interaction charges between Pc and cyt*f* are interchanged[109]. The complex of *Ph. laminosum* Pc and cyt*f* demonstrated that the charge interactions are not absolutely necessary for a functional complex. In this case, the proteins mostly interact through hydrophobic contacts. The structure showed poorer convergence to a well-defined state, suggesting more dynamics within the complex[40].

Pc from cyanobacterium *P. hollandica* contains two unusual residues located in the hydrophobic patch, which have been mutated to the residues normally found in these positions (Tyr12Gly/Pro14Leu). The mutant Pc has been shown to react differently with PSI[201] and was suggested to be more dynamic in complex with cyt*f* from *Ph. laminosum*[87]. Here, we report the structure of the physiological complex between *P. hollandica* Pc and cyt*f* and show that the existing equilibrium between encounter and well-defined state in the complex is shifted towards the encounter state by the mutation of two unusual hydrophobic patch residues (Y12G/P14L). It is concluded that this complex is on the border between dynamic and well-defined states.

Materials and Methods

Protein expression & purification

Mutant and wt ^{15}N-labelled *P. hollandica* plastocyanin were expressed and purified as described before[87]. Cyt*f* was expressed and purified essentially as described[202], in which the coding sequence of the *P. hollandica* cyt*f* soluble domain (GenBank AF486288) was ligated in-frame to the *Ph. laminosum* Pc leader coding sequence and expressed in *Escherichia coli*. The purification procedure followed the protocol for the *Ph. laminosum* protein[202]. Yields of pure cyt*f* were typically 3 mg protein per litre of culture.

Cd-substitution of Pc

Cd-substitution of plastocyanin was essentially done as described[166] with the following modifications. Of a 200 mM KCN, 500 mM Tris/HCl, pH 7.0 solution, 0.5 mL was added to 0.5 mL of 1 mM oxidised Pc. The sample was then loaded on a G25 Sephadex column pre-equilibrated with 1 mM CdCl$_2$, 50 mM HEPES, pH 7.0. The buffer was exchanged to water and then to 10 mM sodium phosphate, pH 6.0.

NMR samples

All protein samples contained 10 mM sodium phosphate, pH 6.0, 6% D_2O. Protein concentrations were determined by optical spectroscopy using ε_{602} of 4.9 mM^{-1} cm^{-1} for oxidised PCu, ε_{554} of 24.9 mM^{-1} cm^{-1} for reduced cyt*f* and ε_{278} of 7.6 mM^{-1} cm^{-1} for PCd (ε_{278} based on atomic absorption measurements). The pH was adjusted with microlitre aliquots of 0.1 or 0.5 M HCl. Samples for assignment contained 1.0 mM ^{15}N-labelled PCd. For titrations, both Cu(II) and Cd-substituted ^{15}N-labelled Pc were concentrated to 0.2 mM. Wt PCd could not be used for titrations because of unfolding in the presence of high amounts of cyt*f*. This was not the case for the mutant PCd, which is more stable in both the Cu- and Cd-substituted form. The copper proteins were reduced by addition of 2.0 mM ascorbate and flushed with argon to prevent reoxidation. Aliquots of a 1.33 mM cyt*f* stock solution were added to the Pc containing samples. Samples for determination of PCS contained 85 μM ^{15}N-labelled wt or mutant PCd and 50 or 100 μM oxidised cyt*f*, respectively. Cyt*f* was subsequently reduced in the sample by addition of 20 equivalents of sodium ascorbate. The pH was measured before and after each experiment.

NMR spectroscopy

All NMR spectra were recorded at 300 K on a Bruker DMX600 spectrometer equipped with a triple-resonance TCI-ZGRAD ATM Cryoprobe (Bruker, Karlsruhe, Germany). Chemical shift perturbation and PCS studies were performed by acquiring ^{15}N,^{1}H HSQC spectra. Spectral widths of 40 ppm (^{15}N) and 13.5 ppm (^{1}H) were used, and 1024 and 256 complex points were acquired in the direct and indirect dimension, respectively. Cd-substituted wt and mutant Pc resonances were assigned using 3D NOESY-HSQC and 3D TOCSY-HSQC experiments. Data were processed with AZARA 2.7 [203] and analysed in ANSIG for Windows[204].

Binding curves and chemical shift mapping

Averaged chemical shift perturbations ($\Delta\delta_{avg}$) were derived from equation 3a:

$$\Delta\delta_{avg} = \sqrt{\frac{1}{2}(\frac{\Delta\delta_N^{\ 2}}{25} + \Delta\delta_H^{\ 2})} \qquad (3a)$$

where $\Delta\delta_N$ and $\Delta\delta_H$ are the chemical shift perturbation after extrapolation to the 100% bound state of the amide nitrogen and proton, respectively[205]. Chemical shift titration curves were analysed with a two-parameter non-linear least-squares global fit to a 1:1 binding model, which corrects for dilution effects [16,38]:

$$\Delta\delta_{bind} = \frac{1}{2}\Delta\delta_{max}(A - \sqrt{(A^2 - 4R)}) \quad (3b)$$

$$A = 1 + R + \frac{PR + C}{PCK_a} \qquad (3c)$$

where R is the [cyt*f*]:[^{15}N-Pc] ratio, $\Delta\delta_{bind}$ is the chemical shift perturbation at a given R, $\Delta\delta_{max}$ is the chemical shift perturbation at 100% bound ^{15}N-Pc, P is the initial [^{15}N-Pc], C is the stock concentration of cyt*f* and K_a is the association constant of the complex.

Table 3.1. Restraint groups

Type	Number	Scale	Number x scale
Interface	22	10	220
Pseudocontact	36	10	360
Minimal distance	94	3	282
Angle	36	*a*	*a*

a Scaling of the angle restraints is not comparable to the other (distance) restraints.

Structure determination

The coordinates for *P. hollandica* Pc were taken from the solution structure (PDB entry 1B3I [76]). Mutations Y12G and P14L were introduced *in silico*, using DeepView/Swiss-PdbViewer version 3.7 [206]. A model of *P. hollandica* cyt*f* based on *Ph. laminosum* cyt*f* (PDB entry 1CI3 [107]) was created with MODELLER 6v2 [207]. Docking of Pc onto cyt*f* was done using restrained rigid-body molecular dynamics in XPLOR-NIH 2.9.9 [208]. The coordinates of cyt*f* were fixed, while Pc was placed at a random position and allowed to

move under the forces of restraints and a van der Waals repel function. Only the interactions between the backbone and C_β atoms of Pc and all atoms of cyt*f* were considered at this stage. The restraints were divided into three classes. Chemical shift perturbations in the presence of reduced cyt*f* were attributed to the proximity of the protein. The average relative solvent-accessible surface area of each Pc residue was calculated with NACCESS 2.1.1 [209]. Residues with a surface accessible surface area of more than 50% and $\Delta\delta_{bind} \geq 0.1$ (^{15}N) or 0.02 (^{1}H) were included in the class for interface restraints. Pseudocontact and angle restraints based on PCS were defined as described[29]. Residues that do not experience a PCS were included in a minimal distance restraint class. A summary of the restraints is given in Table 3.1. The product of the number of restraints and the scale used in the calculations indicates the weight of each group. The rigid-body molecular dynamics was essentially done as described before[29,30,40,109]. A run comprised 3000 cycles, each of 1000 steps. Structures below an energy threshold were saved, yielding ~200 structures per run. To obtain multiple independent dockings during a run Pc was randomly displaced after having reached an energy minimum, with energies changing less than two-fold during 10 cycles. Approximately 130 displacements occurred per run. The resulting structures were ranked according to total restraint energy, and the lowest energy structures were subjected to energy minimisation of the side chains in the interface. This ensemble of 20 lowest energy structures has been deposited in the Protein Data Bank under (entry 2P80). The buried interface area was calculated using NACCESS.

Pseudocontact simulations

The PCS simulations were done using XPLOR-NIH. The lowest energy structure of wt Pc - cyt*f* was used as the initial orientation of the Y12G/P14L Pc - cyt*f* complex. The relative diffusional movement in the mutant complex of Pc - cyt*f* was decomposed into two types of rotations. Pc was rotated around its centre of mass (wobble) and around the origin of the magnetic susceptibility tensor frame; the haem iron in cyt*f* (rotation). For this purpose three pseudoatoms, representing the magnetic susceptibility tensor were placed at 2 Å from the haem metal centre in cyt*f*. They were used as a reference frame

with the χ_{zz} component of the tensor placed along the Fe-Tyr1N vector. Each rotation was again decomposed in three directions (*X, Y* and *Z*), resulting in six variables for the complete movement. For a given set (for example, 40º, 80º, 35º / 60º, 60º, 60º) an ensemble of 50 structures was created by six rotations over random angles within the range given for each of the six variables (i.e., between 0º and 40º for the first angle, and so on), and this procedure was repeated 50 times. For such an ensemble the average PCS was calculated for each Pc nucleus. The equation used to calculate PCS, assuming an axial magnetic susceptibilty tensor, oriented along the Fe-Tyr1N vector[8] is:

$$\Delta\delta_{PC} = \frac{10^{36} F}{12\pi N_A r^3} \chi_{ax} \left(3\cos^2\theta - 1\right)$$
(3d)

where $\Delta\delta_{PC}$ is the size of the PCS in ppm, r is the distance (Å) from the Pc nucleus to the iron, and θ is the angle between the nucleus, the iron and the nitrogen of the N-terminal amino group of cyt*f*. *F* reflects the fraction Pc in complex with cyt*f*; the value used in these simulations is 0.7. N_A is Avogadro's number and χ_{ax} the size of the magnetic susceptibility tensor, taken to be 2.0×10^{-8} m^3 mol^{-1}, on the basis of other *c*-type cytochromes[210].

If the rotations caused the structures to either clash or not touch, the distance was increased or decreased in steps of 1 Å, respectively, until both proteins were just in contact. To determine the correlation between the observed and simulated PCS the *Q*-factor was calculated with equation 3e:

$$Q = \left[\sum_i \left\{ \Delta\delta_{PC}^{obs}(i) - \Delta\delta_{PC}^{sim}(i) \right\}^2 / \sum_i \Delta\delta_{PC}^{obs}(i)^2 \right]^{1/2}$$
(3e)

where $\Delta\delta_{PC}^{obs}$ is the size of the observed PCS in ppm and $\Delta\delta_{PC}^{sim}$ is the size of the average simulated PCS for residue *i*.

Results and discussion

Complex of P. hollandica PCu and cytf: wild type versus Y12G/P14L Pc

To compare the effects of binding, chemical shift perturbations were analyzed for wt and Y12G/P14L *P. hollandica* Pc upon titration with cyt*f*. The presence of reduced cyt*f* gives rise to distinct changes in the ^{1}H-^{15}N HSQC spectrum of ^{15}N-PCu(I). A single averaged resonance was observed for each amide indicating that exchange between free and bound Pc is fast on the NMR-time scale. The observed chemical shift changes ($\Delta\delta_{bind}$) of the most affected residues were plotted against the molar ratio of cyt*f*: ^{15}N-PCu (Fig. 3.2) and fitted to a 1:1 binding model[16]. This yields a K_a of 25 ($\pm$ 2) x10^3 M^{-1} for wt PCu and 20 ($\pm$ 1) x10^3 M^{-1} for Y12G/P14L PCu. Although the binding constants are very similar, there is a significant difference in the size of the chemical shift perturbations. This becomes apparent when the average

Figure 3.2. Binding curves for complex formation between *P. hollandica* Pc and cyt*f*. The $|\Delta\delta_{bind}|$ of individual residues is plotted as a function of the cyt*f*:Pc ratio. Global non-linear least-squares fits (solid lines) to a 1:1 binding model[16] yielded a K_a of 25 ($\pm$ 2) x10^3 M^{-1} for wild type PCu (A) and 20 ($\pm$ 1) x10^3 M^{-1} for Y12G/P14L Pc (B).

chemical shift perturbations ($\Delta\delta_{avg}$) per residue are considered (Fig. 3.3). From the figure, it is clear that the hydrophobic patch surrounding the copper site is the main site involved in complex formation, as seen in Pc - cyt*f* complexes from other organisms[8,29,30,40,109]. The residues that are affected in the wt complex are generally also affected in the mutant complex, but the size of the chemical shift changes is clearly smaller, by about 40%. This is comparable to the results obtained for the complex of *P. hollandica* Pc and cyt*f* from *Ph. laminosum*[87], and suggests increased dynamics in the complex of Y12G/P14L Pc and

cyt*f*. A comparison of the size of the PCS found for the complex with wt and mutant Pc (see later, Fig. 3.7A) supports this notion.
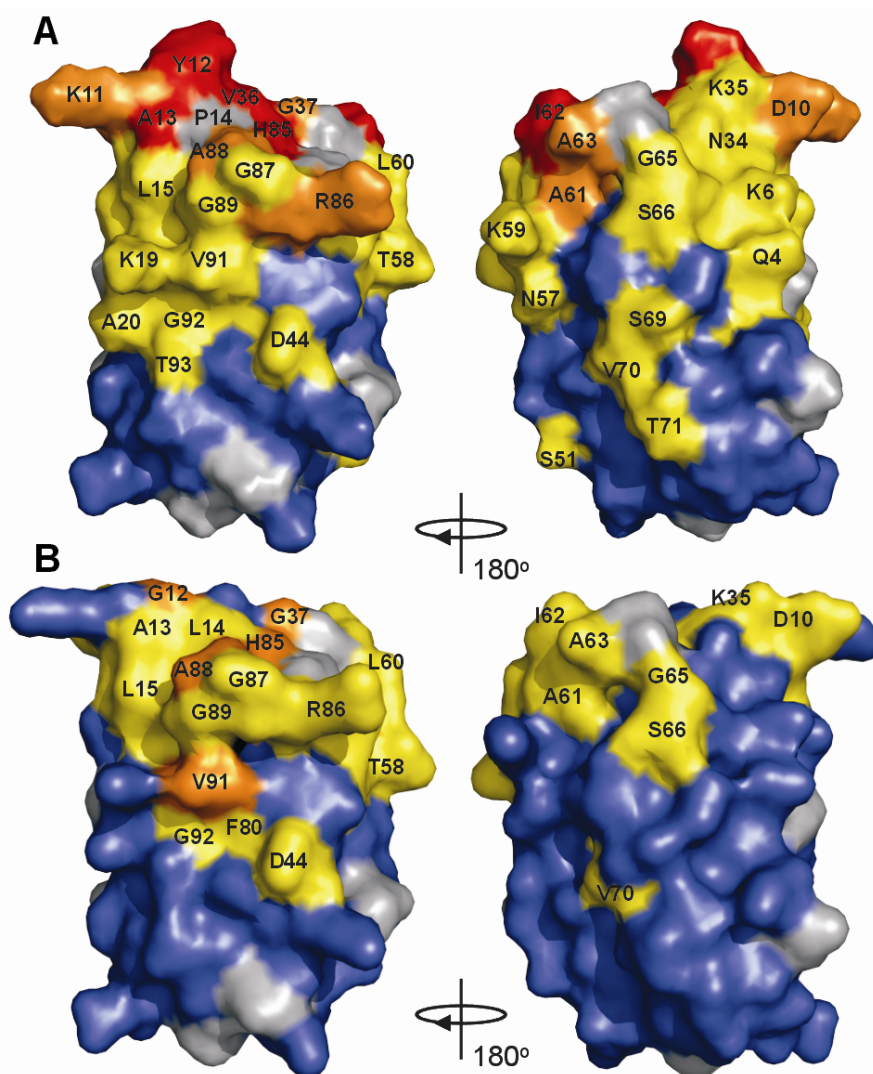
Figure 3.3. Surface representations of A) *P. hollandica* Pc (PDB file 1BI3) and B) a model of *P. hollandica* Pc Y12G/P14L. Average chemical shift perturbations ($\Delta\delta_{avg}$) for PCu are colour coded as follows; blue $\Delta\delta_{avg} \leq 0.025$ ppm, yellow $\Delta\delta_{avg} \geq 0.025$ ppm, orange $\Delta\delta_{avg} \geq 0.10$ ppm, and red $\Delta\delta_{avg} \geq 0.175$ ppm.

The affinity between Pc and cyt*f* decreases with increasing ionic strength (Fig. 3.4). A reduction of $\Delta\delta_{bind}$ of 46% at 200 mM NaCl is observed, indicating electrostatics play a role in complex formation. The Pc Y12G/P14L complex is similarly affected by ionic strength, with $\Delta\delta_{bind}$ reduced by 42%. This demonstrates that the effect of ionic strength on complex formation is similar in the wt and mutant complexes.
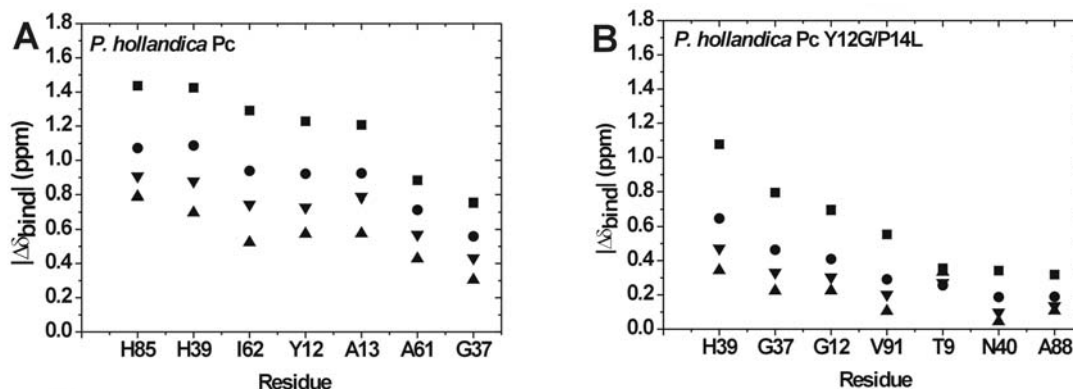
Figure 3.4. Salt dependence of the $|\Delta\delta_{bind}|$ of the most shifted residues of wild type PCu (A) and Y12G/P14L PCu (B) in complex with cyt*f* (the ratio cyt*f*:PCu is 3:1). Symbols indicate the presence of 0 mM NaCl (■), 50 mM NaCl (●), 100 mM NaCl (▼) and 200 mM NaCl (▲).

Structure of the complex of P. hollandica Pc – cytf

The structure of *P. hollandica* Pc - cyt*f* complex has been determined by rigid-body structure calculations using restraints obtained by NMR spectroscopy. Two types of NMR data were used. One is chemical shift perturbations of solvent exposed Pc residues, which give information on the proximity of these residues to cyt*f*. The other is intermolecular pseudocontact shifts (PCS), which are observed in the presence of paramagnetic, oxidised cyt*f* and give both distance and angular information on the proximity of Pc residues to the Fe(III)[29]. To be able to study the interaction of Pc with both oxidised and reduced cyt*f* without interference from electron transfer reactions, the Cu in Pc was substituted with Cd (PCd).

A titration followed by ^{1}H-^{15}N HSQC spectra showed that the complex of PCd Y12G/P14L has a K_a of 26 ($\pm$ 3) x10^3 M^{-1}, similar to that of the complex with PCu Y12G/P14L. The observed $\Delta\delta_{avg}$ in the mutant PCd complex are identical for forty percent of the perturbed residues, while for residues in the vicinity of the metal site and the 'eastern patch' $\Delta\delta_{avg}$ values differ between Pc containing Cu(I) and Cd(II). Similar differences have been observed before for *Ph. laminosum* Cd-substituted Pc in complex with cyt*f*[211] and are most likely caused by the charge difference between the metals. Comparison of $\Delta\delta_{avg}$ or K_a between the wt PCu and PCd complexes was not possible because of experimental limitations (see Materials and Methods).
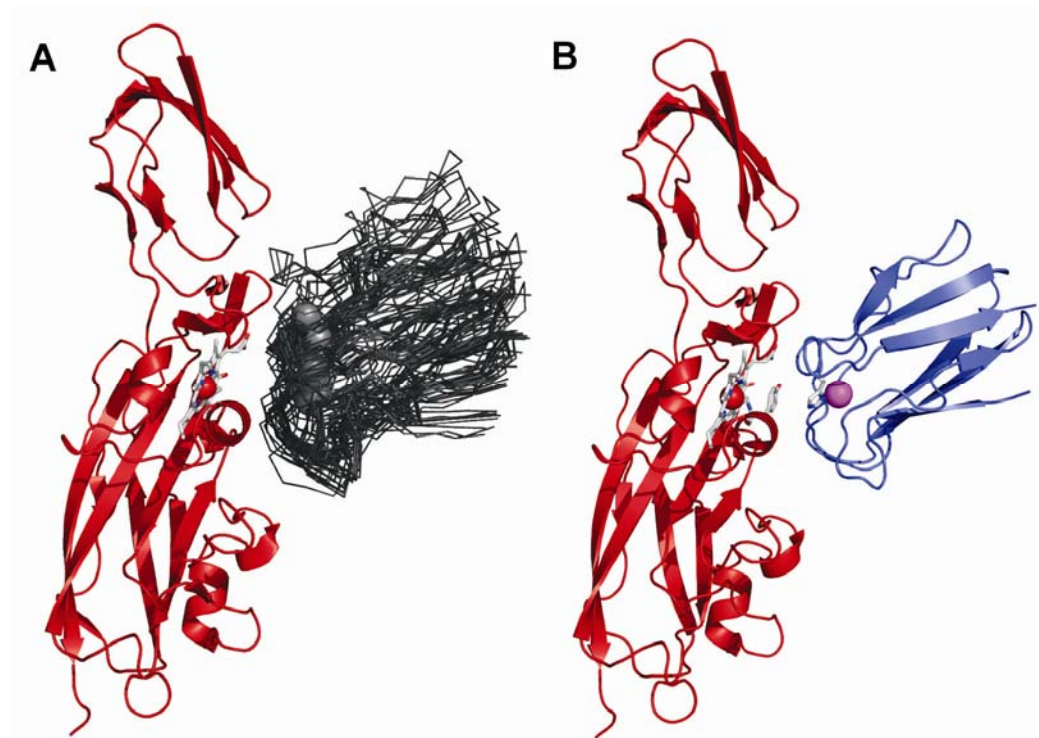
Figure 3.5. Structure of *P. hollandica* Pc – cyt*f* complex. A) Superposition of the 20 lowest energy conformers. Cyt*f* is shown as a red ribbon, the haem as sticks and the Fe ion as a sphere; the backbone of Pc is shown as a black C^{α} trace, with the copper ion as a grey sphere. B) Lowest energy representation, Pc is shown as a blue ribbon, with the Cu ion in magenta. Copper ligand His85 and haem ligand Tyr1 are shown as sticks.

The rigid-body calculations with the restraints summarised in Table 3.1 converge to an ensemble of complexes, which is depicted by an overlay of the twenty lowest energy structures in Fig. 3.5A. The ensemble is characterised by a Cu-Fe distance of 13.4 ± 1.4 Å. The average positional rmsd from the mean structure of the Pc backbone atoms in the 20 lowest energy structures is 4.6 ± 2.7 Å. This variability is mainly due to a relative translational displacement of the Pc on the cyt*f* surface. Violations analysis of both angles and PCS (Fig. 3.6) shows that there is a large degree of variation between the structures. In structure calculations of other Pc - cyt*f* complexes better convergence was observed using similar input[29,30,109]. Therefore, we believe the limited convergence is an indication of real dynamics rather than a lack of sufficient restraints. The observed restraints in this case represent an average that can be approximated by an ensemble of structures. For residues in the loop regions 35-41 and 46-51 of Pc, negative PCS are predicted in part of the structures. This is related to the angle between the nucleus-iron vector and the Fe-

Tyr1 N bond, which exceeds 54.7°, resulting in a sign change of the PCS[42]. Both the rmsd and violations for the ensemble indicate that the *P. hollandica* Pc - cyt*f* complex is much more dynamic than the plant and *Nostoc* sp. PCC 7119 complexes[29,109] and more closely resembles the highly dynamic *Ph. laminosum* complex[40].
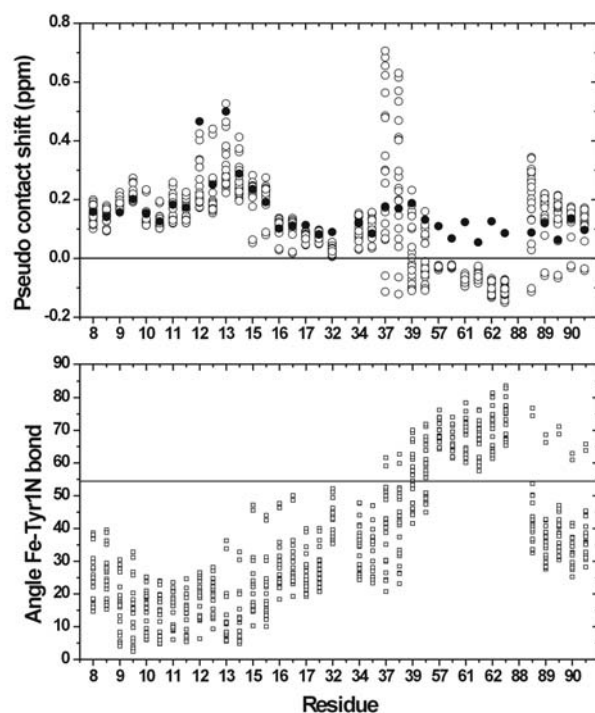
Figure 3.6. Violations for the wild type Pc - cyt*f* complex. The top panel shows the observed PCS (●) and the back-calculated PCS (○) for the backbone amide atoms in the 20 lowest energy structures. For every residue the ^{15}N value is shown (major tick), followed by the ^{1}H value (minor tick). The bottom panel shows the back-calculated angles (□) between the nucleus, the haem iron, and the Tyr1 N atom. Positive PCS are expected to give an angle <54.7° (solid line).

The orientation of wt Pc in the lowest energy *P. hollandica* Pc - cyt*f* complex (Fig. 3.5B) is reminiscent of the orientation found for the *Nostoc* sp. PCC 7119 Pc - cyt*f* complex[109]. The binding interface comprises 15 Pc residues, all located in the hydrophobic patch, including Tyr12 and Pro14. The buried interface area for Pc is calculated to be ~860 Å^2. Similarly, 15 cyt*f* residues and the propionate side chains of the haem contribute to a buried interface area of ~725 Å^2. Although the chemical shift changes in the complex are salt dependent (see earlier) the only charged residues in the interface are Asp63 in cyt*f*, which interacts with Thr58 in Pc and Arg86 in Pc, which could interact with Tyr162 in cyt*f*. Some polar residues are present in the interface, mainly on the cyt*f* side, but clear

electrostatic contributions as seen in the plant and *Nostoc* Pc - cyt*f* complexes are not found. The lack of interaction between the eastern patch on Pc and the small domain of cyt*f* as found in the plant and *Nostoc* sp. PCC 7119 complex could account for the more dynamic nature of the *P. hollandica* complex. Such interactions are lacking in the *Ph. laminosum* Pc - cyt*f* complex, which is also very dynamic. In the lowest energy structure the coupling pathway for electron transfer comprises the haem ligand Tyr1 N and the solvent exposed copper ligand His85. This pathway has also been found in plant Pc - cyt*f* complexes[29,30]. It has to be noted that because of the variation in the ensemble a detailed analysis of electron transfer pathways is not possible.

Dynamics in P. hollandica Y12G/P14L Pc - cytf complex

When the PCS in the wt and Y12G/P14L Pc - cyt*f* complexes are compared a clear decrease in their size for the mutant complex can be observed (Fig. 3.7A), except for the last 10 residues. The decrease in size of chemical shift perturbations (see earlier) and PCS in the mutant complex leads to less and weaker restraints, which in turn cause more possible orientations with similar energies. As a result, rigid-body structure calculations for the *P. hollandica* Y12G/P14L Pc - cyt*f* complex did not lead to any converged ensemble of structures, contrary to the case of the wt complex. The inhomogeneous decrease in PCS and lack of convergence of the calculations can be attributed to a more dynamic nature of the Y12G/P14L Pc - cyt*f* complex.
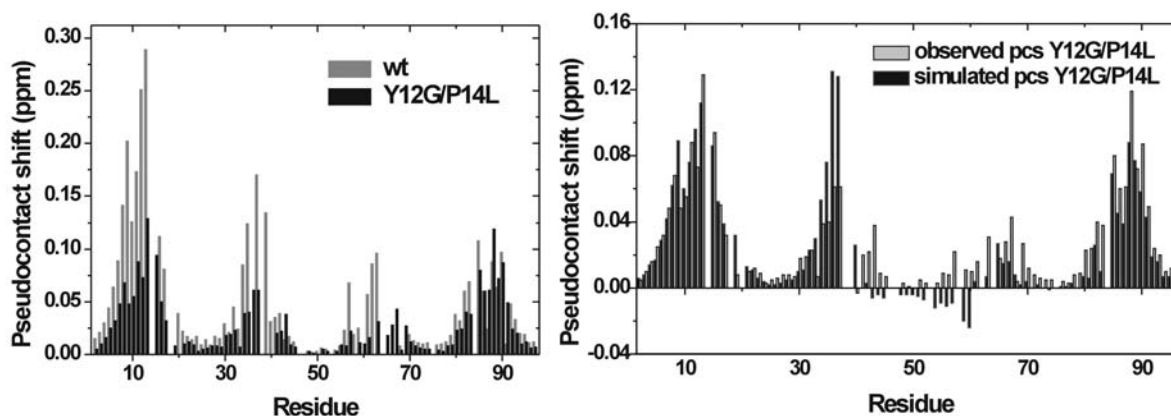
Figure 3.7. A) ^{1}H PCS in wild type and mutant Pc in complex with cyt*f*, B) Observed and simulated ^{1}H PCS in mutant Pc in complex with cyt*f*. The ratio cyt*f* : wt PCd is 1:1.7 and the ratio cyt*f* : Y12G/P14L PCd is 1.2:1.

Simulations were done to determine the degree of movement in the mutant complex sufficient to result in the observed averaged PCS (Fig. 3.7B). The orientation of the lowest energy complex between wt Pc and cyt*f* was used as a starting point. Rotation of Pc around the Fe axis in each direction was analysed, an example for 60º is shown in Figure 3.8. It was concluded that rotation in a single direction does not result in an ensemble of orientations that closely matches the observed and simulated PCS. The effect of rotation around the centre of mass of Pc Y12G/P14L (wobble) of various degrees was analysed as well (Fig. 3.9). This movement clearly affects the overall size of the average PCS. It has to be noted though, that the binding site is localised mostly at the hydrophobic patch. Thus, an ensemble of orientations that results from this movement over the example 180º is unrealistic.
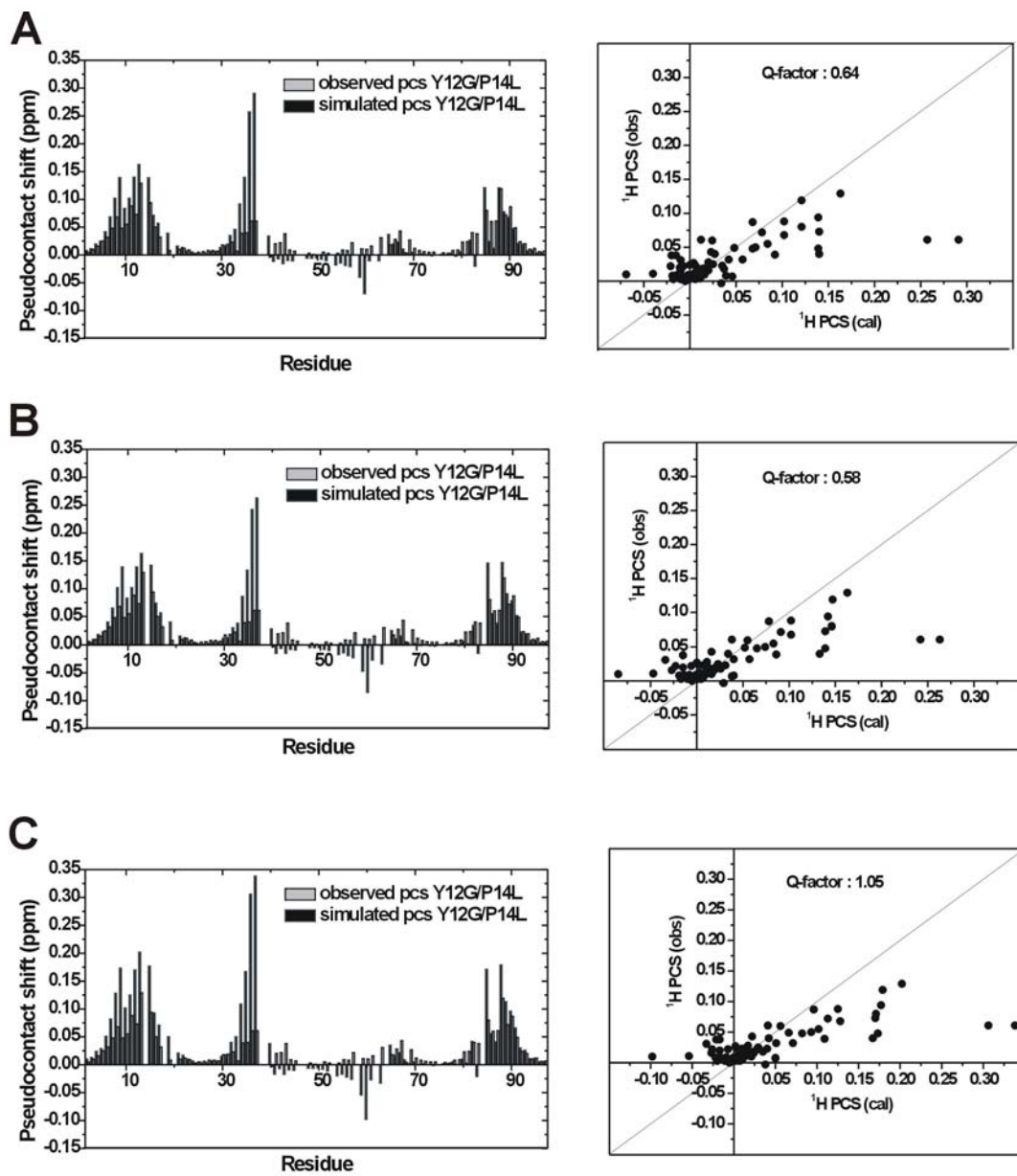
Figure 3.8. Observed and simulated ^{1}H PCS for mutant Pc in complex with cyt*f*. Left panels show the PCS per residue and right panels the correlation between the PCS. Simulations consist of 50 positions rotated over 60º in the A) *x*-, B) *y*-, C) *z*-direction around the Fe-Tyr1 N axis.
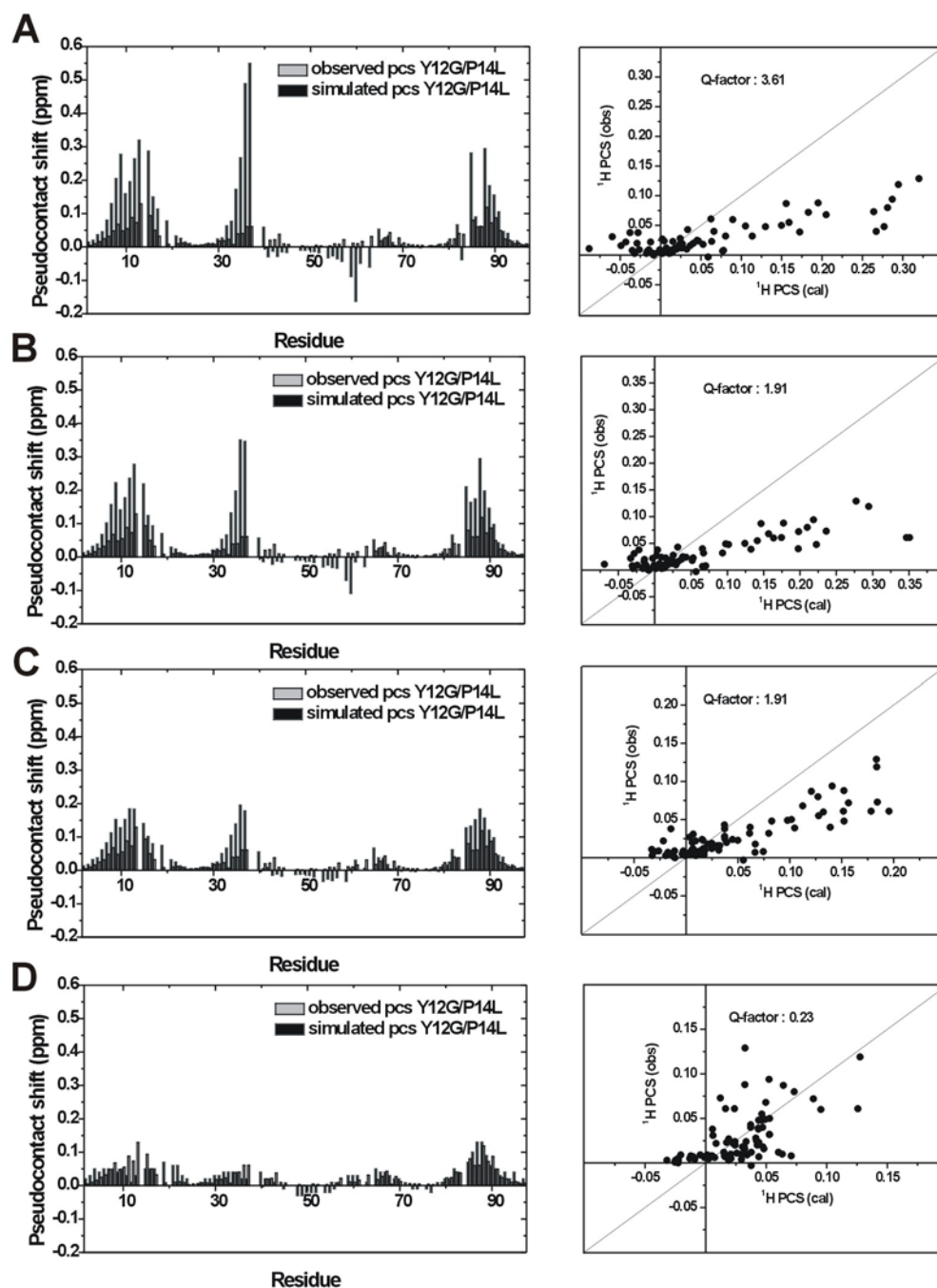
Figure 3.9. Observed and simulated ¹H PCS for mutant Pc in complex with cyt*f*. Left panels show the PCS per residue and right panels the correlation between the PCS. Simulations consist of 50 positions wobbled over A) 10º, B) 45º, C) 90º and 180º in all directions around the centre of mass of Pc.

By trying systematicly combinations of rotation and wobbling, it was found that rotation of Pc around the Fe with amplitudes of 40º, 80º and 35º in the *x*-, *y*- and *z*-direction, respectively, combined with rotation around the centre of mass of Pc Y12G/P14L (wobble) of 60º in all directions results in an ensemble of orientations with average PCS values that closely resemble those observed (Fig. 3.7B). This solution is not unique; there are more combinations of variables that lead to similar results. For example rotation of 60º, 90º, and 45º in the *x*-, *y*- and *z*-direction, respectively, combined with rotation around the centre of mass of Pc Y12G/P14L (wobble) of 60º in all directions was found to result in very similar average PCS and a similar spread in PC positions (Fig. 3.10). Some Pc Y12G/P14L residues have deviating PCS values in all simulations. These residues (33-37 and 57-59) are found in the interface and are also the most violated in the wt structure (Fig. 3.6), which suggests that these deviations are not specific for the Y12G/P14L Pc - cyt*f* complex. It must be noted, however, that residues 33-37 are found to be the most affected by the mutations Y12G/P14L apart from residues neighbouring the mutations[87], perhaps indicating a structural difference in this part of the mutant Pc, as compared to the wt.
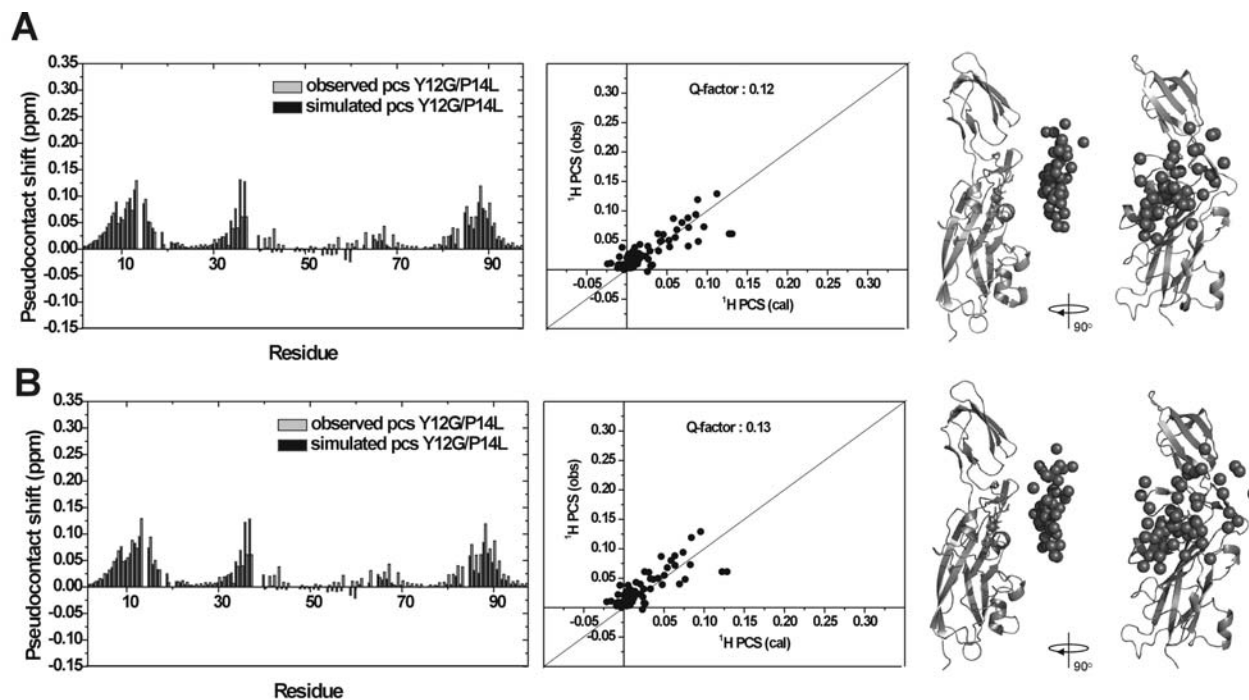
Figure 3.10. Observed and simulated ^{1}H PCS for mutant Pc in complex with cyt*f*. Left panels show the PCS per residue and middle panels the correlation between the PCS. Simulations consist of 50 positions resulting from A) rotation of Pc around the Fe-Tyr1 N axis of 40º, 80º and 35º in the *x*-, *y*- and *z*-direction, respectively, combined with rotation around the center of mass (wobble) of 60º in all directions and B) rotation of Pc around the Fe-Tyr1 N axis of 60º, 90º and 45º in the *x*-, *y*- and *z*-direction, respectively, combined with rotation around the center of mass (wobble) of 50º in all directions. The ensembles created are depicted in the right panels. The 50 positions of the copper atoms in Pc are represented by spheres.

The 50 orientations of Pc Y12G/P14L that result from the simulation mentioned above are visualised in Figure 3.11. From these simulations, it is clear that a considerable range of orientations is sampled in the mutant complex. It also demonstrates that merely the observation of PCS cannot be used as evidence for a well-defined complex.
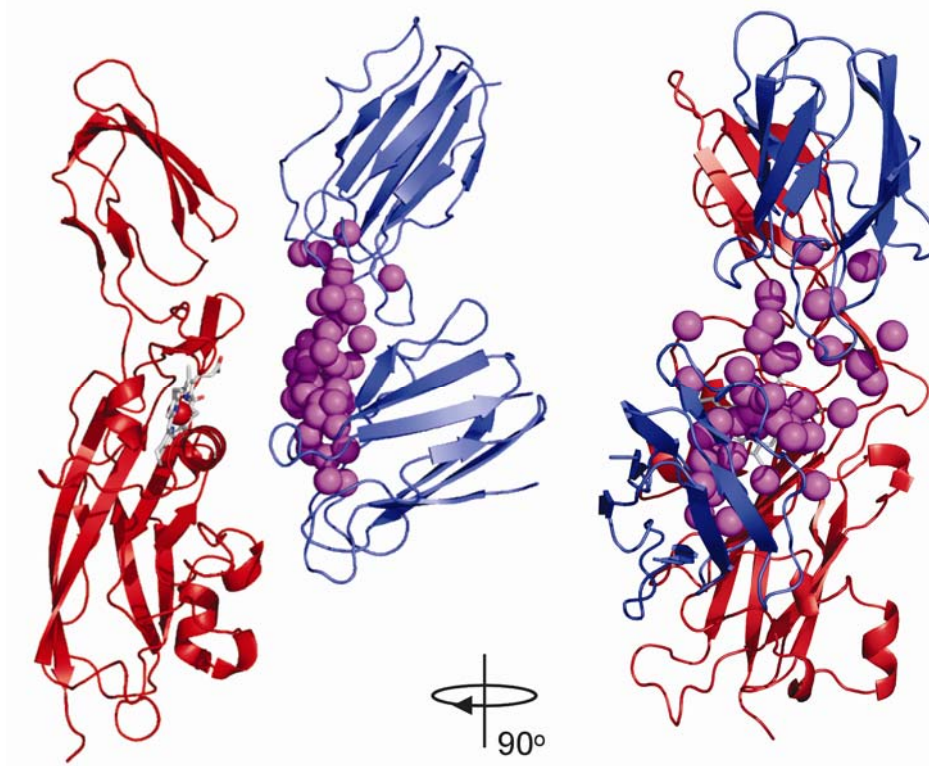
Figure 3.11. Representation of the dynamics in the Pc Y12G/P14L – cyt*f* complex. Cyt*f* is shown as a red ribbon, the haem as sticks and the Fe ion as a sphere. The Cu ion in a set of 50 Pc Y12G/P14L molecules is shown as magenta spheres. The two most extreme orientations of Pc Y12G/P14L are shown as blue ribbons.

The Cu-Fe distances are mostly too large for electron transfer, so only a subset of states will be suitable for electron transfer. Since the wt and mutant complex have similar binding constants and the electron transfer rates to Pc are similar (k_2 = 2-3 x 10^8 M^{-1} s^{-1}; Baranova and Bullerjahn, manuscript in preparation), it provides an example of two complexes that differ mainly in their dynamics.

It can be concluded that the mutation of the two hydrophobic patch residues Tyr12 and Pro14 to the residues found in other plastocyanins, results in a more dynamic complex of Pc and cyt*f*. These mutations provide a way to compare the reasonably well-defined wt Pc - cyt*f* complex with one that is more dynamic, presenting an opportunity to examine the movements and dynamics in the encounter state of a transient protein-protein complex.

Dynamics in the complex of *Nostoc* sp. PCC 7119 cytochrome c_6-cytochrome f

Abstract

The role of electron carrier between cyt*f* and PSI can be carried out by Pc and cytc_6. A docking model for the physiological cytc_6 – cyt*f* complex from *Nostoc* sp. PCC 7119 based on chemical shift perturbations revealed that the orientation of cytc_6 in the complex is similar to the orientation of Pc in the Pc - cyt*f* complex. Additional information from pseudocontact shifts (PCS) and paramagnetic relaxation enhancement (PRE) has been used to investigate the structure and dynamics of this complex. Including PCS data into docking calculations leads to a single structure which has a similar orientation to the structure from chemical shift data only. When PRE from five different spin labels on the surface of cyt*f* are used in docking, single structures are also found, but with different orientations depending on which combination is used. Furthermore, the violations for each of the structures determined remain large, especially for the spin label furthest away from the site of electron transfer. This suggests that the complex is dynamic and cannot be described by a single structure. Simulation of dynamics in the complex by creating an ensemble of structures around the structure determined by chemical shift perturbations and PCS (or by chemical shift perturbations alone) as described in Chapter III did not reduce the violations of the distances derived from PRE. This shows that the complex of cytc_6 and cyt*f* cannot be described by a single model of stochastic excursions from a single structure. Most likely, cytc_6 has multiple preferred orientations.

Introduction

During oxygenic photosynthesis electrons are shuttled between the cytochrome *b$_6$f* complex and PSI by a mobile electron carrier. In plants this role is performed by the copper protein Pc, while in some cyanobacteria and algae cytc$_6$ is produced instead. Other photosynthetic organisms adapt to the copper and iron availability in their environment by producing either of the two proteins[111]. While the complex between Pc and cyt*f* has been well characterised, only a limited amount of studies have been done on the cytc$_6$ - cyt*f* complex. The first clues on the binding characteristics were found in an NMR study on the non-physiological cyanobacterial complex of cyt*f* from *Ph. laminosum* and cytc$_6$ from *Nostoc* sp. PC 7119 (former *A. variabilis*)[136]. This revealed a binding interface typical of electron transfer proteins and suggested it is a well-defined complex. More information on the behaviour of cytc$_6$ in a physiological transient complex comes from its interaction with PSI[212]. It was found that hydrophobic and electrostatic patches, which surround the haem cleft of cytc$_6$, are affected by binding. These patches had been identified before by site-directed mutagenesis studies[213,214]. Recently, a docking model for the physiological cytc$_6$ – cyt*f* complex from *Nostoc* sp. PC 7119 based on chemical shift perturbations was reported[135]. It revealed that the orientation of cytc$_6$ in the complex is reminiscent of the orientation of Pc in the Pc - cyt*f* complex from the same species. As described in Chapter III, and from other recent studies[31,188], additional NMR data such as pseudocontact shifts (PCS) and paramagnetic relaxation enhancement (PRE) can provide insight into the dynamics of transient protein-protein complexes. Here, we describe an attempt to combine these approaches to resolve the dynamics in the *Nostoc* sp. PC 7119 cytc$_6$ – cyt*f* complex.

Materials and Methods

Protein preparation

Uniformly ^{15}N-labelled M58C cytc_6 was kindly provided by Dr. Fernando Molina-Heredia and Prof. Miguel A. De la Rosa (Seville, Spain). *E. coli* cell pellets containing cyt$f$ 'Cys' variants were kindly provided by Michela Finiguerra (Leiden, the Netherlands). Cells were resuspended in the minimal volume of buffer (5 mM TRIS pH 8.0, 3 mM DTT), followed by addition of 5 mg DNase and lysozyme and 1 mM PMSF. Extracts of the harvested cells were obtained through use of the French press cell. Cell debris was removed by ultra-centrifugation at 30.000 rpm after which the supernatant was dialysed against 5 L of 5 mM TRIS pH 8.0, 3 mM DTT for 3 hours and overnight at 4°. Cyt$f$ was purified using ion exchange chromatography with DEAE sepharose (Amersham Biosciences) in 5 mM TRIS pH 8.0, 3 mM DTT. The protein was eluted with a gradient of 0-500 mM NaCl. The fractions containing cyt$f$ were concentrated and size exclusion chromatography was performed with Superdex-G75 (Amersham Pharmacia Biotech) in 5 mM TRIS pH 8.0, 3 mM DTT, 100 mM NaCl. DTT was removed from cyt$f$ solutions by ultrafiltration (Amicon, MW cut-off 10 kDa). The protein was subsequently exchanged to 10 mM NaPi, pH 6.0 and concentrated to ~40 μM. The protein was oxidised by a 100-fold excess of $K_3[Fe(CN)_6]$ and a 10-fold excess of either MTSL or MTS was added. MTSL [(1-oxyl-2,2,5,5-tetramethyl-3-pyrroline-3-methyl)-methanethiosulfonate] and MTS [(1-acetyl-2,2,5,5-tetramethyl-3-pyrroline-3-methyl)-methanethiosulfonate] were purchased from Toronto Research Chemicals (North York, Ontario, Canada) and used without further purification. Stock solutions of 0.1 M MTS(L) in DMSO were used. The protein solution was kept for 2 hours at RT and O/N at 4° after which the excess $K_3[Fe(CN)_6]$ and MTS(L) was removed by ultrafiltration. Modification of cyt$f$ with MTS(L) was confirmed by mass spectroscopy and an estimate of the labelling ratio was made from EPR experiments[31].

NMR experiments

All samples contained 10 mM NaPi, pH 6.0 and 6% D_2O. Protein concentrations were determined by optical spectroscopy using ε_{419} of 85.5 mM⁻¹ cm⁻¹ for M58C cytc_6 and ε_{556} of 31.5 mM⁻¹ cm⁻¹ for reduced cyt$f$ [215]. The pH was adjusted with μL aliquots of 0.1/0.5 M HCl. The concentration of cyt$f$-MTS or cyt$f$-MTSL stock solutions was carefully set to 0.7 mM. Samples contained 0.3 mM ¹⁵N M58C cytc_6 and 0.1 mM cyt$f$-MTS or cyt$f$-MTSL. The diamagnetic and paramagnetic experiments were performed on cytc_6 from the same stock solution. All NMR spectra were recorded at 300 K on a Bruker DMX600 spectrometer equipped with a triple-resonance TCI-ZGRAD ATM Cryoprobe (Bruker, Karlsruhe, Germany). ¹⁵N,¹H HSQC were obtained with spectral widths of 32 ppm (¹⁵N) and 13.5 ppm (¹H) and 1024 and 256 complex points were acquired in the direct and indirect dimension, respectively. Data were processed with AZARA 2.7 [203] and analysed in ANSIG for Windows[204]. Sequence specific assignments of the backbone resonances of M58C cytc_6 were kindly provided by Dr. Irene Díaz-Moreno (Seville, Spain).

Determination of distance restraints (PRE)

From the intensities of the recorded M58C cytc_6 resonances the paramagnetic relaxation enhancement (PRE) effects were calculated using equation 4a [52]:

$$\frac{I_{para}}{I_{dia}} = \frac{R_{2,dia}\exp(-tR_{2,para})}{R_{2,dia} + R_{2\,para}} \quad (4a)$$

where I_{para} and I_{dia} are the intensities of the ¹⁵N M58C cytc_6 peaks in the presence of cyt$f$-MTSL and cyt$f$-MTS, respectively; $R_{2,dia}$ is the transverse relaxation rate of M58C cytc_6 backbone amides in the presence of cyt$f$-MTS ; $R_{2,para}$ is the paramagnetic contribution to the relaxation rate (PRE) and t is the INEPT evolution time of the recorded HSQC (9 ms). For residues of which the resonances disappear from the spectrum, the maximal intensity was estimated from the noise level. These residues were classified in the 'upper limit' distance class for docking calculations (see below).

The $R_{2,dia}$ values were determined from the peaks in the HSQC spectrum of M58C cytc_6 in the presence of cyt$f$-MTS. For this purpose the FIDs were zero-filled up to 2048 and

512 complex points in the direct and indirect dimension, respectively. The resulting FIDs were multiplied with a 2 Hz line-broadening single exponential window function in the ^{1}H dimension. The width at half-height ($\Delta v_{1/2}$) of each peak was determined from a Lorentzian fit performed in the program MestRe-C 4.8.6.0 (Mestrelab Research S.L., Santiago de Compostela, Spain). After correction for artificial line-broadening the $R_{2,dia}$ was calculated ($R_{2,dia} = \pi \Delta v_{1/2}$) and converted into distances using equation 4b [52]:

$$r = \sqrt[6]{\frac{\gamma^2 g^2 \beta^2 \tau_c}{20 R_{2,para}} \left(4 + \frac{3}{1 + \omega_h^2 \tau_c^2} \right)} \qquad (4b)$$

where r is the distance of the amide proton in M58C cytc_6 to the spin label (attached to cyt$f$); γ is the gyromagnetic ratio of ^{1}H; g is electronic g-factor; β is the Bohr magneton; ω_h is the ^{1}H Larmor frequency and τ_c is the correlation time of the electron-nucleus vector. The τ_c values used for the five positions of the MTSL on cyt$f$ were 6 ns for Q7C, 14 ns for A63C, 6 ns for N71C, 3 ns for Q104C and 7 ns for S192C. These values were derived from EPR spectra on the cyt$f$ – cytc_6 complexes and were kindly provided by Francesco Scarpelli and Dr. Martina Huber (Leiden, the Netherlands).

From the K_a of $(6.5 \pm 0.7) \times 10^3$ M^{-1} it was calculated that the fraction bound in the NMR samples with 1:1 stoichiometry of cytc_6 – cyt$f$ is 25%. The $R_{2,para}$ was multiplied with a factor of 1/0.25 because the observed PRE's represent this fraction of the total PRE. The distances calculated from the PRE were divided into three classes. The resonances that disappeared from the spectrum were included in an upper limit restraint class. Resonances that experienced an intensity change of less than 10% were included in a minimal distance restraint class (lower limit). A two-bounds class included the resonances that experience more than 10% of intensity change, but are still observed. A summary of the restraints is given in Table 4.1.

Table 4.1. Number of distance restraints for each spin label on cyt*f*.

Spin label	Upper bound	Lower bound	2-bound	Total
Q7C	2	54	34	90
A63C	10	49	29	88
N71C	11	38	40	89
Q104C	10	53	25	88
S192C	2	67	18	87

Docking with PRE restraints

The XRD structure of M58C cyt*c$_6$* was determined by Dr. Navraj Pannu and Prof. Jan Pieter Abrahams (Leiden, the Netherlands) from crystals prepared by Davide Cavazzini and Prof. Gian Luigi Rossi (Parma, Italy). Coordinates of cyt*f* from a previously described homology model[109] were used. Modifications of the model in order to add the MTSL atoms were performed by Dr. Alexander N. Volkov (Louvain-la-Neuve, Belgium) as described[31]. The five cysteine surface mutations were introduced *in silico* and four orientations representative of all sterically allowed orientations per MTSL spin label were added to account for its mobility[55]. Docking of M58C cyt*c$_6$* onto cyt*f* was done using restrained rigid body molecular dynamics in XPLOR-NIH 2.9.9 [208]. The coordinates of cyt*f* were fixed, while M58C cyt*c$_6$* was placed at a random position and allowed to move under the forces of restraints and a van der Waals repel function. The restraint for a particular residue was defined as the r^{-6} averaged distance between the O atoms of the representative spin label orientations and the amide protons.

Dynamics simulations

Dynamics in the M58C cyt*c$_6$* – cyt*f* complex was simulated in XPLOR-NIH 2.9.9 [208] as described in Chapter III [216]. The initial orientation of the complex was identical to either the published structure determined by docking with restraints derived from chemical shift changes[135] only, or the structure determined by docking with restraints from both chemical shift changes and PCS. Both the structures and PCS data for comparison were kindly provided by Dr. Irene Díaz-Moreno (Seville, Spain).

Results and Discussion

Paramagnetic effects in the ^{15}N M58C cytc$_6$ – cytf-MTSL complex

To characterise the dynamics in the physiological complex between cytc_6 and cyt$f$ from cyanobacterium *Nostoc* sp. PCC 7119 a series of paramagnetic spin labels was attached to cyt$f$. For this purpose five surface-exposed cyt$f$ residues were singly mutated to cysteines (Finiguerra M.G. *et al.*, in preparation), to which a thiol-specific paramagnetic spin label (MTSL) was subsequently connected. The selected positions of the spin labels on the surface of cyt$f$ are close to the haem, the site of electron transfer, except S192C, which is positioned on the small domain of cyt$f$ (Fig. 4.1).
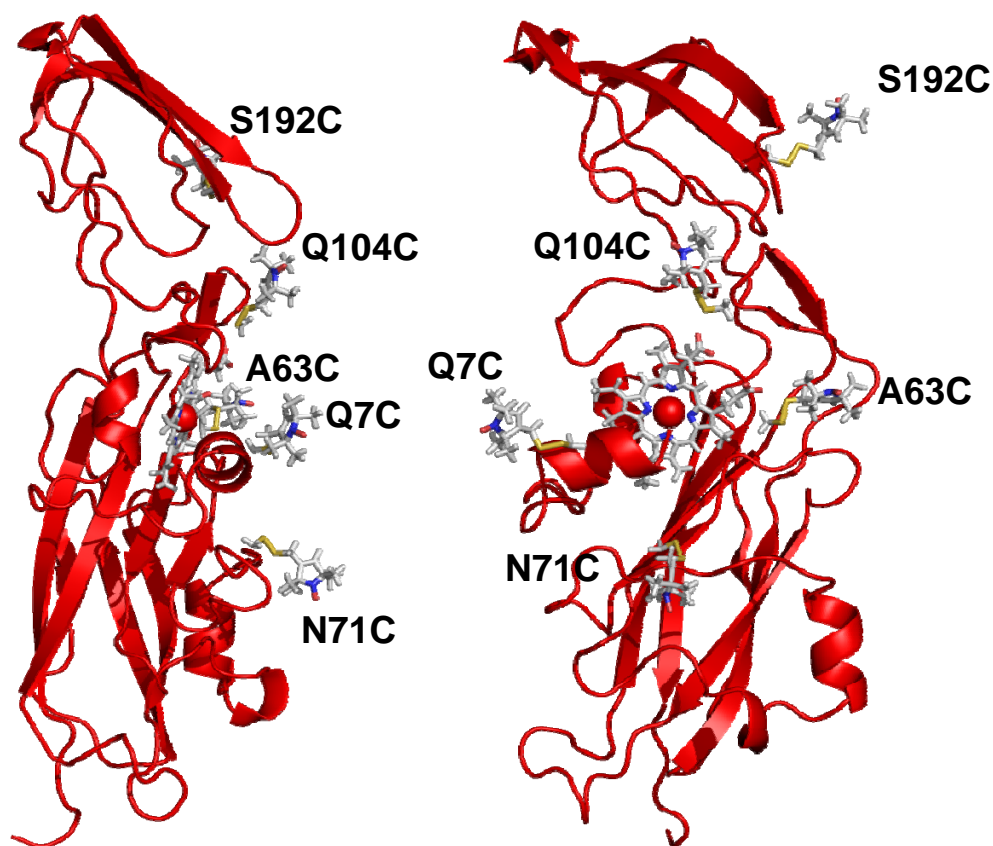
Figure 4.1. Positions of the MTSL spin labels on cyt$f$. The molecule on the right has been rotated over 90° relative to the one on the left.

The spin labels were attached to cyt*f* in order to induce an intermolecular paramagnetic relaxation enhancement (PRE) on amide nuclei of ^{15}N-M58C cytc_6. Cytc_6 is prone to autoreduction, which can lead to spin label reduction. Therefore, the M58C mutant variant of cytc_6 was used. Replacement of the Met58 Fe ligand with Cys causes a reduction of the midpoint potential of several hundred mV, yielding a variant with a midpoint potential of +265 mV (Dr. Lange, personal communication), that does not show any autoreduction. XRD analysis of wt and M58C cytc_6 showed that the crystal structures are almost identical with rmsd values of 0.16 and 0.23 Å for backbone and all heavy atoms (Dr. Pannu, personal communication).
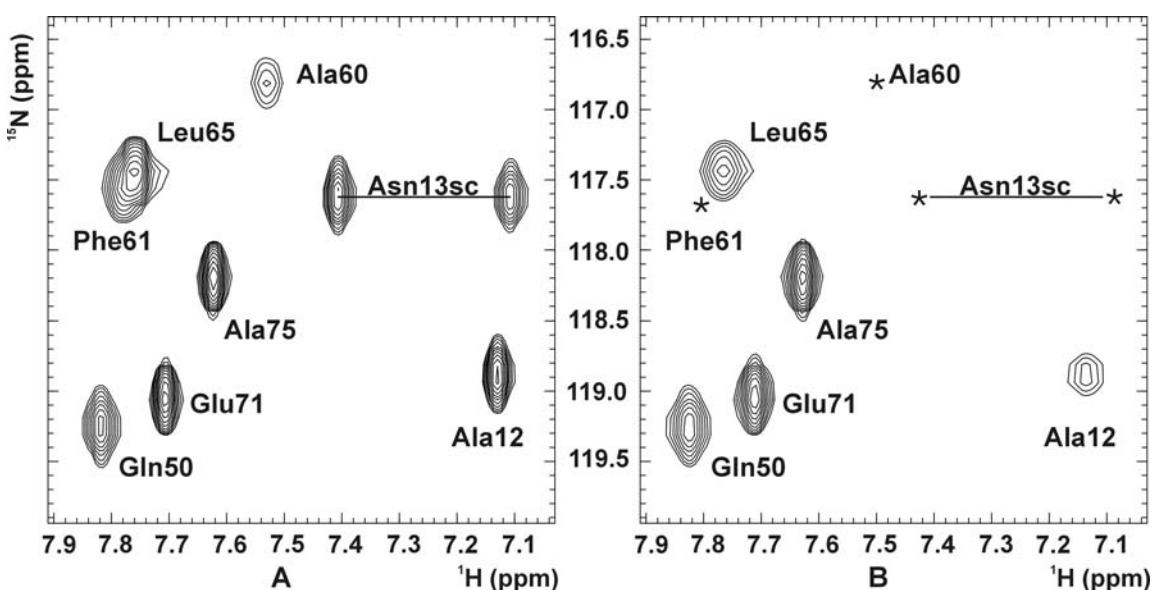
Figure 4.2. Part of the ^{1}H-^{15}N-HSQC spectrum of M58C cytc_6 in the presence of Q104C cyt*f* modified with A) diamagnetic spin label and B) paramagnetic spin label. The ratio ^{15}N M58C cytc_6 : cyt*f* is 3:1. Asterisks denote the position of peaks in A), which are no longer observed in B).

In five separate experiments the effect of paramagnetically labelled cyt*f* on the ^{1}H-^{15}N HSQC spectrum of ^{15}N-M58C cytc_6 was compared to the effect of diamagnetically labelled cyt*f*. When, for example, Q104C-cyt*f* is introduced a number of resonances in ^{15}N-M58C cytc_6 broaden out and several disappear entirely from the spectrum (Fig. 4.2). These effects are observed in the presence of the other four cyt*f* mutants as well. To ensure the labels themselves do not interfere with binding of cyt*f* to ^{15}N M58C cytc_6 the ^{1}H chemical shift changes brought about by the cyt*f*-MTS mutants are compared with the

^{1}H chemical shift changes in the unlabelled complex (Fig. 4.3). A similar pattern of chemical shift changes is observed for the unlabelled and MTS-labelled complexes, although small variations are noticeable. General scaling differences represent small differences in fractions bound between experiments with spin labelled cyt*f*. These were taken into account by the use of a scaling factor in docking calculations (see below).
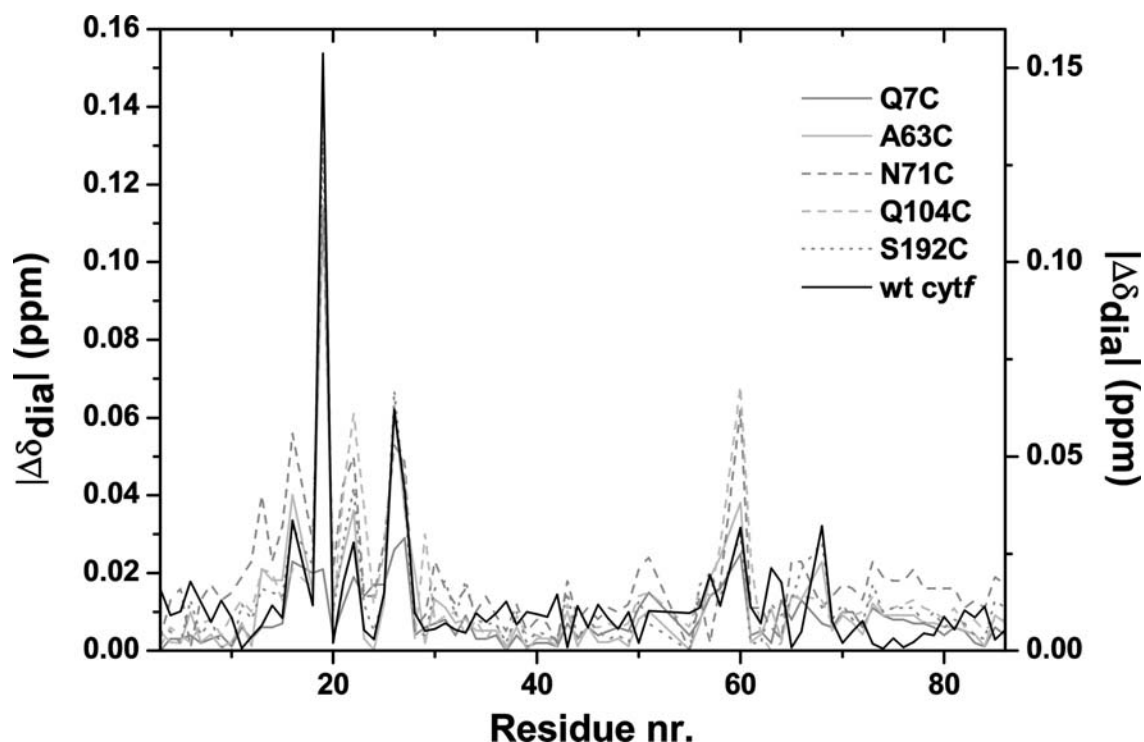
Figure 4.3. ^{1}H chemical shift changes observed at 3:1 ^{15}N M58C cyt*c$_6$*: cyt*f*-MTS for all five cyt*f* mutants (left y-axis) and for the 1:3 ^{15}N M58C cyt*c$_6$* : cyt*f* complex (right y-axis).

It can be concluded that the observed changes in intensity are caused by an increase in the relaxation rate ($R_{2, para}$) of the affected protons, due to their proximity to the unpaired electrons of MTSL. PRE effects are distance dependent and they were converted into five sets of restraints for docking. Rigid-body calculations with all possible combinations of three pairs of these sets have been performed. It was observed that all these runs converge strongly towards a single structure. Also, when all five sets of restraints together were used a single structure is found.
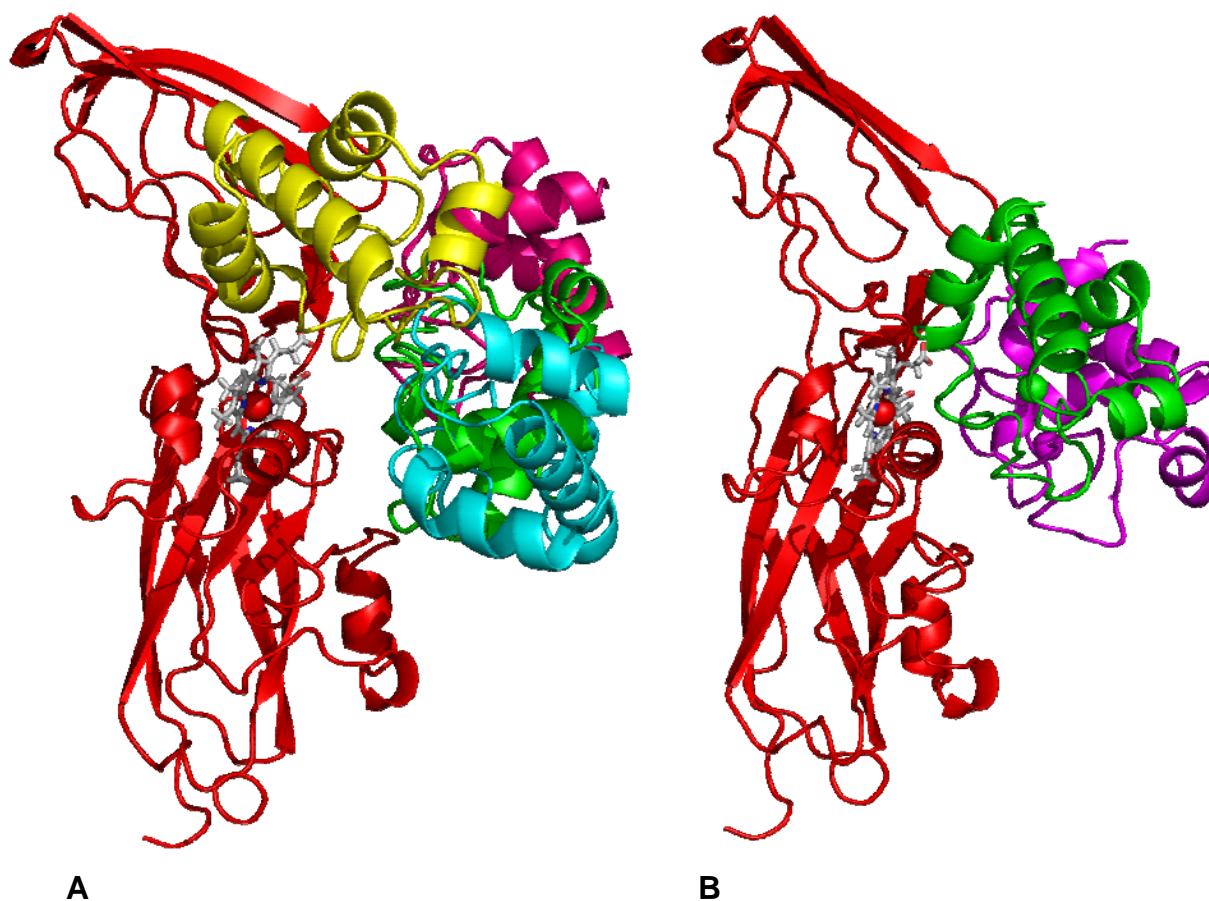
Figure 4.4. A) Overlay of structures of the M58C cyt*c$_6$* - cyt*f* complex determined by docking with distance restraints from all five spin labels (green), spin labels Q7C, A63C and Q104C (cyan), Q7C, A63C and S192C (yellow) and A63C, N71C and S192C (pink). B) Overlay of the structures determined with chemical shifts perturbation data as restraints (magenta) and chemical shifts perturbation data and PCS as restraints (dark green).

From an overlay of several of these structures (Fig. 4.4A), it is evident that the positions and orientations of cyt*c$_6$* to cyt*f* diverge remarkably between the different spin label sets used. This can also be concluded from the violations summarised in Table 4.2. The spin labels corresponding to the sets of restraints that are not used in a particular docking show a higher number of violated residues and a larger average distance violation. When all five sets of restraints are used, the average distance violations are more evenly distributed over the restraints sets. The spin label attached to S192C on cyt*f*, furthest away from the haem, generally has high average distance violations from a relatively

small number of violated residues. The observations from docking with PRE derived restraints suggest it is not possible to meet all restraints in a single structure. Similarly, the previously published structure determined by docking with chemical shift data[135] and a structure previously determined by docking with chemical shift perturbation and PCS data together (Fig. 4.4B) (Dr. Irene Díaz-Moreno, personal communication) demonstrate the variability in results obtained from docking with various types of NMR data. When all these NMR data are considered it is likely that dynamics play a role in complex formation between cytc_6 and cyt$f$.

Table 4.2. Statistics on distance violations for the lowest energy structures of M58C cytc_6 – cyt$f$-MTSL complexes from docking with restraints from all 5 spin labels (5SL) and all combinations of 3 spin labels (numbers indicate position of spin label on cyt$f$). The number of violated residues (Nr.) and the average distance violation (Av.) are shown for each spin label (SL). The statistics for spin labels which were excluded from a particular combination are shown in bold.

Docking:	5SL		7/63/71		7/63/104		7/63/192		7/71/104		7/71/192	
SL	Nr.	Av.	Nr.	Av.	Nr.	Av.	Nr.	Av.	Nr.	Av.	Nr.	Av.
Q7C	23	5.7	20	5.5	18	2.5	26	3.8	21	3.3	29	5.1
A63C	38	2.1	18	2.7	30	2.5	28	3.1	**46**	**4.5**	**65**	**5.3**
N71C	32	2.0	15	3.6	**32**	**7.0**	**39**	**8.1**	36	3.0	25	3.2
Q104C	34	4.8	**35**	**4.4**	23	3.3	**24**	**10.7**	23	3.3	**26**	**8.2**
S192C	12	9.4	**12**	**13.1**	**14**	**16.6**	12	9.8	**11**	**14.9**	12	5.5
Total	139	4.8	100	5.9	117	6.4	129	7.1	137	5.8	157	5.5

Docking:	7/104/192		63/71/104		63/71/192		63/104/192		71/104/192	
SL	Nr.	Av.	Nr.	Av.	Nr.	Av.	Nr.	Av.	Nr.	Av.
Q7C	20	3.2	**30**	**5.1**	**26**	**13.7**	**19**	**8.4**	**36**	**6.1**
A63C	**60**	**5.7**	21	2.2	23	2.9	22	2.1	**60**	**6.0**
N71C	**49**	**5.6**	26	3.0	32	2.1	**27**	**2.0**	12	2.8
Q104C	20	6.2	43	3.9	**26**	**13.2**	23	6.2	29	5.0
S192C	20	5.6	**12**	**13.7**	10	5.1	12	8.1	14	6.7
Total	169	5.3	132	5.6	117	7.4	103	5.4	151	5.3
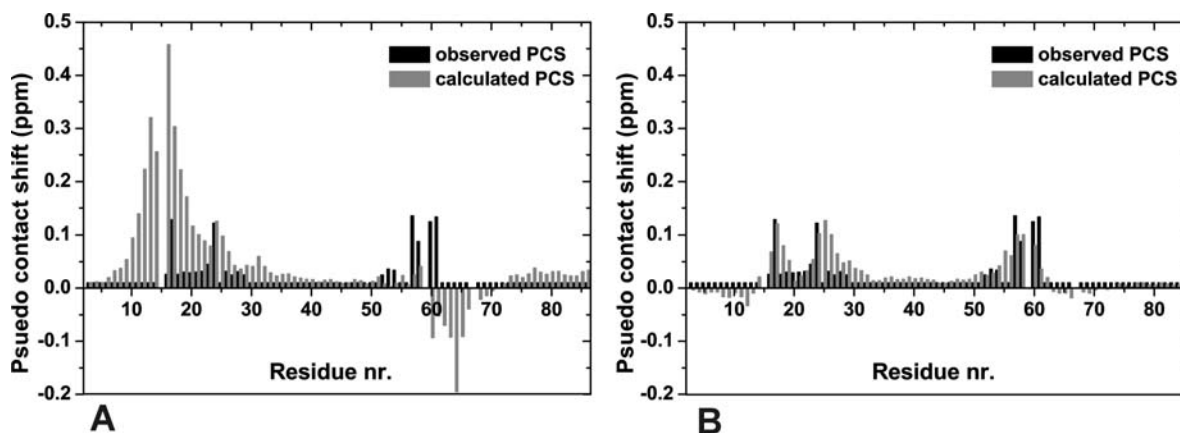
Figure 4.5. Observed and calculated ^{1}H PCS for the structure of the M58C cytc_6 – cyt$f$ complex determined with A) chemical shifts perturbation data as restraints and B) chemical shifts perturbation data and PCS as restraints. All non-significant PCS are indicated with a bar of 0.01 ppm.

Dynamics simulations

When the PCS are back-calculated for both structures in Figure 4.4B and compared to the observed PCS it is clear that the PCS data improve the structure of the cytc_6 - cyt$f$ complex (Fig. 4.5). In order to determine if increased dynamics in the M58C cytc_6 - cyt$f$ complex can result in both the observed PCS and PRE simultaneously, simulations were performed. For comparison, the orientation of the protein in the structure based on chemical shift data[135] and the structure based on chemical shift and PCS data together were used as a starting point.
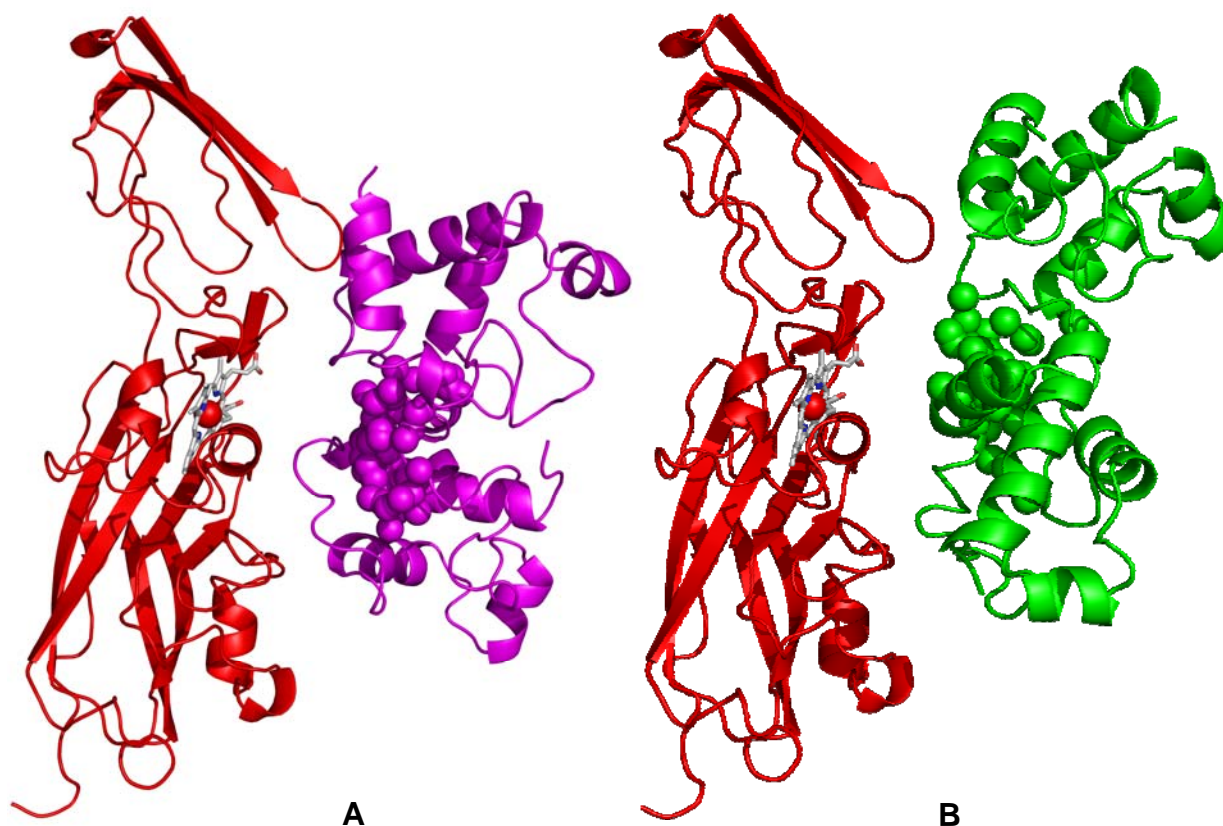
Figure 4.6. Representation of the dynamics in the M58C cytc_6 – cyt$f$ complex. The starting position for the random rotations is found by A) docking with chemical shift changes or B) docking with chemical shift changes and PCS. The Fe in a set of fifty M58C cytc_6 molecules is shown as A) magenta or B) green spheres. The two most extreme orientations of M58C cytc_6 are shown as ribbons. Cyt$f$ is shown as a red ribbon with the haem in sticks and the Fe ion as a sphere.

Random rotation of M58C cytc_6 around the Fe-Tyr1 N axis within the range of 30º, 30º and 90º in the x-, y- and z-direction, respectively, combined with random rotation around the centre of mass of M58C cytc_6 (wobble) of up to 60º in all directions (Fig. 4.6) was found to be in best agreement with the observed data. As shown in Chapter III, these simulations cannot determine which set of variables represents the actual movements found in the complex, but give an indication of the minimal amplitude. PCS violation analysis of the averaged PCS in the simulated ensemble of 50 positions indicates that when the structure determined with PCS data is used as starting position for the random rotations, the averaged PCS match quite well the observed PCS (Fig. 4.7). However, comparison with PCS calculated from the single orientation structure (Fig. 4.5B) shows that this way of creating an ensemble does not improve the match between observed and

calculated PCS in the ensemble. When the structure determined with just chemical shift data is considered the averaged PCS deviate, especially for the first twenty residues. The binding interface in both structures is similar, but the PCS probably refine the orientation of cytc_6 towards the haem in cyt$f$.
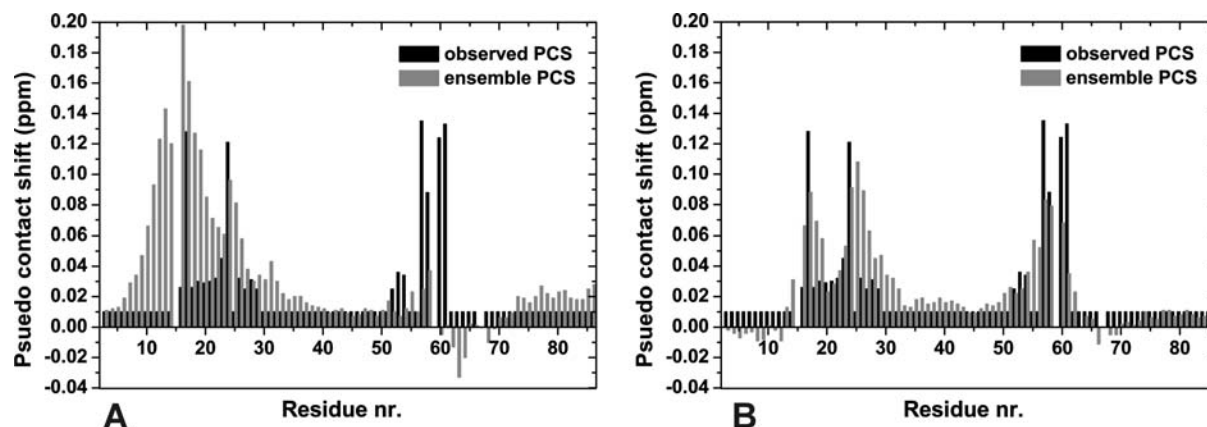
Figure 4.7. Observed and averaged, simulated ^{1}H PCS for the ensemble generated around the structure of the M58C cytc_6 – cyt$f$ complex determined with A) chemical shifts perturbation data as restraints and B) chemical shifts perturbation data and PCS as restraints. All non-significant PCS are indicated with a bar of 0.01 ppm
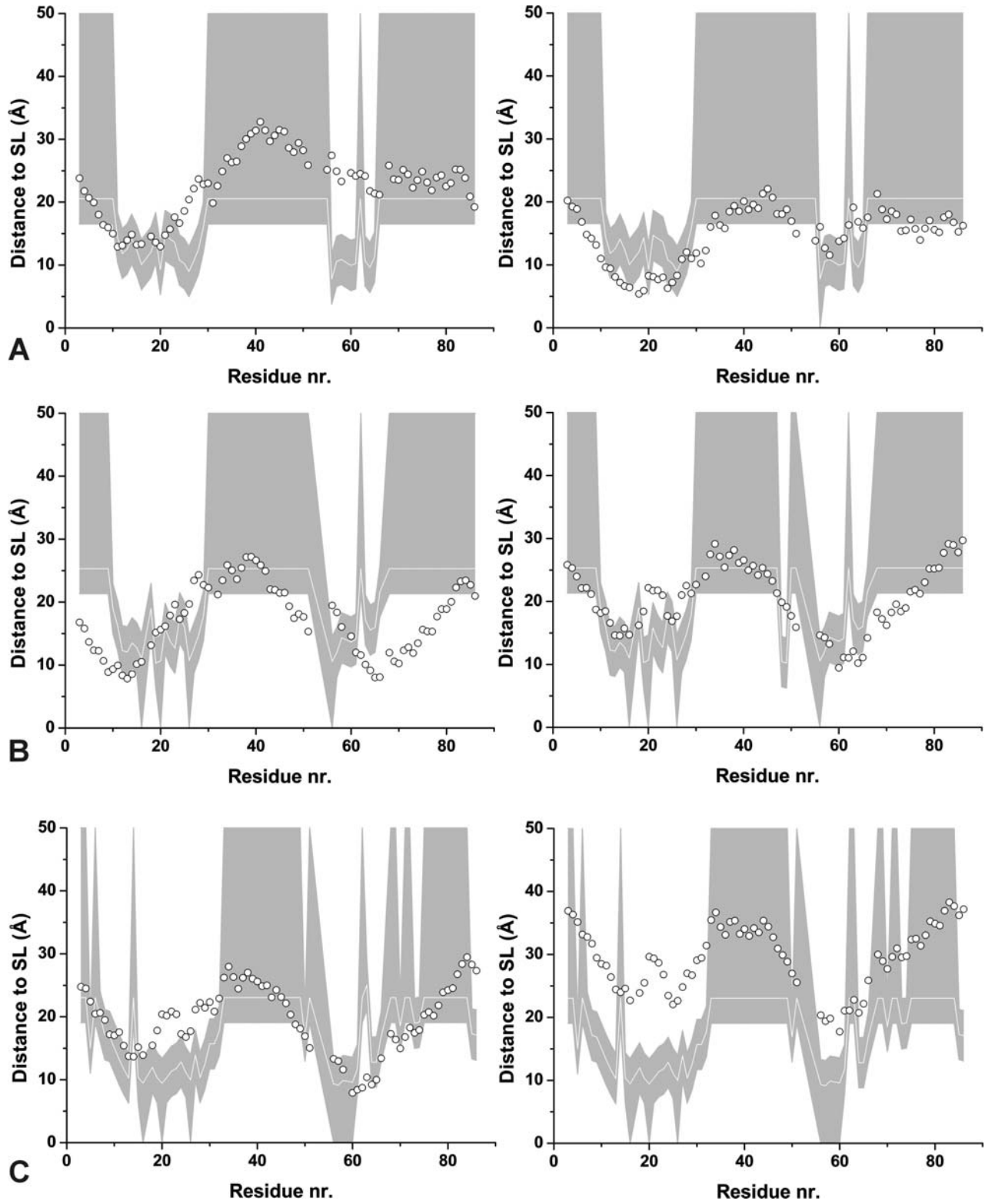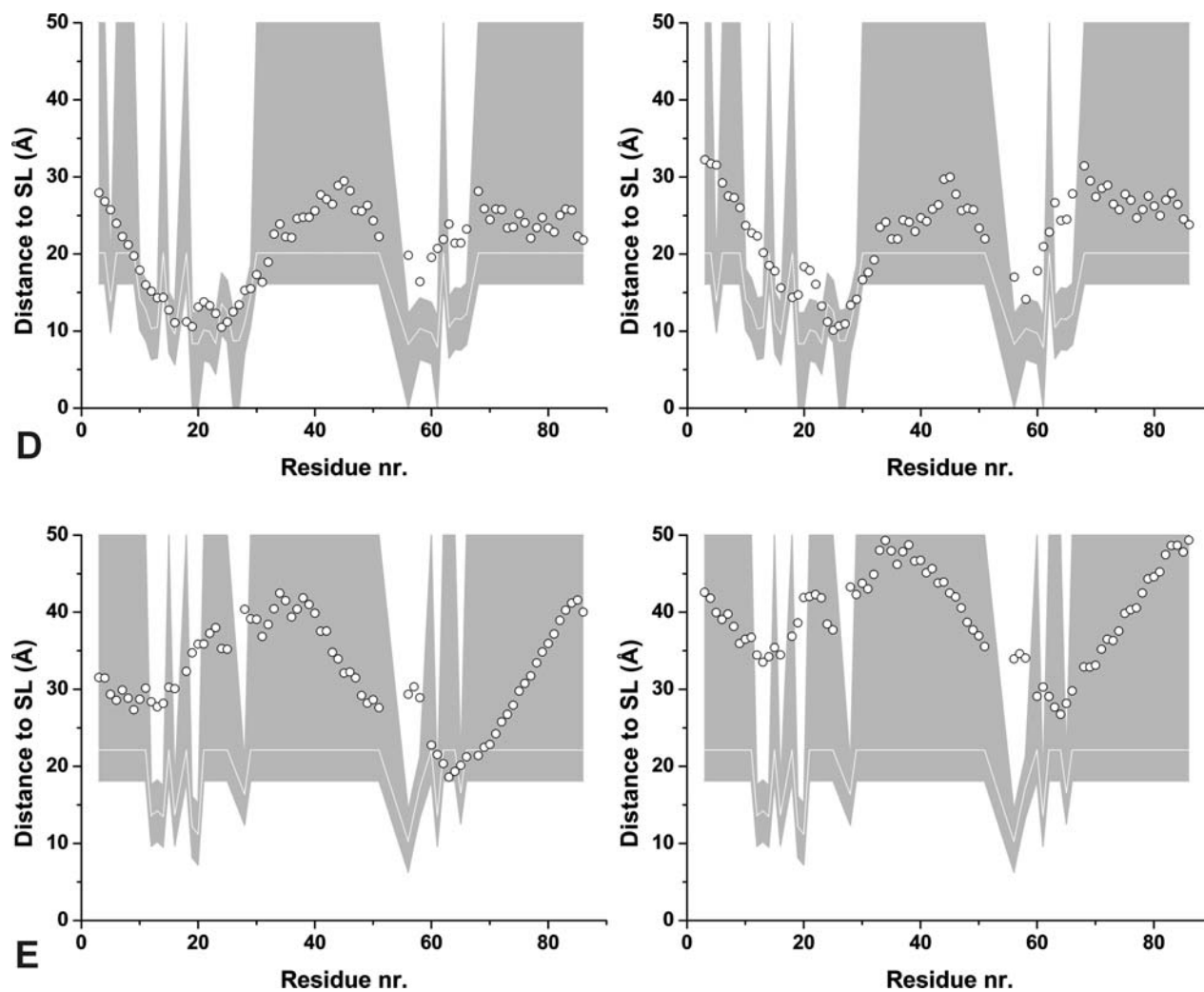
Figure 4.8. Ensemble averaged distances of residues in M58C cytc_6 to spin label at A) Q7C, B) A63C, C) N71C, D) Q104C and E) S192C on cyt$f$. On the left of every panel the ensemble with random rotations around the position of M58C cytc_6 found by docking with chemical shift changes and on the right the ensemble around the position found by docking with chemical shift changes and PCS. The grey area represents the allowed area for each residue and the white line the experimentally determined, PRE-derived distances used as input in docking. Open circles denote r^{-6} averaged distances for an ensemble of 50 structures.

Violations of distances derived from PRE for all five spin label positions are shown for the two ensembles created around the two starting structures (Fig. 4.8). These violations remain large (Table 4.3), indicating that the simple model used here to simulate movement in the complex does not account for all PRE effects observed. This is most obvious for the spin label S192C, furthest away from the haem. For both starting structures, when the S192C spin label is considered, only a few residues are actually violated but the average violation distance is notably larger than for the other spin labels. This indicates that cytc_6 spends more time close to this spin label than simulated here. It is concluded that the ensemble must have an uneven distribution, with certain preferred orientations. The approach to create an ensemble of randomly rotated orientations based on a single starting position appears unsuitable to sample all the dynamics in this complex, contrary to what was found for the Pc - cyt*f* complex of *P. hollandica* (Chapter III).

Table 4.3. Statistics on distance violations for simulated ensemble of cytc_6 – cyt*f* complexes. The total number of restraints is shown in parenthesis.

Spin label	**Chem. shift based structure**		**Chem. shift and PCS based structure**	
	Nr. of violated residues	Avg. violation (Å)	Nr. of violated residues	Avg. violation (Å)
Q7C	17 (90)	6.6	38 (90)	1.6
A63C	28 (88)	3.1	31 (88)	3.2
N71C	30 (89)	3.7	38 (89)	7.5
Q104C	15 (88)	4.6	20 (88)	5.8
S192C	12 (87)	14.1	12 (87)	17.3
Total	102 (442)	6.4	139 (442)	7.1

Interaction of *Silene pratensis* plastocyanin with lysine peptides studied by NMR

Abstract

Charged peptides of lysine residues have been used to study the role of electrostatics in protein-protein association. It was shown they inhibit the electron transfer between *S. pratensis* Pc and cyt*f*. In order to study this interaction with NMR ^{15}N-labelled *S. pratensis* Pc was produced and its backbone amides were assigned. The association constant for the interaction between tetra-Lys and *S. pratensis* Pc of 5 (± 2) x10^3 M^{-1}, determined by NMR, is found to be similar to the one previously determined. As expected, the chemical shift perturbation map shows that the negatively charged patches on Pc are affected by binding of tetra-Lys. Surprisingly, the amount of affected residues and the size of the chemical shift changes indicate the complex between tetra-Lys and Pc is relatively dynamic.

To include apolar interactions, several hydrophobic residues were added to the peptide. The association constant between this peptide and Pc is found to be 6 (± 2) x10^3 M^{-1}. Apparently the addition of hydrophobic residues does not significantly change the binding. The chemical shift perturbations map shows similar binding to Pc as well, supporting the idea that surfaces of electron transfer proteins are designed to interact weakly but specifically with their partners.

Introduction

Transient protein complexes formation can be described in a two step model (Fig. 1.1). The free proteins associate to form a short-lived, dynamic encounter complex, which is in equilibrium with a well-defined complex. Electrostatic interactions are involved in the initial association step and influence the orientation of the proteins in the complex[18]. Charged peptides can be useful to investigate the molecular interaction and recognition between proteins[217,218]. For example, it was discovered that lysine peptides inhibit electron transfer between *S. pratensis* Pc and cyt*f* as well as between Pc and cytochrome *c*[219], demonstrating that they can serve as models for interaction.

Pc from plants contains negatively charged patches which serve as recognition sites for positively charged residues on cyt*f*[29,30]. In the cyanobacterial *Nostoc* sp. 7119 Pc - cyt*f* complex the charges are reversed, but the patches are similarly positioned[41,215]. The Pc - cyt*f* complex from cyanobacterium *Ph. laminosum*, however, does not show these charged patches and is found to be more dynamic than the other complexes[40]. Yet, electrostatics do influence the overall reaction rate between *Ph. laminosum* Pc and cyt*f* [131].

Peptides of various numbers of consecutive lysines show binding to *S. pratensis* Pc, of which tetra-Lys was found to inhibit electron transfer most effectively. A recent study to compare the distribution of lysines revealed that the tetra-Lys peptide, with a uniform distribution of Lys, is most efficient in binding to *S. pratensis* Pc[220] (Fig. 5.1A).

Apart from electrostatics a major part of transient protein-protein associations is dependent on hydrophobic interactions, in particular in the formation of the final, active complex. Electron transfer between Pc and cyt*f* takes place through a copper coordinating histidine located in a hydrophobic patch. We combined both aspects in one peptide by adding hydrophobic residues to four lysines, connected by a flexible stretch of glycine and serine resulting in the KKKKGSGSMFIQ peptide (Fig. 5.1B). The interaction of both tetra-Lys and this peptide with ^{15}N labelled *S. pratensis* Pc was studied by NMR. The effects of the added hydrophobic residues on the binding constant and binding map were compared.
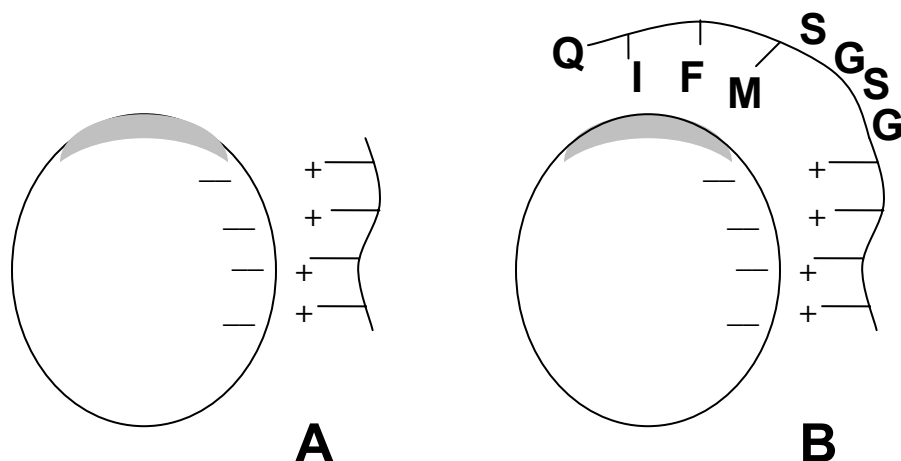
Figure 5.1. Schematic representation of the interaction between *S. pratensis* Pc and peptides A) tetra-Lys and B) KKKKGSGSMFIQ. The hydrophobic patch on Pc is shown as a grey area.

Materials and Methods

Protein expression & purification

For the production of *S. pratensis* ^{15}N-Pc competent BL21 *E. coli* cells were transformed with the pETiPc plasmid[221], which was kindly provided by Prof. Shun Hirota (Nagoya, Japan). The cells were incubated overnight at 37° on a LB/Amp (0.1 g/L ampicillin) plate. A single colony was inoculated in 10 mL LB/Amp medium and incubated overnight at 37°, shaking at 250 rpm. Five mL of the pre-culture was inoculated in 0.5 L M9 minimal medium[222] supplemented with 0.3 g/L [15]NH$_4$Cl and 0.1 g/L ampicillin in a 2L flask. For additional ^{13}C labelling the minimal medium was supplemented with1 g/L ^{13}C-glucose. The cultures were grown at 37°, shaking at 250 rpm to an OD$_{600}$ of 0.7 before induction with 1 mM IPTG. At the same time the temperature was lowered to 30° and growth was continued overnight before harvesting. A periplasmic extract of the harvested cells was obtained by cold osmotic shock. Oxidised Pc was purified using ion exchange chromatography with DEAE sepharose (Amersham Biosciences) in 10 mM potassium phosphate pH 7.0. Pc was eluted with a gradient of 0-500 mM NaCl. The fractions containing Pc were concentrated and size exclusion chromatography was

performed with Superdex-G75 (Amersham Pharmacia Biotech) in 10 mM potassium phosphate pH 7.0, 100 mM NaCl. Pc was oxidised with potassium ferricyanide and reduced with sodium ascorbate. Protein concentrations were determined by optical spectroscopy using $\varepsilon_{597} = 4.5$ mM^{-1} for oxidised Pc[221]. The protein was considered pure when $A_{278}/A_{597} \leq 1.2$ [223]. The yield of pure ^{15}N-Pc after purification was 5 mg/L.

NMR samples

Pc was concentrated by ultra filtration (Amicon, MW cut-off 5 kDa). Samples for peptide titration contained 0.2 mM of reduced ^{15}N-Pc protein in 10 mM sodium phosphate, pH 7.0, 6% D$_2$O and 2 mM sodium ascorbate. The sample for assignment of the backbone amide resonances consisted of 2 mM ^{13}C/^{15}N labelled protein in 10 mM potassium phosphate, pH 6.7, 6% D$_2$O and 2 mM sodium ascorbate. The pH was adjusted with μL aliquots of 0.1 or 0.5 M HCl. Argon was flushed through Pc samples to prevent reoxidation. Peptides LysLysLysLys (KKKK or tetra-Lys) and LysLysLysLysGlySerGly SerMetPheIleGln (KKKKGSGSMFIQ) were kindly provided by Prof. Shun Hirota (Kyoto, Japan). Stock solutions of 1.5 mM tetra-Lys peptide and 0.9 mM KKKKGSGSMFIQ in 10 mM sodium phosphate, pH 7.0 were prepared. The concentration of the stock solutions was determined by single scan ^{1}H experiments with 100 μM of (trimethylsilyl)-propionic acid (TSP) as an internal reference. The area under the resonance of the nine equivalent protons in TSP was used as a calibration for a single methyl resonance in the peptides.

NMR spectroscopy

All NMR spectra were recorded at 303 K on a Bruker DMX600 spectrometer. ^{15}N,^{1}H HSQC were obtained with spectral widths of 32 ppm (^{15}N) and 13.0 ppm (^{1}H). Data were processed with AZARA 2.7 [203] and analysed in ANSIG for Windows[204]. Resonances in the HSQC spectrum of *S. pratensis* Pc were assigned using 3D HNCACB and HN(CA)CO experiments.

Binding curves and chemical shift mapping

Averaged chemical shift perturbations ($\Delta\delta_{avg}$) were derived from equation 3a:

$$\Delta\delta_{avg} = \sqrt{\frac{1}{2}\left(\frac{\Delta\delta_N{}^2}{25} + \Delta\delta_H{}^2\right)} \qquad (3a)$$

where $\Delta\delta_N$ and $\Delta\delta_H$ are the chemical shift perturbation of the amide nitrogen and proton, respectively[205]. The chemical shift perturbations were recorded at 93% or 94% bound ^{15}N-Pc to the tetra-Lys and KKKKGSGSMFIQ peptide, respectively. Chemical shift titration curves were analysed with a two-parameter non-linear least-squares global fit to a 1:1 binding model, which corrects for dilution effects [16,38]:

$$\Delta\delta_{bind} = \frac{1}{2}\Delta\delta_{max}(A - \sqrt{(A^2 - 4R)}) \qquad (3b)$$

$$A = 1 + R + \frac{PR + C}{PCK_a} \qquad (3c)$$

where R is the [peptide]:[^{15}N-Pc] ratio, $\Delta\delta_{bind}$ is the chemical shift perturbation at a given R, $\Delta\delta_{max}$ is the chemical shift perturbation at 100% bound ^{15}N-Pc, P is the initial [^{15}N-Pc], C is the stock concentration of peptide and K_a is the association constant of the complex.

Results and discussion

In order to study *S. pratensis* Pc with NMR a protocol for the expression of the ^{15}N-labelled protein in minimal medium supplemented with 0.3 g/L ^{15}NH$_4$Cl was developed (see Materials & Methods) and ^{15}N labelled Pc was obtained. For assignment of the backbone amide resonances in the well-dispersed ^{15}N,^{1}H HSQC (Fig. 5.2), the minimal medium was supplemented with 1 g/L ^{13}C-glucose. Subsequently, 3D HNCACB and HN(CA)CO experiments were performed on ^{13}C, ^{15}N-labelled PCu(I) enabling in the assignment of all backbone amides (Table 5.1).
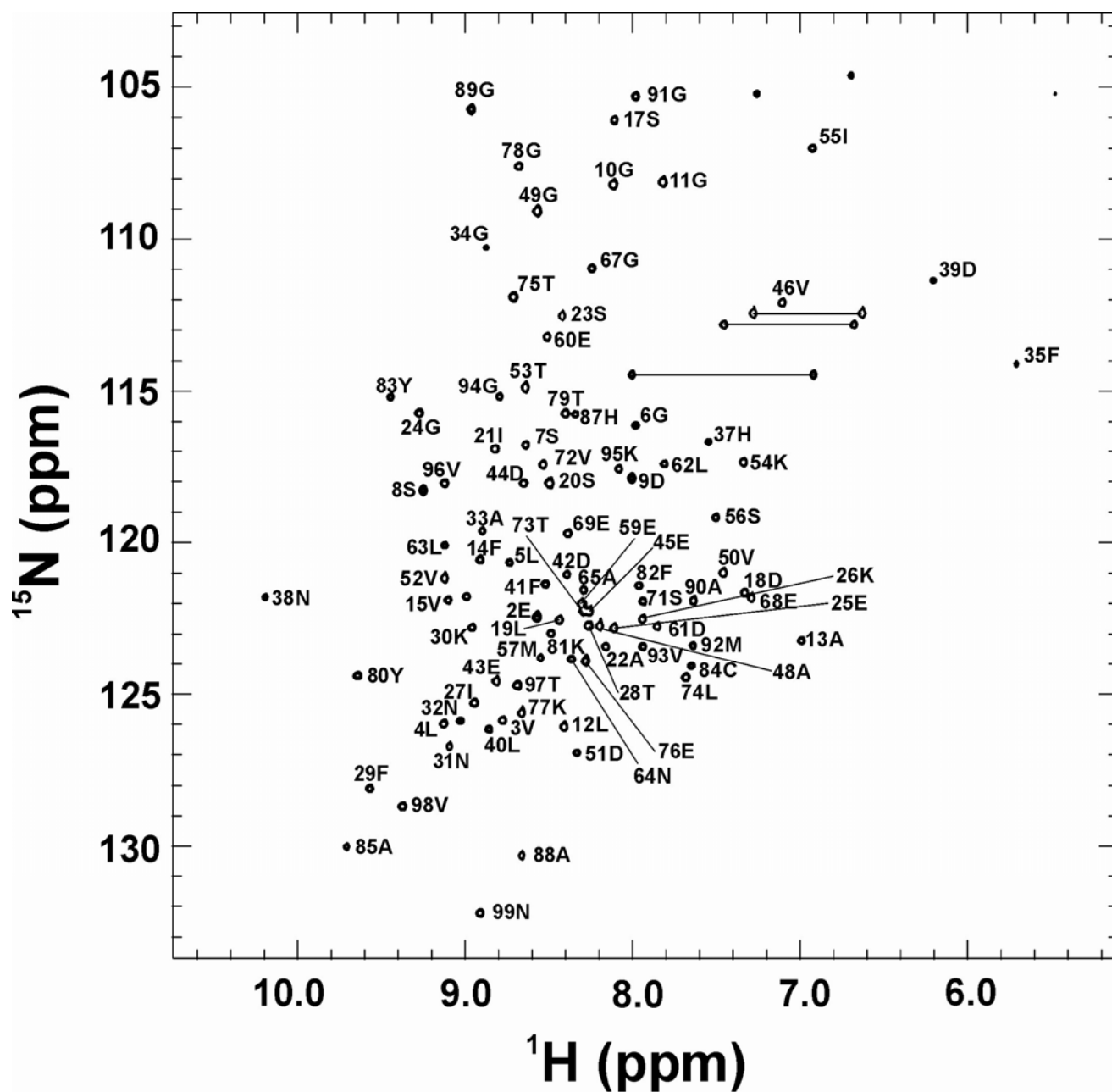
Figure 5.2. 2D ^{1}H-^{15}N HSQC spectrum of *S. pratensis* PCu(I). Labels indicate the assignment at 303 K, 10 mM potassium phosphate, pH 6.7. Side chain NH$_2$ resonances are connected by horizontal bars.

Table 5.1. ¹H and ¹⁵N resonance assignments of *S. pratensis* Pc at 303 K, 10 mM potassium phosphate, pH 6.7.

Residue	¹⁵N	¹Hᴺ	¹³Cᵅ	¹³Cᵝ	¹³CO
Ala1			49.71	18.52	171.28
Glu2	122.46	8.572	53.17	30.88	172.75
Val3	125.86	8.758	58.59	33.42	173.37
Leu4	126.00	9.114	52.05	40.61	175.03
Leu5	120.64	8.719	51.93	38.90	173.50
Gly6	116.11	7.948	42.17		171.84
Ser7	116.75	8.620	54.57	62.74	175.20
Ser8	118.23	9.218		60.53	172.61
Asp9	117.86	7.989			174.67
Gly10	108.19	8.102	42.78		172.76
Gly11	108.12	7.804	43.18		172.09
Leu12	126.09	8.400			171.83
Ala13	123.24	6.987	48.22	20.34	174.99
Phe14	120.6	8.904	56.11	38.02	174.32
Val15	121.91	9.083	56.99	31.83	173.09
Pro16				33.01	171.96
Ser17	106.13	8.098	56.21	62.31	172.38
Asp18	121.64	7.316	56.09		173.12
Leu19	122.57	8.425	53.05	42.48	173.53
Ser20	118.11	8.485	54.97	63.04	171.81
Ile21	116.92	8.809	56.93	40.17	172.44
Ala22	123.44	8.140	48.29	18.34	175.91
Ser23	112.53	8.405	58.66	60.86	174.84
Gly24	115.72	9.254	42.73		171.86
Glu25	122.83	8.099	54.11	28.73	171.83
Lys26	122.58	7.935	53.42	32.10	174.81
Ile27	125.31	8.933	58.05	37.92	173.38
Thr28	122.70	8.247	59.81	68.15	170.85
Phe29	128.07	9.557	54.30	37.02	173.29
Lys30	122.77	8.940	52.37	34.03	174.27
Asn31	126.75	9.079	52.29	36.62	174.63
Asn32	125.92	9.004	53.39	39.97	171.99
Ala33	119.58	8.857	50.40	20.16	175.80
Gly34	110.16	8.814	44.43		169.94
Phe35	114.10	5.699	49.66	34.32	171.41
Pro36			60.60		171.93
His37	116.49	7.543	52.51	36.68	173.50
Asn38	121.66	10.15	52.51	36.69	168.89
Asp39	111.36	6.187	60.04	31.77	171.63
Leu40	126.19	8.837	58.60	32.75	172.73
Phe41	121.39	8.505	55.37	38.31	173.03
Asp42	121.02	8.396	51.62	41.38	174.71
Glu43	124.58	8.814	56.51	27.53	174.72
Asp44	117.98	8.635	53.36	39.52	175.05
Glu45	122.19	8.235	53.58	28.80	171.73
Val46	112.04	7.091	56.75	31.35	172.15
Pro47					173.76
Ala48	122.76	8.192	60.64	30.09	177.29
Gly49	109.11	8.554	42.93		173.11
Val50	120.98	7.441	60.92	30.09	173.00

Table 5.1: continued

Residue	^{15}N	^{1}H^{N}	^{13}C^{α}	^{13}C^{β}	^{13}CO
Asp51	126.96	8.337	49.52	38.73	176.92
Val52	121.11	9.096			176.83
Thr53	114.93	8.629			175.08
Lys54	117.41	7.324	54.33	30.94	175.91
Ile55	106.92	6.903	59.44	36.71	174.34
Ser56	119.14	7.484	57.03	63.47	172.97
Met57	123.78	8.526	54.17	29.16	172.29
Pro58					
Glu59	122.07	8.294	57.70		175.25
Glu60	113.15	8.497	54.41	27.22	174.68
Asp61	122.68	7.842	51.79	39.34	172.50
Leu62	117.57	7.809			174.60
Leu63	120.13	9.102	52.03	38.16	175.40
Asn64	123.83	8.343	52.67	39.85	172.55
Ala65	121.53	8.257	47.45	70.05	173.69
Pro66					176.15
Gly67	110.97	8.239	43.65		172.01
Glu68	121.76	7.269	55.93	29.45	173.52
Glu69	119.73	8.383	52.28	32.50	174.43
Tyr70	121.75	8.973	55.59	41.17	172.40
Ser71	121.97	7.925	54.60	64.04	170.48
Val72	117.48	8.520	57.60	33.28	171.15
Thr73	122.17	8.288	59.94	67.60	171.69
Leu74	124.45	7.672			174.36
Thr75	111.91	8.695	60.17	67.57	173.99
Glu76	123.90	8.267	54.45	26.18	175.89
Lys77	125.65	8.650	55.82	31.37	174.09
Gly78	107.60	8.665	41.54		170.89
Thr79	115.66	8.388	60.77	68.31	171.66
Tyr80	124.43	9.634	53.93	37.98	173.36
Lys81	122.87	8.461	53.08	33.09	172.80
Phe82	121.29	7.946	52.03	38.54	171.51
Tyr83	115.23	9.434	53.90	38.60	168.93
Cys84	124.02	7.630	54.91	31.06	176.42
Ala85	111.29	9.699	54.96	66.53	
Pro86					177.98
His87	115.57	8.307	53.98	31.23	175.87
Ala88	111.79	8.634	54.47	69.26	180.38
Gly89	105.77	8.948	44.03		173.04
Ala90	121.87	7.610	49.21	70.26	176.08
Gly91	105.29	7.969	42.97		172.96
Met92	123.27	7.616	55.54	28.79	170.51
Val93	123.43	7.929	58.32	34.33	173.52
Gly94	115.07	8.765	42.58		168.79
Lys95	117.63	8.072	52.79	34.83	172.78
Val96	118.10	9.110	55.60	32.66	171.85
Thr97	124.74	8.673	59.98	68.21	170.88
Val98	128.66	9.354	59.13	30.19	174.23
Asn99	106.58	8.899	52.70	39.89	177.48
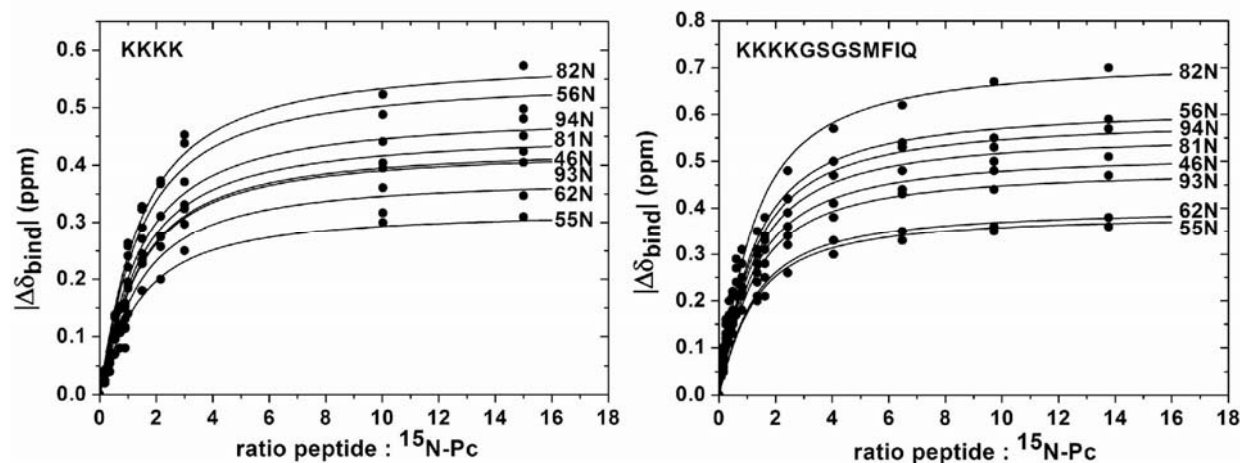
Figure 5.3. Binding curves for the interaction between *S. pratensis* ^{15}N-Pc and tetra-Lys or KKKKGSGSMFIQ. The $|\Delta\delta_{bind}|$ of individual residues is plotted as a function of the peptide : Pc ratio. Global non-linear least squares fits (solid lines) to a 1:1 binding model[16] yield a K_a of 5 ($\pm$ 2) x 10^3 M^{-1} for tetra-Lys and 6 ($\pm$ 2) x 10^3 M^{-1} for KKKKGSGSMFIQ.

To determine the effects of binding, chemical shift perturbations were analyzed for *S. pratensis* Pc upon titration with the two Lys-peptides. The presence of both of the peptides gives rise to distinct changes in the ^{1}H-^{15}N HSQC spectrum of ^{15}N-PCu(I). A single averaged resonance was observed for each amide indicating that exchange between free and bound Pc is fast on the NMR-timescale. The observed chemical shift changes ($\Delta\delta_{bind}$) of the most affected residues were plotted against the molar ratio of peptide: ^{15}N-PCu (Fig. 5.3) and fitted to a 1:1 binding model[16]. This yields a K_a of 5 ($\pm$ 2) x10^3 M^{-1} for the tetra-Lys peptide and 6 ($\pm$ 2) x10^3 M^{-1} for the KKKKGSGSMFIQ peptide. The K_a is in agreement with the spectroscopically determined association constant of 8 ($\pm$ 2) x10^3 M^{-1} for the tetra-Lys : Pc interaction[224]. The association constant does not significantly change by the addition of the hydrophobic residues to the peptide.
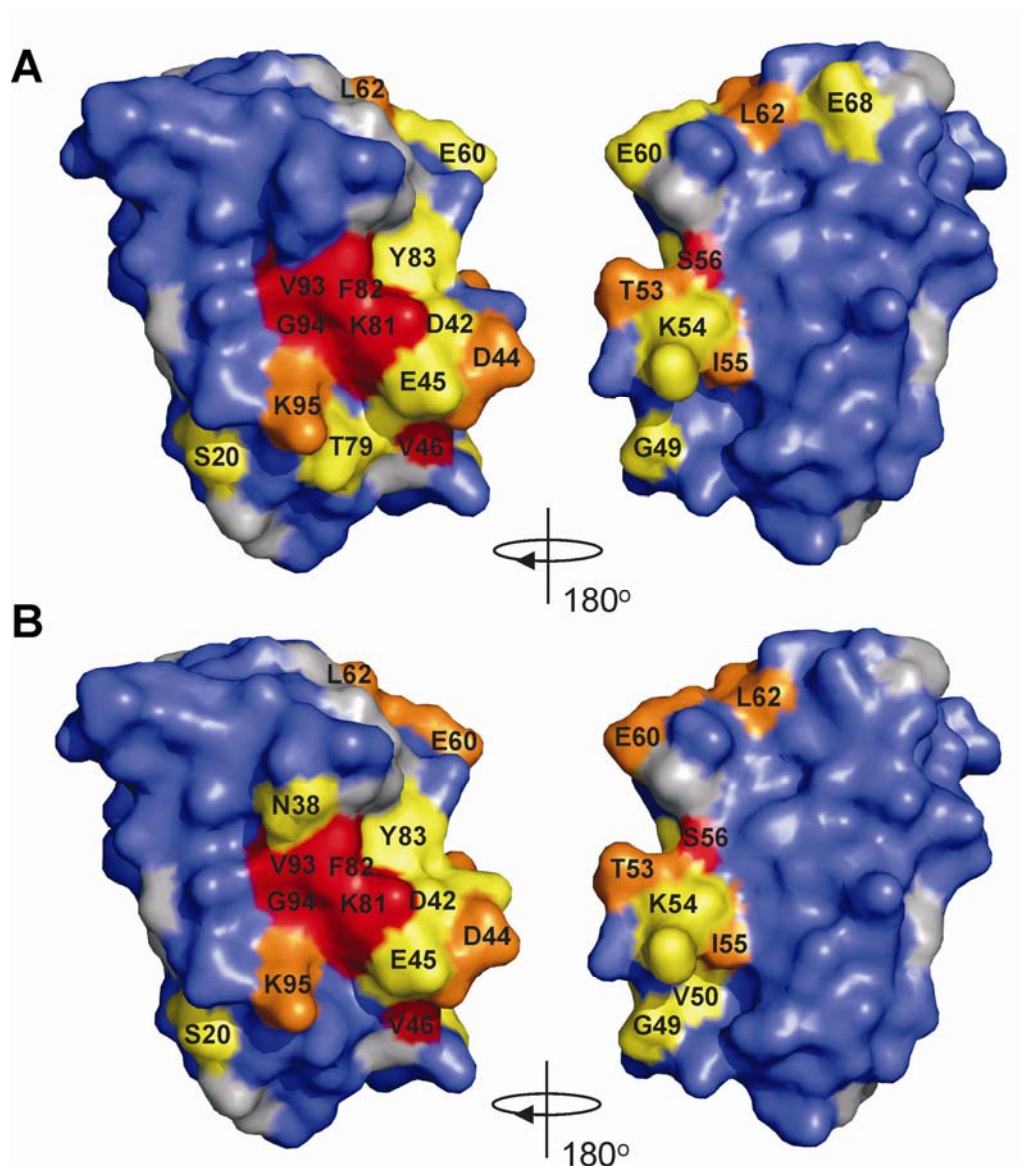
Figure 5.4. Surface representations of *S. pratensis* Pc (PDB file 1BYO) in the presence of A) tetra-Lys or B) KKKKGSGSMFIQ. Residues that experience chemical shift changes ($\Delta\delta_{bind}^{15N}$) are colour coded as follows; blue $\Delta\delta_{bind} \leq 0.1$ ppm, yellow $\Delta\delta_{bind} \geq 0.1$ ppm, orange $\Delta\delta_{bind} \geq 0.2$ ppm, and red $\Delta\delta_{bind} \geq 0.3$ ppm.

The chemical shift perturbations experienced by the backbone amide have been colour coded and plotted on the surface of *S. pratensis* Pc (PDB file 1BYO)[79], creating a binding map (Fig. 5.4). The binding map of the tetra-Lys: Pc interaction confirms that the two negatively charged patches of Pc are involved in binding with the peptide. Surprisingly though, these residues do not experience the largest shift changes. These are found for the

residues next to the lower acidic patch, and are experienced by mainly hydrophobic residues. It is conceivable that the C-terminus of the peptide interacts with the side chain of Lys81 in Pc, which is the most affected residue. The chemical shift changes are not confined to a specific patch or set of residues, which suggest a relatively dynamic interaction between Pc and the tetra-Lys peptide. This is supported by the size of $\Delta\delta_{Avg}$ for all residues in Pc (Fig. 5.5), which are smaller than those found in a single-orientation complex and larger than those found in a complex that consists of a dynamic ensemble of orientations[33].
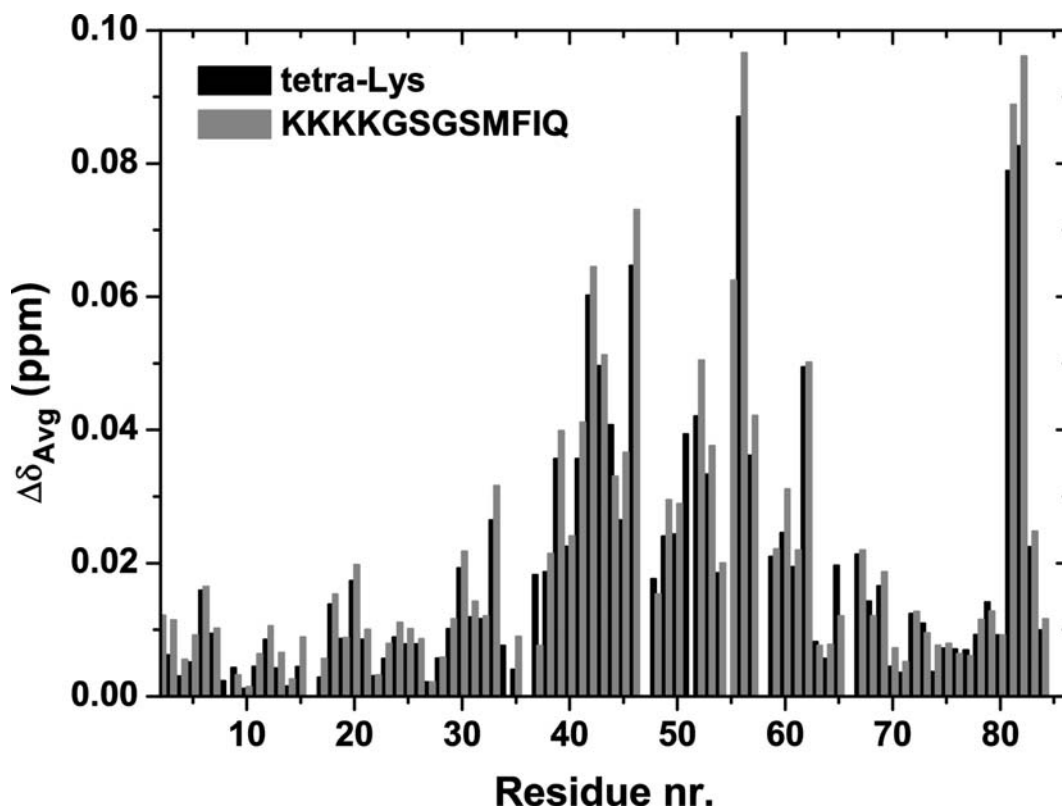
Figure 5.5. $\Delta\delta_{Avg}$ experienced by *S. pratensis* Pc in complex with tetra-Lys and KKKKGSGSMFIQ peptide.

Small perturbations of the residues that coordinate the copper indicate that the copper site is not the main binding site of the peptide. The reported inhibition of electron transfer to cytochrome *c* and cyt*f* [219,225] can therefore be best explained by the interference of electrostatic interactions by the charged peptides. The binding map of the KKKKGSGSMFIQ: Pc interaction shows a similar pattern of chemical shift changes. Again the copper site is not the site of interaction with the peptide. This indicates that the

addition of the hydrophobic residues does not decrease the dynamics in the interaction with Pc. Interestingly, the copper coordinating His37 experiences a smaller chemical shift, indicating the copper site geometry might be differentially affected by the two peptides. However, the lack of a significant change in the binding constant indicates that the hydrophobic residues do not influence the interaction of the peptide with Pc. This supports the idea that surfaces of electron transfer proteins are designed to interact weakly but specifically with their partners, keeping a fine balance between hydrophobic, electrostatic and solvent interactions. Perhaps the peptides used here are too flexible to mimic the entire interaction between Pc and its partners.

Chapter VI

Effect of macromolecular crowders on the transient *Ph. laminosum* plastocyanin - cytochrome *f* complex

Abstract

The presence of large amounts of macromolecules in the cellular environment, described by the term macromolecular crowding affects proteins and protein-protein complexes. The effect of macromolecular crowding on transient protein-protein association was investigated by NMR. Initially, the effect of four high molecular weight crowders on the 2D NMR spectrum of ^{15}N-Src-SH2, a small globular protein was tested. It was found that addition of up to 20% Ficoll70 leads to minimal line broadening and the least amount of signal loss. For this reason, *Ph. laminosum* ^{15}N-Pc was titrated with increasing amounts of cyt*f* in the presence of 20% Ficoll70. The resulting binding constant of the Pc- cyt*f* complex is not significantly different from the binding constant in the absence of crowder. The similarity between the chemical shift perturbation maps in the absence and presence of crowding agent also indicates that the binding is not detectably affected by the presence of Ficoll70. Both observations support the idea that high molecular weight crowders show low 'microviscosity' and are not uniformly distributed. The question remains whether this is a appropriate representation of *in vivo* crowding conditions.

Introduction

The dilute solutions in which proteins and protein complexes are often studied are different from the cellular environment in which these proteins normally function[226]. Inside an *E. coli* cell, for example, the total concentration of proteins and RNA is approximately 300-400 g/l^{-1} [227]. The presence of a large amount of other macromolecules in high concentrations, described by the term macromolecular crowding can have effects on both diffusion and the effective volume available to proteins and protein complexes[228-234]. Generally, reaction rates can decrease due to diffusion limitations or increase because the activity of reactants rises through a decline in effective volume. Alternatively, both effects can cancel each other out. The effective volume available depends on the size of the proteins with respect to the other molecules crowding the solution. In order to mimic this situation *in vitro* macromolecular crowders are added to the reactants. The effects of these crowders on protein-protein association have been studied by a multitude of approaches including stopped-flow kinetics, fluorescence spectroscopy and isothermal titration calorimetry[235-239]. All results indicated crowders have detectable effects on protein-protein association. It was also suggested that the properties of high molecular weight crowders better mimic the intracellular environment then low molecular weight crowders[237]. NMR studies have shown that the presence of crowders stabilises intrinsically disordered proteins, such as FlgM[240] and α-synuclein[241]. Also, a ^{13}C-NMR off-resonance rotating frame spin-lattice relaxation study has shown that high concentrations of γ-crystallin in the ocular mammalian lens leads to self-association[242]. However, the effects of macromolecular crowding on the binding interface and structure of protein-protein complexes have not been studied. Here, we investigated the transient complex of Pc and cyt*f* under crowding conditions with NMR. The complex plays an important role in photosynthetic electron transport in all oxygenic organisms. Cyt*f* is part of a membrane protein complex (cytochrome b_6f) and the interactions with Pc takes place in the lumen of chloroplasts. Therefore, the *in vivo* conditions in which the complex functions might be different to those in the *E. coli* cytoplasm. Still, it was shown that effects of molecular crowding can provide an insight in the well-studied reaction kinetics of this complex[238]. The SH2 domain of Src from mouse was used as a test system for the

effect of molecular crowders on the 2D NMR spectrum of small globular proteins (~13 kDa). Four different crowders were compared to assess the influence of their different physical properties.

Materials and Methods

Removal of leader peptide from Ph. laminosum Pc

A new construct for cytoplasmic expression of the *Ph. laminosum* Pc gene (*petE*) was created. In order to remove the endogenous leader sequence from *petE*, an oligonucleotide encoding the translation initiation site and 13 subsequent bases was designed as forward primer (5'-pCGTATACCATGGAAACCTTCACCG-3'). A standard T7 primer (Isogen Life Science) was taken as backward primer. The pET11Pc plasmid was used as a template in a PCR reaction consisting of one cycle of 5 minute denaturation at 95°C, 30 cycles of 1 minute of hybridization at 53°C, 1 minute of elongation at 70°C, 1 minute of denaturation at 95°C and finally 10 minutes of elongation at 70°C. The resulting fragment was cloned back into the pET11d vector (Novagen) using the NcoI and BamHI restriction sites. Sequencing of the resulting plasmid pET11Pcnl showed the removal of the leader sequence and an unaltered coding sequence.

Protein production and purification

For the production of *Ph. laminosum* ^{15}N-Pc competent BL21 *E. coli* cells were transformed with the pET11Pcnl plasmid and incubated overnight at 37° on a LB/Amp (0.1 g/L ampicillin) plate. A single colony was inoculated in 10 mL LB/Amp medium and incubated overnight at 37°, shaking at 250 rpm. Five mL of the pre-culture was inoculated in 0.5 L M9 minimal medium[222] supplemented with 0.3 g/L [15]NH$_4$Cl and 0.1 g/L ampicillin in a 2 L flask. The cultures were incubated at 37°, shaking at 250 rpm before induction with 1 mM IPTG at an OD$_{600}$ of 0.7. At the same time the temperature was lowered to 30° and growth was continued for five hours before harvesting. Cells were resuspended in the minimal volume of buffer (5 mM TRIS pH 7.5), followed by

addition of 5 mg DNase and lysozyme, 1 mM PMSF and 5 mM $CuNO_3$. Cytoplasmic extracts of the harvested cells were obtained through use of the French press cell. Cell debris was removed by ultra-centrifugation at 30.000 rpm after which the supernatant was dialysed against 5 L of 5 mM TRIS pH 7.5 for 3 hours and overnight at 4°. Reduced Pc was purified using ion exchange chromatography with DEAE sepharose (Amersham Biosciences) in 5 mM TRIS pH 7.5. Pc was eluted with a gradient of 5-50 mM TRIS pH 7.5. The fractions containing Pc were concentrated and the ion exchange chromatography was repeated with oxidised Pc. Size exclusion chromatography was performed with Superdex-G75 (Amersham Pharmacia Biotech) in 50 mM TRIS pH 7.5, 100 mM NaCl. Pc was oxidised with potassium ferricyanide and reduced with sodium ascorbate. The Pc concentration was determined by optical spectroscopy using $\varepsilon_{597} = 4.3$ mM^{-1} for oxidised Pc[243]. Pc was considered pure when $A_{278}/A_{597} \leq 2.5$ [202]. The yield of pure ^{15}N-Pc after purification was 5 mg/L. Comparison with periplasmically expressed Pc was made with optical spectroscopy, mass spectroscopy and 2D NMR.

Ph. laminosum cyt*f* was produced and purified as described before[40], with the exception that growth under semi-anaerobic conditions was achieved by rotation of 1.7 L culture in 2L flasks at 180 rpm, instead of 100 rpm. The cyt*f* concentration was determined by optical spectroscopy using $\varepsilon_{556} = 31.5$ mM^{-1} for reduced cyt*f* [202]. Yields of up to 10 mg/L of cyt*f* after purification were obtained.

^{15}N-Src-SH2 was produced from plasmid pSRC_mouse in BL21 *E. coli* cells in M9 minimal medium[222] supplemented with 0.3 g/L ^{15}NH$_4$Cl and 50 mg/L kanamycin. Gene expression was induced with 0.5 mM IPTG when OD$_{600}$ reached 0.6 and incubation at 37° and 250 rpm was continued for three hours. Cells were lysed as described above. The protein was purified using affinity chromatography with Ni-NTA (Qiagen) in 20 mM TRIS pH 8.0, 0.5 M NaCl, 10 mM imidazole. The protein was eluted with 100 mM imidazole. Protein concentration was determined with the theoretical[244] $\varepsilon_{280} = 14.4$ mM^{-1} cm^{-1}.

NMR experiments

All protein samples were concentrated by ultrafiltration (Amicon, MW cut-off 10 kDa for cyt*f* and 5 kDa for Pc and Src-SH2). The pH was adjusted with μL aliquots of 0.1 or 0.5 M HCl.[15]N-Src-SH2 samples contained 1 mM of the protein in 20 mM sodium phosphate pH 6.5, 6% D_2O. Pc samples contained 10 mM sodium phosphate, pH 6.0, 6% D_2O and 2 mM sodium ascorbate. Argon was flushed through Pc samples to prevent reoxidation. Aliquots of a 1.33 mM cyt*f* stock solution were added to samples of 0.6 mM ^{15}N-Pc. Ficoll70 (Sigma-Aldrich), dextran T70 (Fluka), poly-ethylene glycol 6000 (PEG-6000, Merck) and bovine serum albumin (BSA, Sigma-Aldrich) were purchased and used without further purification. Stock solutions of 40% (w/v) crowder in 20 mM sodium phosphate, pH 6.5, 6% D_2O were prepared.

NMR spectroscopy

All NMR spectra were recorded at 300 K on a Bruker DMX600 spectrometer. ^{15}N,^{1}H HSQC were obtained with spectral widths of 27 ppm (^{15}N) and 13.5 ppm (^{1}H) for ^{15}N-Src-SH2 and 31.3 ppm (^{15}N) and 12 ppm (^{1}H) for ^{15}N-Pc. Data were processed with AZARA 2.7 [203] and analysed in ANSIG for Windows[204].

Binding curves and chemical shift mapping

Chemical shift titration curves were analysed with a two-parameter non-linear least-squares global fit to a 1:1 binding model, which corrects for dilution effects [16,38]:

$$\Delta\delta_{bind} = \frac{1}{2}\Delta\delta_{max}(A - \sqrt{(A^2 - 4R)}) \qquad (3b)$$

$$A = 1 + R + \frac{PR + C}{PCK_a} \qquad (3c)$$

where R is the [cyt*f*] : [^{15}N-Pc] ratio, $\Delta\delta_{bind}$ is the chemical shift perturbation at a given R, $\Delta\delta_{max}$ is the chemical shift perturbation at 100% bound ^{15}N-Pc, P is the initial [^{15}N-Pc], C is the stock concentration of cyt*f* and K_a is the association constant of the complex.
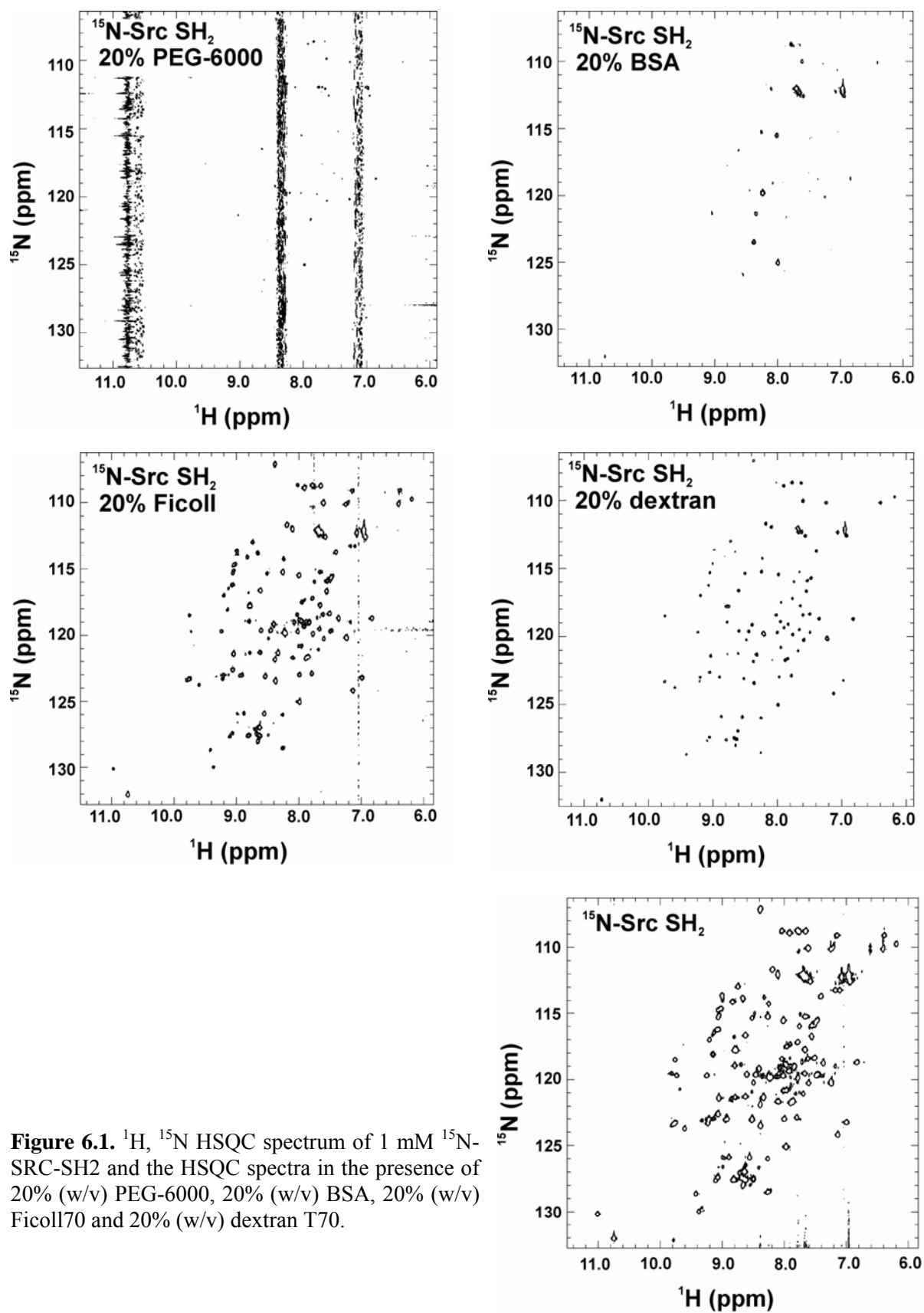
Figure 6.1. ^{1}H, ^{15}N HSQC spectrum of 1 mM ^{15}N-SRC-SH2 and the HSQC spectra in the presence of 20% (w/v) PEG-6000, 20% (w/v) BSA, 20% (w/v) Ficoll70 and 20% (w/v) dextran T70.

Results and discussion

Effects of various high molecular weight crowders on ^{15}N-Src-SH2

In order to determine the effect of four high molecular weight crowders on the ^{15}N,^{1}H HSQC spectrum of a small globular protein, ^{15}N-labelled Src-SH2 (~13 kDa) was titrated with dextran T70, Ficoll70, PEG-6000 and BSA. Dextran T70 (average MW 70 kDa) is a non-ionic, linear flexible, polysaccharide with few and short branches[245,246]. Ficoll70 (average MW 70 kDa) is a non-ionic, highly branched, synthetic polymer of sucrose and epichlorohydrin which approximates a sphere more closely than dextran[245,246]. PEG-6000 (average MW 60 kDa) is a non-ionic, linear, non-branched polymer of ethylene glycol. Bovine serum albumin is the only charged crowder with pI of 4.7 and a molecular weight of 66 kDa. It has been shown for several crowders that the macroscopic viscosity is not equal to the microscopic viscosity experienced by proteins or probes. In fact, diffusion of molecules was much faster than expected from the macroscopic viscosity of these crowders[237,247-250]. Spectra were recorded at 1%, 5%, 10% and 20 % (w/v) of each crowder. Comparison of the resulting spectra at 20% of each crowder (Fig. 6.1) shows a clear difference between these crowders. The presence of charged BSA leads to an inhomogeneous decrease in the intensity of the resonances, indicating a large increase in the rotational correlation time, which may be attributed to interactions between BSA and SH2. However, the same effect is observed for uncharged PEG-6000, which in addition disturbs the spectrum in the ^{1}H dimension. It can therefore not be ruled out that microscopic viscosity influences the rotational correlation time in the presence of both PEG-6000 and BSA. Both dextran T70 and Ficoll70 have only small effects on the SH2 signal. The presence of 20% Ficoll70 leads to the least decrease in intensity of the SH2 resonances. From these results it was expected that a reasonable signal to noise ratio can also be recorded for ^{15}N-Pc in a solution with up to 20% Ficoll70. Higher concentrations of crowders could not be investigated due to experimental limitations. This is still well in the range of physiological significance because, for instance, 5% Ficoll70 represents the approximate volume occupancy found *in vivo*[251].
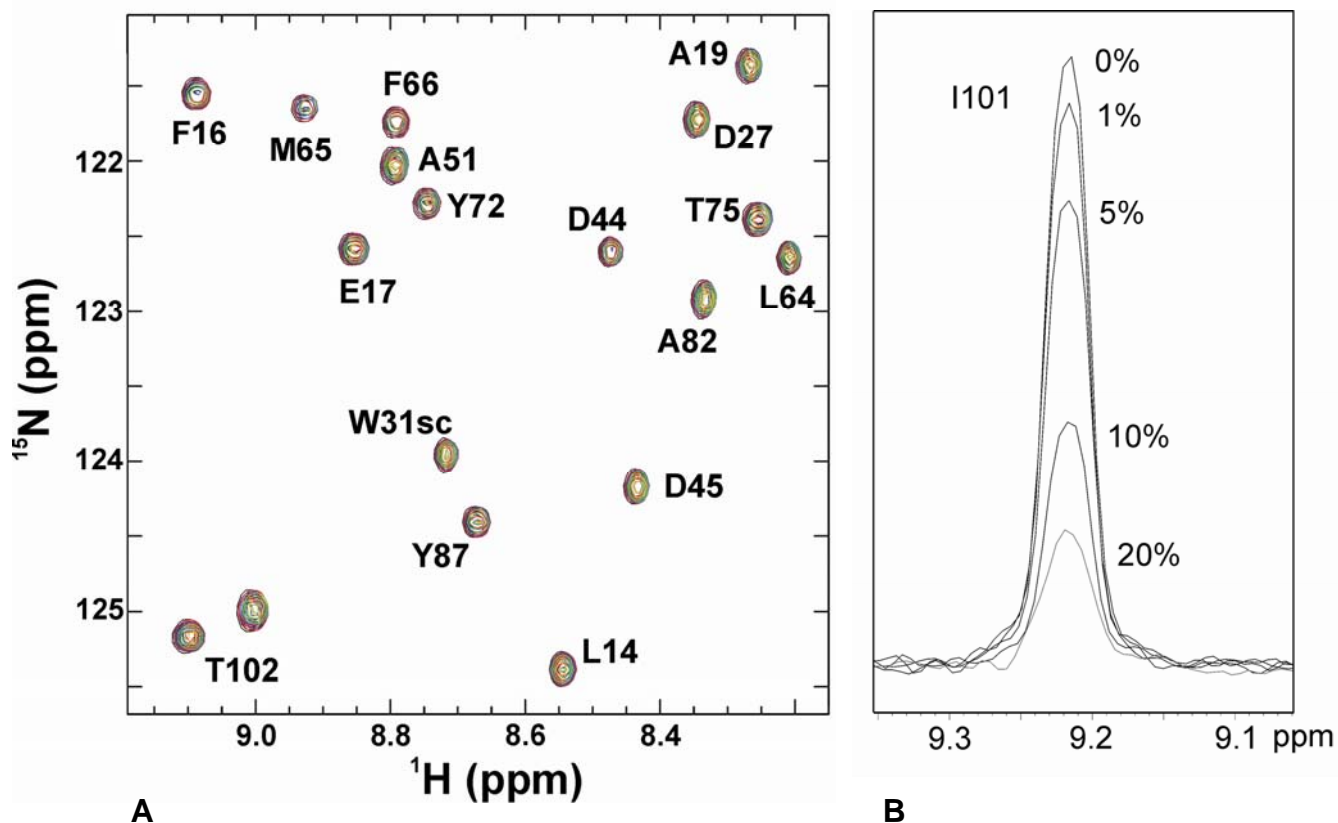
Figure 6.2. A) Overlay of part of ^{1}H-^{15}N HSQC of *Ph. laminosum* Pc in the presence of 0% (black), 1% (red), 5% (blue), 10% (green), 20% (orange) Ficoll70. B) Cross-sections through ^{1}H^N Pc resonance of Ile101 at various concentrations of Ficoll70.

Effects of Ficoll70 on the NMR spectrum of ^{15}N- Pc

Resonances of *Ph. laminosum* ^{15}N-Pc produced in the cytoplasm have similar chemical shifts to those reported for *Ph. laminosum* Pc from the periplasm[40], with the exception of one extra peak, most likely corresponding to the amide of Glu1. Mass spectroscopy on cytoplasmic Pc revealed that initial Met is not cleaved off from Pc produced in the cytoplasm. In the case of periplasmic expression it is removed together with the leader peptide. This means that Glu1 in cytoplasmically expressed Pc is no longer the N-terminal residue and the Glu1 amide is detectable in the 2D NMR spectrum.

In order to assess the effects of Ficoll70 on ^{15}N-Pc, a titration with 1%, 5%, 10% and 20% Ficoll70 was performed. An overlay of part of the recorded spectra is shown in Figure 6.2A. A representative cross-section of one of the resonances (Fig. 6.2B) indicates

that line-broadening is only limited. This shows that the rotational correlation of Pc is not dramatically changed by the addition of 20% Ficoll70. The decrease in intensity can partly be explained by the decrease in protein concentration due to the addition of crowder stock solution as well as a little protein precipitation at higher crowder concentration. As has been reported before[237], semi-dilute solutions of high molecular mass crowders can be inhomogeneous at the microscopic level. This could lead to a fraction of immobilised and therefore NMR-undetectable protein and a fraction of protein which is affected only by a small increase in (microscopic) viscosity. This would explain the observed decrease in intensity and lack of significant change in rotational correlation time. Apparently Ficoll70 can be used as macromolecular crowder without interfering too much with the 2D NMR spectrum of ^{15}N-Pc.
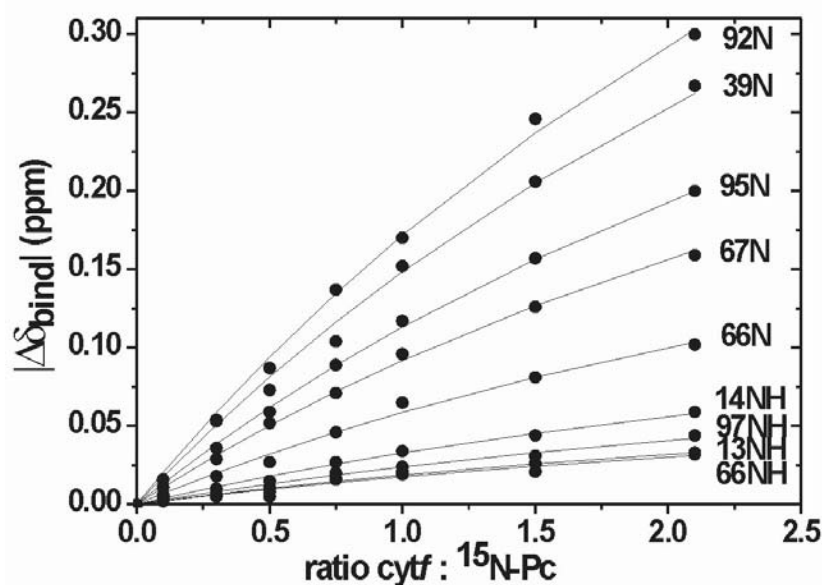
Figure 6.3. Binding curves for complex formation between *Ph. laminosum* ^{15}N-Pc and cyt*f* in presence of 20% Ficoll70. The $|\Delta\delta_{bind}|$ of individual residues is plotted as a function of the cyt*f* : Pc ratio. Global non-linear least squares fits (solid lines) to a 1:1 binding model[16] yielded a K_a of ~10^2 M^{-1}.

Effects of Ficoll70 on Ph. laminosum Pc - cytf complex

To study the effect of crowding on the *Ph. laminosum* Pc- cyt*f* complex cyt*f* was titrated into Pc in the presence of 20% Ficoll70. As in the absence of crowder, the presence of cyt*f* gives rise to changes in the ^{1}H-^{15}N HSQC spectrum of ^{15}N-Pc. A single averaged resonance was observed for each amide indicating that exchange between free and bound Pc is fast on the NMR-timescale. The observed chemical shift changes ($\Delta\delta_{bind}$) of the most affected residues were plotted against the molar ratio of cyt*f*: ^{15}N-PCu (Fig. 6.3) and fitted to a 1:1 binding model[16]. This yields a very low K_a, of $\sim 10^2$ M^{-1}, which is similar to the K_a in the absence of Ficoll70 [40]. It has to be noted that due to weak binding the K_a cannot be determined with high accuracy. Only large differences would be detectable. The ^{15}N chemical shift changes were colour-coded and plotted on a surface representation of the crystal structure of Pc[74] to create a chemical shift perturbation map (Fig. 6.4). Compared to the chemical shift perturbation map previously determined for the complex[40], no major differences are observed. In both cases the hydrophobic patch, located at the northern end of the protein is most involved in complex formation. In the presence of 5% Ficoll70 similar results are obtained.

It can be concluded the presence of crowder does not detectably change the binding in the *Ph. laminosum* Pc - cyt*f* complex. This is in agreement with the report that the overall electron transfer rate (k_2) is not affected by the presence of high molecular weight crowders[238]. It supports the idea that high molecular weight crowders such as Ficoll70 are not uniformly distributed in solution and form a 'porous' medium[237] in which relatively small proteins can move as they would in dilute solution. The question remains whether this is an appropriate model for the physiological conditions the proteins encounter and which crowder or combination of crowders is most successful in mimicking the cellular environment.
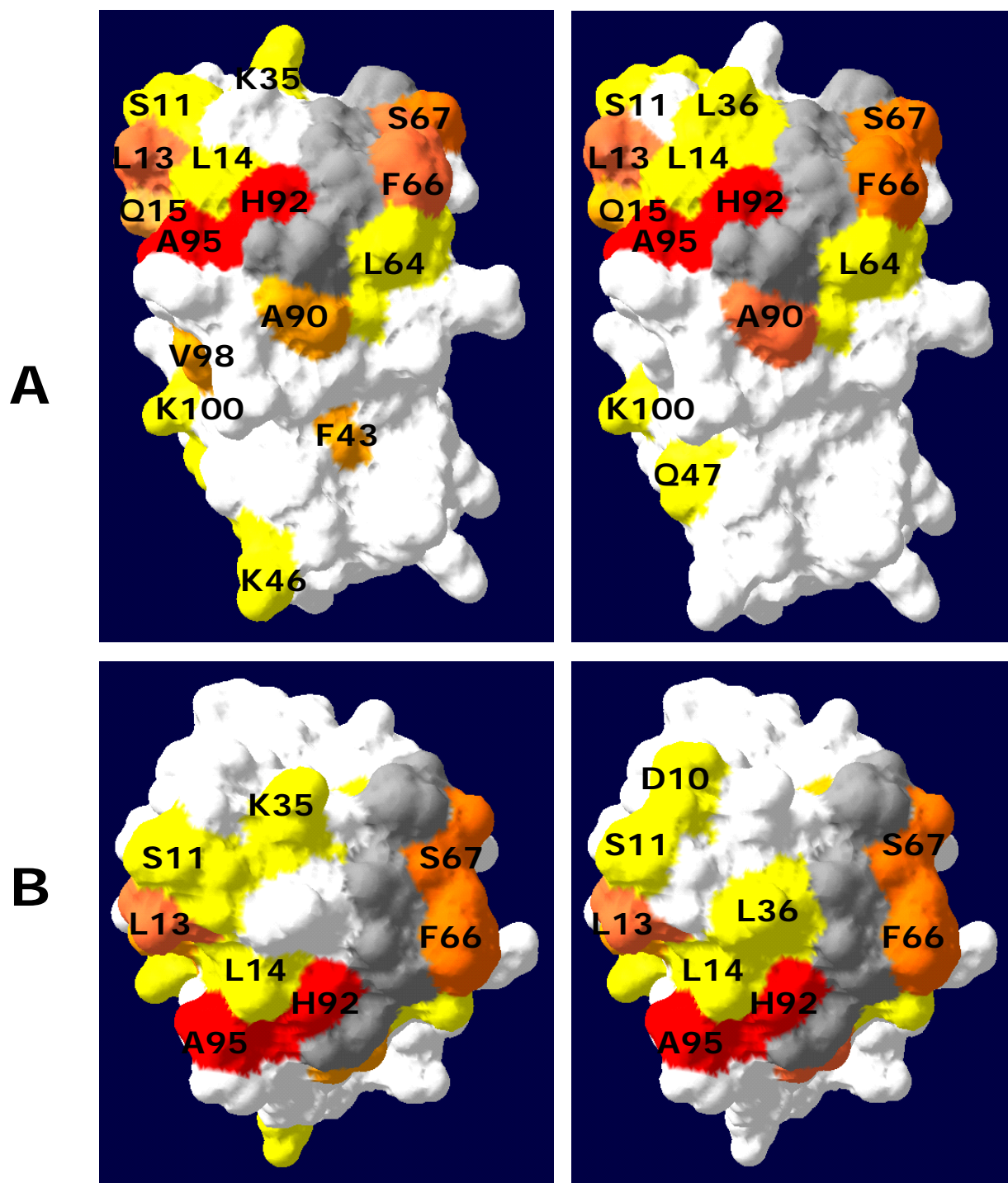
Figure 6.4. Surface representations of Pc in the presence of 0% (left) and 20% (right) Ficoll70. Chemical shift changes ($\Delta\delta_{Bind}^{15N}$) in the presence of ferrous cyt*f*. Residues with $\Delta\delta_{Bind}^{15N} \leq 0.05$ ppm in white, $\Delta\delta_{Bind} \geq 0.05$ ppm in yellow, $\Delta\delta_{Bind} \geq 0.1$ ppm in orange, $\Delta\delta_{Bind} \geq 0.3$ ppm in red and proline residues in gray. A) side view B) top view.

Concluding remarks

Concluding remarks

NMR chemical shift perturbation analysis

Throughout this work NMR titration experiments have been used as a tool to study protein properties and several aspects of transient protein interactions. Typically, a ^{15}N-labelled protein is presented with for instance a change in pH or the addition of a partner protein or peptide. The resulting changes in the 2D [^{1}H, ^{15}N] NMR spectrum are followed and resonances are recorded at every step. This technique has been used extensively in our group and proved to be very useful to characterise transient protein complexes[8,9].

In Chapter II this technique is used to investigate the protonation behaviour of a histidine copper ligand. Previously, crystallography and 1D NMR spectroscopy studies suggested that histidine protonation does not occur in fern Pc[77,85]. We show that 2D NMR spectroscopy can overcome aggregation problems and provides a detailed picture of the protonation event that occurs at a lower pK_a than expected for Pc.

It has been suggested before that the size of the chemical shift changes that arise due to the addition of the partner protein can be used as a diagnostic tool for the dynamics in a transient protein complex[33,35,38]. This work supports that view (Chapter III). A new approach was used that creates an ensemble of randomly distributed orientations in the complex between mutant Pc and cyt*f*. The average PCS are calculated for each ensemble to determine which ensemble of orientations corresponds to the experimental PCS. Results show that changes on the surface of *P. hollandica* Pc can increase the dynamics, which was previously inferred from the decrease in size of the chemical shifts changes (Chapter III and reference 87).

Dynamics in transient protein complexes

The two-step model proposed for transient protein complex formation (Fig. 1.1) has slowly emerged from increasing amounts of experimental data and theoretical studies. The first step of protein association has been extensively studied and the role of electrostatic interactions is well established. The second stage, characterised by an

----

equilibrium between the dynamic encounter and the well-defined state has come into the focus of recent research, for which paramagnetic NMR techniques are indispensable. The approach of creating an ensemble of orientations was used to study the Pc - cyt*f* (Chapter III) and cyt*c*$_6$ - cyt*f* complex (Chapter IV). In the latter case the PCS data were complemented with intermolecular paramagnetic relaxation enhancement (PRE) data, caused by five spin labels on cyt*f*. This type of paramagnetic data is fundamentally different from PCS. It has been used to determine the conformational space occupied by the cytochrome *c* – cytochrome *c* peroxidase complex, which is a mostly well-defined complex[31]. Both complexes studied in this work are found to be balanced between encounter and well-defined state, which complicates the characterisation of the interaction. This is illustrated by the violations of the PRE restraints from five spin labels, which cannot be met all at the same time. This is a strong indication of the dynamic nature of the complex. The creation of an ensemble of orientations around a starting structure works well for the *P. hollandica* mutant Pc in complex with cyt*f* (Chapter III), for which the single orientation determine for the wt complex is most likely the centre of the ensemble. In the case of *Nostoc* cyt*c*$_6$ - cyt*f* it is likely that the distribution of orientations in the ensemble is less symmetric. This suggests that the use of methods that do not require a starting structure, such as Brownian dynamics, might be more successful in precisely describing the encounter state of this complex.

Surface interactions in the Pc - cytf complex

The mutation of residues in the interface between *P. hollandica* Pc and cyt*f* has a profound effect on the dynamics of the complex, indicative of the role that geometric compatibility plays in complex formation (Chapter III). In Chapter V the interaction of a positively charged peptide with the negative eastern patch of Pc shows why this peptide can inhibit the electron transfer from cyt*f*. The addition of hydrophobic residues to the peptide does not significantly change the interaction with Pc. From these results it can be concluded that surfaces of electron transfer proteins are designed to interact specifically with their partners, keeping a fine balance between hydrophobic, electrostatic and solvent interactions (Chapter III and V).

The Pc - cytf complex in vivo

The work described here is all performed on proteins that were removed from their original environment. *In vitro* studies on proteins and protein complexes has delivered a wealth of knowledge on their function and on the mechanisms involved. While drawing conclusions from *in vitro* work, however, it is not only important to keep in mind that there is a difference with the cellular environment, but also to assess how these differences effect the system under investigation. Macromolecular crowders have been used to determine to what extent the *in vitro* data can be representative for *in vivo* behaviour of bio-macromolecules. The addition of the high molecular weight crowder Ficoll70 to the Pc - cyt*f* complex does not cause significant changes in the binding (Chapter VI) or overall reaction rate[238]. It is in agreement with the view that these type of crowders form a 'low-viscosity', porous medium. Whether this is the most appropriate model for the cellular environment in general and the lumen in which the Pc - cyt*f* complex functions remains to be seen.

Reference List

1. Schreiber, G. and Fersht, A. R. Interaction of barnase with its polypeptide inhibitor barstar studied by protein engineering. *Biochemistry* **32,** 5145-5150 (1993).

2. Shapiro, R. Cytoplasmic ribonuclease inhibitor. W. N. Allen, Ed. Volume 341, Academic Press, p. 611-628 (2001).

3. Shapiro, R. and Vallee, B. L. Interaction of human placental ribonuclease with placental ribonuclease inhibitor. *Biochemistry* **30,** 2246-2255 (1991).

4. Clackson, T. and Wells, J. A. A hot spot of binding energy in a hormone-receptor interface. *Science* **267,** 383-386 (1995).

5. Bogan, A. A. and Thorn, K. S. Anatomy of hot spots in protein interfaces. *J. Mol. Biol.* **280,** 1-9 (1998).

6. Reichmann, D., Rahat, O., Cohen, M., Neuvirth, H. and Schreiber, G. The molecular architecture of protein-protein binding sites. *Curr. Opin. Struct. Biol.* **17,** 67-76 (2007).

7. Moreira, I. S., Fernandes, P. A. and Ramos, M. J. Hot spots - A review of the protein-protein interface determinant amino-acid residues. *Proteins Struc. Funct. Bioinf.* **68,** 803-812 (2007).

8. Crowley, P. B. and Ubbink, M. Close encounters of the transient kind: protein interactions in the photosynthetic redox chain investigated by NMR spectroscopy. *Acc. Chem. Res.* **36,** 723-730 (2003).

9. Prudêncio, M. and Ubbink, M. Transient complexes of redox proteins: structural and dynamic details from NMR studies. *J. Mol. Recognit.* **17,** 524-539 (2004).

10. Kang, C. H., Ferguson-Miller, S. and Margoliash, E. Steady-state kinetics and binding of eukaryotic cytochromes *c* with yeast cytochrome *c* peroxidase. *J. Biol. Chem.* **252,** 919-926 (1977).

11. Sétif, P. Q. Y. and Bottin, H. Laser flash absorption spectroscopy study of ferredoxin reduction by photosystem I: spectral and kinetic evidence for the existence of several photosystem I-ferredoxin complexes. *Biochemistry* **34,** 9059-9070 (1995).

12. Hervás, M., Navarro, J. A., Díaz, A., Bottin, H. and De la Rosa, M. A. Laser-flash kinetic analysis of the fast electron transfer from plastocyanin and cytochrome c_6 to photosystem I. Experimental evidence on the evolution of the reaction mechanism. *Biochemistry* **34,** 11321-11326 (1995).

----

13. Schlarb-Ridley, B. G., Bendall, D. S. and Howe, C. J. Role of electrostatics in the interaction between cytochrome *f* and plastocyanin of the cyanobacterium *Phormidium laminosum. Biochemistry* **41,** 3279-3285 (2002).

14. Crowley, P. B. and Carrondo, M. A. The architecture of the binding site in redox protein complexes: Implications for fast dissociation. *Proteins Struc. Funct. Bioinf.* **55,** 603-612 (2004).

15. Matthew, J. B., Weber, P. C., Salemme, F. R. and Richards, F. M. Electrostatic orientation during electron transfer between flavodoxin and cytochrome c. *Nature* **301,** 169-171 (1983).

16. Kannt, A., Young, S. and Bendall, D. S. The role of acidic residues of plastocyanin in its interaction with cytochrome *f. Biochim. Biophys. Acta* **1277,** 115-126 (1996).

17. Janin, J. The kinetics of protein-protein recognition. *Proteins* **28,** 153-161 (1997).

18. Sheinerman, F. B., Norel, R. and Honig, B. Electrostatic aspects of protein-protein interactions. *Curr. Opin. Struct. Biol.* **10,** 153-159 (2000).

19. Smoluchowski, M. V. Versuch einer matematischen Theorie der Koagulationskinetik kolloider Lösungen. *Z. Phys. Chem.* **92,** 129-168 (1917).

20. Tsai, C. J., Lin, S. L., Wolfson, H. J. and Nussinov, R. Studies of protein-protein interfaces: a statistical analysis of the hydrophobic effect. *Protein Sci.* **6,** 53-64 (1997).

21. Berg, O. G. and von Hippel, P. H. Diffusion-controlled macromolecular interactions. *Annu. Rev. Biophys. Biophys. Chem.* **14,** 131-160 (1985).

22. Northrup, S. H. and Erickson, H. P. Kinetics of protein-protein association explained by Brownian dynamics computer simulation. *Proc. Natl. Acad. Sci. U. S. A* **89,** 3338-3342 (1992).

23. Schreiber, G. and Fersht, A. R. Rapid, electrostatically assisted association of proteins. *Nat. Struct. Biol.* **3,** 427-431 (1996).

24. Kang, C. H., Brautigan, D. L., Osheroff, N. and Margoliash, E. Definition of cytochrome *c* binding domains by chemical modification. Reaction of carboxydinitrophenyl- and trinitrophenyl-cytochromes *c* with baker's yeast cytochrome *c* peroxidase. *J. Biol. Chem.* **253,** 6502-6510 (1978).

25. Eltis, L. D., Herbert, R. G., Barker, P. D., Mauk, A. G. and Northrup, S. H. Reduction of horse heart ferricytochrome *c* by bovine liver ferrocytochrome b_5. Experimental and theoretical analysis. *Biochemistry* **30,** 3663-3674 (1991).

----

26. Hervás, M., Navarro, J. A., Molina-Heredia, F. P. and De la Rosa, M. A. The reaction mechanism of Photosystem I reduction by plastocyanin and cytochrome c_6 follows two different kinetic models in the cyanobacterium *Pseudanabaena* sp. PCC 6903. *Photosynth. Res.* **57,** 93-100 (1998).

27. McLendon, G. Control of biological electron-transport via molecular recognition and binding - the Velcro model. *Struc. Bond.* **75,** 159-174 (1991).

28. Qin, L. and Kostic, N. M. Importance of protein rearrangement in the electron-transfer reaction between the physiological partners cytochrome *f* and plastocyanin. *Biochemistry* **32,** 6073-6080 (1993).

29. Ubbink, M., Ejdeback, M., Karlsson, B. G. and Bendall, D. S. The structure of the complex of plastocyanin and cytochrome *f*, determined by paramagnetic NMR and restrained rigid-body molecular dynamics. *Structure* **6,** 323-335 (1998).

30. Lange, C., Cornvik, T., Díaz-Moreno, I. and Ubbink, M. The transient complex of poplar plastocyanin with cytochrome *f*: effects of ionic strength and pH. *Biochim. Biophys. Acta* **1707,** 179-188 (2005).

31. Volkov, A. N., Worrall, J. A. R., Holtzmann, E. and Ubbink, M. Solution structure and dynamics of the complex between cytochrome *c* and cytochrome *c* peroxidase determined by paramagnetic NMR. *Proc. Natl. Acad. Sci. U. S. A* **103,** 18945-18950 (2006).

32. Liang, Z. X., Jiang, M., Ning, Q. and Hoffman, B. M. Dynamic docking and electron transfer between myoglobin and cytochrome b_5. *J. Biol. Inorg. Chem* **7,** 580-588 (2002).

33. Worrall, J. A. R., Liu, Y. J., Crowley, P. B., Nocek, J. M., Hoffman, B. M. and Ubbink, M. Myoglobin and cytochrome b_5: A Nuclear Magnetic Resonance study of a highly dynamic protein complex. *Biochemistry* **41,** 11721-11730 (2002).

34. Hoffman, B. M., Celis, L. M., Cull, D. A., Patel, A. D., Seifert, J. L., Wheeler, K. E., Wang, J. Y., Yao, J., Kurnikov, I. V. and Nocek, J. M. Differential influence of dynamic processes on forward and reverse electron transfer across a protein-protein interface. *Proc. Natl. Acad. Sci. U. S. A* **102,** 3564-3569 (2005).

35. Volkov, A. N. *Transient complexes of haem proteins*. Ph.D. Thesis (Leiden University, Leiden, the Netherlands, 2007).

36. Henzler-Wildman, K. and Kern, D. Dynamic personalities of proteins. *Nature* **450,** 964-972 (2007).

37. Zuiderweg, E. R. Mapping protein-protein interactions in solution by NMR spectroscopy. *Biochemistry* **41,** 1-7 (2002).

----

38.   Worrall, J. A. R., Reinle, W., Bernhardt, R. and Ubbink, M. Transient protein interactions studied by NMR spectroscopy: The case of cytochrome *c* and adrenodoxin. *Biochemistry* **42,** 7068-7076 (2003).

39.   Iwahara, J. and Clore, G. M. Detecting transient intermediates in macromolecular binding by paramagnetic NMR. *Nature* **440,** 1227-1230 (2006).

40.   Crowley, P. B., Otting, G., Schlarb-Ridley, B. G., Canters, G. W. and Ubbink, M. Hydrophobic interactions in a cyanobacterial plastocyanin-cytochrome *f* complex. *J. Am. Chem. Soc.* **123,** 10444-10453 (2001).

41.   Díaz-Moreno, I., Díaz-Quintana, A., De la Rosa, M. A., Crowley, P. B. and Ubbink, M. Different modes of interaction in cyanobacterial complexes of plastocyanin and cytochrome *f*. *Biochemistry* **44,** 3176-3183 (2005).

42.   Arnesano, F., Banci, L. and Piccioli, M. NMR structures of paramagnetic metalloproteins. *Q. Rev. Biophys.* **38,** 167-219 (2005).

43.   Iwahara, J., Anderson, D. E., Murphy, E. C. and Clore, G. M. EDTA-derivatized deoxythymidine as a tool for rapid determination of protein binding polarity to DNA by intermolecular paramagnetic relaxation enhancement. *J. Am. Chem. Soc.* **125,** 6634-6635 (2003).

44.   Gaponenko, V., Sarma, S. P., Altieri, A. S., Horita, D. A., Li, J. and Byrd, R. A. Improving the accuracy of NMR structures of large proteins using pseudocontact shifts as long-range restraints. *J. Biomol. NMR* **28,** 205-212 (2004).

45.   Prudêncio, M., Rohovec, J., Peters, J. A., Tocheva, E., Boulanger, M. J., Murphy, M. E. P., Hupkes, H. J., Kosters, W., Impagliazzo, A. and Ubbink, M. A caged lanthanide complex as a paramagnetic shift agent for protein NMR. *Chem. Eur. J.* **10,** 3252-3260 (2004).

46.   Iwahara, J., Schwieters, C. D. and Clore, G. M. Characterization of nonspecific protein-DNA interactions by ^{1}H paramagnetic relaxation enhancement. *J. Am. Chem. Soc.* **126,** 12800-12808 (2004).

47.   Rodriguez-Castañeda, F., Haberz, P., Leonov, A. and Griesinger, C. Paramagnetic tagging of diamagnetic proteins for solution NMR. *Magn. Reson. Chem.* **44,** S10-S16 (2006).

48.   Vlasie, M. D., Comuzzi, C., van den Nieuwendijk, A. M. C. H., Prudêncio, M., Overhand, M. and Ubbink, M. Long-range-distance NMR effects in a protein labeled with a lanthanide-DOTA chelate. *Chem. Eur. J.* **13,** 1715-1723 (2007).

49.   Keizers, P. H. J., Desreux, J. F., Overhand, M. and Ubbink, M. Increased paramagnetic effect of a lanthanide protein probe by two-point attachment. *J. Am. Chem. Soc.* **129,** 9292-+ (2007).

----

50.   Gillespie, J. R. and Shortle, D. Characterization of long-range structure in the denatured state of staphylococcal nuclease. I. Paramagnetic relaxation enhancement by nitroxide spin labels. *J. Mol. Biol.* **268,** 158-169 (1997).

51.   Gaponenko, V., Howarth, J. W., Columbus, L., Gasmi-Seabrook, G., Yuan, J., Hubbell, W. L. and Rosevear, P. R. Protein global fold determination using site-directed spin and isotope labeling. *Protein Sci.* **9,** 302-309 (2000).

52.   Battiste, J. L. and Wagner, G. Utilization of site-directed spin labeling and high-resolution heteronuclear nuclear magnetic resonance for global fold determination of large proteins with limited nuclear Overhauser effect data. *Biochemistry* **39,** 5355-5365 (2000).

53.   Dedmon, M. M., Lindorff-Larsen, K., Christodoulou, J., Vendruscolo, M. and Dobson, C. M. Mapping long-range interactions in α-synuclein using spin-label NMR and ensemble molecular dynamics simulations. *J. Am. Chem. Soc.* **127,** 476-477 (2005).

54.   Liang, B. Y., Bushweller, J. H. and Tamm, L. K. Site-directed parallel spin-labeling and paramagnetic relaxation enhancement in structure determination of membrane proteins by solution NMR spectroscopy. *J. Am. Chem. Soc.* **128,** 4389-4397 (2006).

55.   Iwahara, J., Schwieters, C. D. and Clore, G. M. Ensemble approach for NMR structure refinement against ^{1}H paramagnetic relaxation enhancement data arising from a flexible paramagnetic group attached to a macromolecule. *J. Am. Chem. Soc.* **126,** 5879-5896 (2004).

56.   Nelson, N. and Ben Shem, A. The complex architecture of oxygenic photosynthesis. *Nat. Rev. Mol. Cell Biol.* **5,** 971-982 (2004).

57.   Kruse, O., Rupprecht, J., Mussgnug, J. H., Dismukes, G. C. and Hankamer, B. Photosynthesis: a blueprint for solar energy capture and biohydrogen production technologies. *Photochem. Photobiol. Sci.* **4,** 957-970 (2005).

58.   Noy, D., Moser, C. C. and Dutton, P. L. Design and engineering of photosynthetic light-harvesting and electron transfer using length, time, and energy scales. *Biochim. Biophys. Acta* **1757,** 90-105 (2006).

59.   Iverson, T. M. Evolution and unique bioenergetic mechanisms in oxygenic photosynthesis. *Curr. Opin. Chem. Biol.* **10,** 91-100 (2006).

60.   Edited from http://www.ualr.edu/botany/psimages.html (2007).

61.   Katoh, S. New copper protein from *Chlorella Ellipsoidea*. *Nature* **186,** 533-534 (1960).

62.   Katoh, S. and Takamiya, A. A new leaf copper protein plastocyanin, a natural Hill oxidant. *Nature* **189,** 665-& (1961).

63. Kimimura, M. and Katoh, S. Studies on electron transport associated with Photosystem I .I. Functional site of plastocyanin: inhibitory effects of HgCl$_2$ on electron transport and plastocyanin in chloroplasts. *Biochim. Biophys. Acta* **283,** 279-& (1972).

64. DeLano, W. L. The PyMOL Molecular Graphics System. http://www.pymol.org (2002).

65. Guss, J. M., Harrowell, P. R., Murata, M., Norris, V. A. and Freeman, H. C. Crystal-structure analyses of reduced Cu(I) poplar plastocyanin at 6 pH values. *J. Mol. Biol.* **192,** 361-387 (1986).

66. Moore, J. M., Case, D. A., Chazin, W. J., Gippert, G. P., Havel, T. F., Powls, R. and Wright, P. E. Three-dimensional solution structure of plastocyanin from the green alga *Scenedesmus obliquus*. *Science* **240,** 314-317 (1988).

67. Collyer, C. A., Guss, J. M., Sugimura, Y., Yoshizaki, F. and Freeman, H. C. Crystal structure of plastocyanin from a green alga, *Enteromorpha prolifera*. *J. Mol. Biol.* **211,** 617-632 (1990).

68. Moore, J. M., Lepre, C. A., Gippert, G. P., Chazin, W. J., Case, D. A. and Wright, P. E. High-resolution solution structure of reduced French bean plastocyanin and comparison with the crystal structure of poplar plastocyanin. *J. Mol. Biol.* **221,** 533-555 (1991).

69. Redinbo, M. R., Cascio, D., Choukair, M. K., Rice, D., Merchant, S. and Yeates, T. O. The 1.5 Å crystal structure of plastocyanin from the green alga *Chlamydomonas reinhardtii*. *Biochemistry* **32,** 10560-10567 (1993).

70. Bagby, S., Driscoll, P. C., Harvey, T. S. and Hill, H. A. High-resolution solution structure of reduced parsley plastocyanin. *Biochemistry* **33,** 6611-6622 (1994).

71. Badsberg, U., Jorgensen, A. M., Gesmar, H., Led, J. J., Hammerstad, J. M., Jespersen, L. L. and Ulstrup, J. Solution structure of reduced plastocyanin from the blue-green alga *Anabaena variabilis*. *Biochemistry* **35,** 7021-7031 (1996).

72. Romero, A., De la Cerda, B., Varela, P. F., Navarro, J. A., Hervás, M. and De la Rosa, M. A. The 2.15 Å crystal structure of a triple mutant plastocyanin from the cyanobacterium *Synechocystis* sp. PCC 6803. *J. Mol. Biol.* **275,** 327-336 (1998).

73. Xue, Y., Okvist, M., Hansson, Ö. and Young, S. Crystal structure of spinach plastocyanin at 1.7 Å resolution. *Protein Sci.* **7,** 2099-2105 (1998).

74. Bond, C. S., Bendall, D. S., Freeman, H. C., Guss, J. M., Howe, C. J., Wagner, M. J. and Wilce, M. C. J. The structure of plastocyanin from the cyanobacterium *Phormidium laminosum*. *Acta Crystallogr. D* **55,** 414-421 (1999).

----

75. Shibata, N., Inoue, T., Nagano, C., Nishio, N., Kohzuma, T., Onodera, K., Yoshizaki, F., Sugimura, Y. and Kai, Y. Novel insight into the copper-ligand geometry in the crystal structure of *Ulva pertusa* plastocyanin at 1.6 Å resolution. Structural basis for regulation of the copper site by residue 88. *J. Biol. Chem.* **274,** 4225-4230 (1999).

76. Babu, C. R., Volkman, B. F. and Bullerjahn, G. S. NMR solution structure of plastocyanin from the photosynthetic prokaryote, *Prochlorothrix hollandica*. *Biochemistry* **38,** 4988-4995 (1999).

77. Kohzuma, T. *et al*. The structure and unusual pH dependence of plastocyanin from the fern *Dryopteris crassirhizoma*. The protonation of an active site histidine is hindered by π-π interactions. *J. Biol. Chem.* **274,** 11817-11823 (1999).

78. Inoue, T., Sugawara, H., Hamanaka, S., Tsukui, H., Suzuki, E., Kohzuma, T. and Kai, Y. Crystal structure determinations of oxidized and reduced plastocyanin from the cyanobacterium *Synechococcus* sp. PCC 7942. *Biochemistry* **38,** 6063-6069 (1999).

79. Sugawara, H., Inoue, T., Li, C., Gotowda, M., Hibino, T., Takabe, T. and Kai, Y. Crystal structures of wild-type and mutant plastocyanins from a higher plant, Silene. *J. Biochem. (Tokyo)* **125,** 899-903 (1999).

80. Bertini, I., Ciurli, S., Dikiy, A., Fernandez, C. O., Luchinat, C., Safarov, N., Shumilin, S. and Vila, A. J. The first solution structure of a paramagnetic copper(II) protein: the case of oxidized plastocyanin from the cyanobacterium *Synechocystis* PCC6803. *J. Am. Chem. Soc.* **123,** 2405-2413 (2001).

81. Bertini, I., Bryant, D. A., Ciurli, S., Dikiy, A., Fernandez, C. O., Luchinat, C., Safarov, N., Vila, A. J. and Zhao, J. Backbone dynamics of plastocyanin in both oxidation states. Solution structure of the reduced form and comparison with the oxidized state. *J. Biol. Chem.* **276,** 47217-47226 (2001).

82. Sykes, A. G. Active-site properties of the blue copper proteins. *Advan. Inorg. Chem.* **36,** 377-408 (1991).

83. Canters, G. W. and Gilardi, G. Engineering type 1 copper sites in proteins. *FEBS Lett.* **325,** 39-48 (1993).

84. Gray, H. B., Malmstrom, B. G. and Williams, R. J. Copper coordination in blue proteins. *J. Biol. Inorg. Chem.* **5,** 551-559 (2000).

85. Dennison, C., Lawler, A. T. and Kohzuma, T. Unusual properties of plastocyanin from the fern *Dryopteris crassirhizoma*. *Biochemistry* **41,** 552-560 (2002).

86. Hulsker, R., Mery, A., Thomassen, E. A., Ranieri, A., Sola, M., Verbeet, M. P., Kohzuma, T. and Ubbink, M. Protonation of a histidine copper ligand in fern plastocyanin. *J. Am. Chem. Soc.* **129,** 4423-4429 (2007).

87. Crowley, P. B., Vintonenko, N., Bullerjahn, G. S. and Ubbink, M. Plastocyanin-cytochrome *f* interactions: The influence of hydrophobic patch mutations studied by NMR spectroscopy. *Biochemistry* **41,** 15698-15705 (2002).

88. Chapman, S. K., Sanemasa, I., Watson, A. D. and Sykes, A. G. Kinetic studies on 1-1 electron-transfer reactions involving blue copper proteins. 5. Reactions of parsley plastocyanin and Pseudomonas aeruginosa azurin with the negatively charged oxidants $[(Nc)_5FeCNCo(CN)_5]^{5-}$ and $[Fe(CN)_6]^{3-}$. *J. Chem. Soc. , Dalton Trans.* 1949-1953 (1983).

89. Chapman, S. K., Watson, A. D. and Sykes, A. G. Kinetic studies on 1-1 electron-transfer reactions involving blue copper proteins. 6. Competitive inhibition of the $[Co(Phen)_3]^{3+}$ (Phen = 1,10-Phenanthroline) oxidation of parsley plastocyanin PCu(I) by redox inactive complexes. *J. Chem. Soc. , Dalton Trans.* 2543-2548 (1983).

90. Chapman, S. K., Sanemasa, I. and Sykes, A. G. Kinetic studies on 1-1 electron-transfer reactions involving blue copper proteins. 7. Effects of pH and redox inactive $[Pt(NH_3)_6]^{4+}$ on reactions of parsley plastocyanin with different inorganic redox partners. *J. Chem. Soc. , Dalton Trans.* 2549-2553 (1983).

91. Chapman, S. K., Knox, C. V., Kathirgamanathan, P. and Sykes, A. G. Kinetic studies on 1-1 electron-transfer reactions involving blue copper proteins. 9. Effects of chromium(III) modification on reactions of plastocyanin with $[Co(Phen)_3]^{3+}$ (Phen = 1,10-phenanthroline), $[Fe(CN)_6]^{3-}$, $[Co(Dipic)_2]^{-}$ (Dipic = Dipicolinate) (Oxidants) and $[Ru(NH_3)_5(Py)]^{2+}$ (Py = Pyridine) (Reductant)PL. *J. Chem. Soc. , Dalton Trans.* 2769-2773 (1984).

92. Chapman, S. K., Knox, C. V. and Sykes, A. G. Kinetic studies on 1-1 electron-transfer reactions involving blue copper proteins. 10. The assignment of binding-sites in the reactions of plastocyanin (and azurin) with non-physiological protein redox partners. *J. Chem. Soc. , Dalton Trans.* 2775-2780 (1984).

93. McGinnis, J., Sinclairday, J. D. and Sykes, A. G. Evidence for reaction at 2 binding-sites in the oxidation of parsley plastocyanin by Tris(1,10-phenanthroline)cobalt(III). *J. Chem. Soc. , Dalton Trans.* 2007-2009 (1986).

94. Sinclairday, J. D. and Sykes, A. G. Kinetic studies on 1-1 electron-transfer reactions involving blue copper proteins. 12. Reactions of spinach plastocyanin with inorganic redox partners. *J. Chem. Soc. , Dalton Trans.* 2069-2073 (1986).

95. Jackman, M. P., Sinclairday, J. D., Sisley, M. J., Sykes, A. G., Denys, L. A. and Wright, P. E. Kinetic studies on 1-1 electron-transfer reactions involving blue copper proteins. 15. The reactivity of *Anabaena variabilis* plastocyanin with inorganic complexes and related NMR studies. *J. Am. Chem. Soc.* **109,** 6443-6449 (1987).

96. Jackman, M. P., McGinnis, J., Sykes, A. G., Collyer, C. A., Murata, M. and Freeman, H. C. Kinetic studies on 1-1 electron-transfer reactions involving blue copper proteins. 14. Reactions of poplar plastocyanin with inorganic complexes. *J. Chem. Soc. , Dalton Trans.* 2573-2577 (1987).

97. McGinnis, J., Sinclairday, J. D., Sykes, A. G., Powls, R., Moore, J. and Wright, P. E. Kinetic studies on 1-1 electron-transfer reactions involving blue copper proteins. 16. Reactivity of plastocyanin from the green-alga *Scenedesmus obliquus* with inorganic redox partners and related NMR studies. *Inorg. Chem.* **27,** 2306-2312 (1988).

98. Albarrán, C., Navarro, J. A., De la Rosa, M. A. and Hervás, M. The specificity in the interaction between cytochrome *f* and plastocyanin from the cyanobacterium *Nostoc* sp. PCC 7119 is mainly determined by the copper protein. *Biochemistry* **46,** 997-1003 (2007).

99. Bendall, D. S. The unfinished story of cytochrome *f. Photosynth. Res.* **80,** 265-276 (2004).

100. Hill, R. and Scarisbrick, R. The haematin compunds of leaves. *New Phytol.* **50,** 98-111 (1951).

101. Takahashi, M. A. and Asada, K. Purification of cytochrome *f* from Japanese radish leaves. *Plant and Cell Physiology* **16,** 191-194 (1975).

102. Gray, J. C., Rochford, R. J. and Packman, L. C. Proteolytic removal of the C-terminal transmembrane region of cytochrome *f* during extraction from turnip and charlock leaves generates a water-soluble monomeric form of the protein. *Eur. J. Biochem.* **223,** 481-488 (1994).

103. Kurisu, G., Zhang, H., Smith, J. L. and Cramer, W. A. Structure of the cytochrome b_6f complex of oxygenic photosynthesis: tuning the cavity. *Science* **302,** 1009-1014 (2003).

104. Stroebel, D., Choquet, Y., Popot, J. L. and Picot, D. An atypical haem in the cytochrome b_6f complex. *Nature* **426,** 413-418 (2003).

105. Martinez, S. E., Huang, D., Szczepaniak, A., Cramer, W. A. and Smith, J. L. Crystal structure of chloroplast cytochrome *f* reveals a novel cytochrome fold and unexpected heme ligation. *Structure.* **2,** 95-105 (1994).

106. Martinez, S. E., Huang, D., Ponomarev, M., Cramer, W. A. and Smith, J. L. The heme redox center of chloroplast cytochrome *f* is linked to a buried five-water chain. *Protein Sci.* **5,** 1081-1092 (1996).

107. Carrell, C. J., Schlarb, B. G., Bendall, D. S., Howe, C. J., Cramer, W. A. and Smith, J. L. Structure of the soluble domain of cytochrome *f* from the cyanobacterium *Phormidium laminosum. Biochemistry* **38,** 9590-9599 (1999).

108. Chi, Y. I., Huang, L. S., Zhang, Z., Fernández-Velasco, J. G. and Berry, E. A. X-ray structure of a truncated form of cytochrome *f* from *Chlamydomonas reinhardtii*. *Biochemistry* **39,** 7689-7701 (2000).

109. Díaz-Moreno, I., Díaz-Quintana, A., De la Rosa, M. A. and Ubbink, M. Structure of the complex between plastocyanin and cytochrome *f* from the cyanobacterium *Nostoc* sp. PCC 7119 as determined by paramagnetic NMR. *J. Biol. Chem.* **280,** 18908-18915 (2005).

110. Moore, G. R. and Pettigrew, G. W. *Cytochrome c: Evolutionary, structural and physiochemical aspects*, Springer-Verlag, Berlin (1990).

111. Wood, P. M. Interchangeable copper and iron proteins in algal photosynthesis. Studies on plastocyanin and cytochrome c-552 in *Chlamydomonas*. *Eur. J. Biochem.* **87,** 9-19 (1978).

112. Nishimura, M. A new hematin compound isolated from *Euglena gracilis*. *J. Biochem.* **46,** 219-223 (1959).

113. Marcaida, M. J., Schlarb-Ridley, B. G., Worrall, J. A. R., Wastl, J., Evans, T. J., Bendall, D. S., Luisi, B. F. and Howe, C. J. Structure of cytochrome c_{6A}, a novel dithio-cytochrome of *Arabidopsis thaliana*, and its reactivity with plastocyanin: Implications for function. *J. Mol. Biol.* **360,** 968-977 (2006).

114. Worrall, J. A. R., Schlarb-Ridley, B. G., Reda, T., Marcaida, M. J., Moorlen, R. J., Wastl, J., Hirst, J., Bendall, D. S., Luisi, B. F. and Howe, C. J. Modulation of heme redox potential in the cytochrome c_6 family. *J. Am. Chem. Soc.* **129,** 9468-9475 (2007).

115. Molina-Heredia, F. P., Wastl, J., Navarro, J. A., Bendall, D. S., Hervás, M., Howe, C. J. and De la Rosa, M. A. A new function for an old cytochrome? *Nature* **424,** 33-34 (2003).

116. Weigel, M., Varotto, C., Pesaresi, P., Finazzi, G., Rappaport, F., Salamini, F. and Leister, D. Plastocyanin is indispensable for photosynthetic electron flow in *Arabidopsis thaliana*. *J. Biol. Chem.* **278,** 31286-31289 (2003).

117. Gupta, R., He, Z. and Luan, S. Functional relationship of cytochrome c_6 and plastocyanin in *Arabidopsis*. *Nature* **417,** 567-571 (2002).

118. Kerfeld, C. A., Anwar, H. P., Interrante, R., Merchant, S. and Yeates, T. O. The structure of chloroplast cytochrome c_6 at 1.9 Å resolution: Evidence for functional oligomerization. *J. Mol. Biol.* **250,** 627-647 (1995).

119. Frazão, C., Soares, C. M., Carrondo, M. A., Pohl, E., Dauter, Z., Wilson, K. S., Hervás, M., Navarro, J. A., De la Rosa, M. A. and Sheldrick, G. M. Ab *initio* determination of the crystal structure of cytochrome c_6 and comparison with plastocyanin. *Structure* **3,** 1159-1169 (1995).

122

---

120. Banci, L., Bertini, I., Quacquarini, G., Walter, O., Díaz, A., Hervás, M. and De la Rosa, M. A. The solution structure of cytochrome c_6 from the green alga *Monoraphidium braunii*. *J. Biol. Inorg. Chem* **1,** 330-340 (1996).

121. Beissinger, M., Sticht, H., Sutter, M., Ejchart, A., Haehnel, W. and Rösch, P. Solution structure of cytochrome c_6 from the thermophilic cyanobacterium *Synechococcus elongatus*. *EMBO J.* **17,** 27-36 (1998).

122. Banci, L., Bertini, I., De la Rosa, M. A., Koulougliotis, D., Navarro, J. A. and Walter, O. Solution structure of oxidized cytochrome c_6 from the green alga *Monoraphidium braunii*. *Biochemistry* **37,** 4831-4843 (1998).

123. Schnackenberg, J., Than, M. E., Mann, K., Wiegand, G., Huber, R. and Reuter, W. Amino acid sequence, crystallization and structure determination of reduced and oxidized cytochrome c_6 from the green alga *Scenedesmus obliquus*. *J. Mol. Biol.* **290,** 1019-1030 (1999).

124. Yamada, S. *et al*. Structure of cytochrome c_6 from the red alga *Porphyra yezoensis* at 1.57 Å resolution. *Acta Crystallogr. D* **56,** 1577-1582 (2000).

125. Sawaya, M. R., Krogmann, D. W., Serag, A., Ho, K. K., Yeates, T. O. and Kerfeld, C. A. Structures of cytochrome c-549 and cytochrome c_6 from the cyanobacterium *Arthrospira maxim*a. *Biochemistry* **40,** 9215-9225 (2001).

126. Dikiy, A., Carpentier, W., Vandenberghe, I., Borsari, M., Safarov, N., Dikaya, E., Van Beeumen, J. and Ciurli, S. Structural basis for the molecular properties of cytochrome c_6. *Biochemistry* **41,** 14689-14699 (2002).

127. Campos, A. P., Aguiar, A. P., Hervás, M., Regalla, M., Navarro, J. A., Ortega, J. M., Xavier, A. V., De la Rosa, M. A. and Teixeira, M. Cytochrome c_6 from *Monoraphidium-Braunii:* A cytochrome with an unusual heme axial coordination. *Eur. J. Biochem.* **216,** 329-341 (1993).

128. Hervás, M., Navarro, J. A. and De la Rosa, M. A. Electron transfer between membrane complexes and soluble proteins in photosynthesis. *Acc. Chem. Res.* **36,** 798-805 (2003).

129. De la Rosa, M. A., Navarro, J. A., Díaz-Quintana, A., De la Cerda, B., Molina-Heredia, F. P., Balme, A., Murdoch, P. D., Díaz-Moreno, I., Durán, R. V. and Hervás, M. An evolutionary analysis of the reaction mechanisms of photosystem I reduction by cytochrome c_6 and plastocyanin. *Bioelectrochemistry* **55,** 41-45 (2002).

130. Qin, L. and Kostic, N. M. Electron-transfer reactions of cytochrome *f* with flavin semiquinones and with plastocyanin. Importance of protein-protein electrostatic interactions and of donor-acceptor coupling. *Biochemistry* **31,** 5145-5150 (1992).

131. Hart, S. E., Schlarb-Ridley, B. G., Delon, C., Bendall, D. S. and Howe, C. J. Role of charges on cytochrome *f* from the cyanobacterium *Phormidium laminosum* in its interaction with plastocyanin. *Biochemistry* **42,** 4829-4836 (2003).

132. Ullmann, G. M., Knapp, E. W. and Kostic, N. M. Computational simulation and analysis of dynamic association between plastocyanin and cytochrome *f*. Consequences for the electron-transfer reaction. *J. Am. Chem. Soc.* **119,** 42-52 (1997).

133. Pearson, D. C. and Gross, E. L. Brownian dynamics study of the interaction between plastocyanin and cytochrome *f*. *Biophys. J.* **75,** 2698-2711 (1998).

134. De Rienzo, F., Gabdoulline, R. R., Menziani, M. C., De Benedetti, P. G. and Wade, R. C. Electrostatic analysis and Brownian dynamics simulation of the association of plastocyanin and cytochrome *f*. *Biophys. J.* **81,** 3090-3104 (2001).

135. Díaz-Moreno, I., Díaz-Quintana, A., Ubbink, M. and De la Rosa, M. A. An NMR-based docking model for the physiological transient complex between cytochrome *f* and cytochrome c_6. *FEBS Lett.* **579,** 2891-2896 (2005).

136. Crowley, P. B., Díaz-Quintana, A., Molina-Heredia, F. P., Nieto, P., Sutter, M., Haehnel, W., De la Rosa, M. A. and Ubbink, M. The interactions of cyanobacterial cytochrome c_6 and cytochrome *f*, characterized by NMR. *J. Biol. Chem.* **277,** 48685-48689 (2002).

137. Gross, E. L. and Pearson, D. C. Brownian dynamics simulations of the interaction of *Chlamydomonas* cytochrome *f* with plastocyanin and cytochrome c_6. *Biophys. J.* **85,** 2055-2068 (2003).

138. Ubbink, M. Complexes of photosynthetic redox proteins studied by NMR. *Photosynth. Res.* **81,** 277-287 (2004).

139. Sykes, A. G. Plastocyanin and the blue copper proteins. *Struc. Bond.* **75,** 175-224 (1991).

140. Canters, G. W., Kolczak, U., Armstrong, F., Jeuken, L. J. C., Camba, R. and Sola, M. The effect of pH and ligand exchange on the redox properties of blue copper proteins. *Faraday Discuss.*205-220 (2000).

141. Solomon, E. I., Szilagyi, R. K., George, S. D. and Basumallick, L. Electronic structures of metal sites in proteins and models: Contributions to function in blue copper proteins. *Chem. Rev.* **104,** 419-458 (2004).

142. Hope, A. B. Electron transfers amongst cytochrome *f*, plastocyanin and photosystem I: kinetics and mechanisms. *Biochim. Biophys. Acta* **1456,** 5-26 (2000).

---

143. Díaz-Quintana, A., Navarro, J. A., Hervás, M., Molina-Heredia, F. P., De la Cerda, B. and De la Rosa, M. A. A comparative structural and functional analysis of cyanobacterial plastocyanin and cytochrome c_6 as alternative electron donors to Photosystem I - Photosystem I reduction in cyanobacteria. *Photosynth. Res.* **75,** 97-110 (2003).

144. Díaz-Moreno, I., Díaz-Quintana, A., De la Rosa, M. A. and Ubbink, M. Structure of the complex between plastocyanin and cytochrome *f* from the cyanobacterium *Nostoc* sp. PCC 7119 as determined by paramagnetic NMR. *J. Biol. Chem.* **280,** 18908-18915 (2005).

145. Hunter, D. M., McFarlane, W., Sykes, A. G. and Dennison, C. Effect of pH on the self-exchange reactivity of the plant plastocyanin from parsley. *Inorg. Chem.* **40,** 354-360 (2001).

146. Dennison, C., Kohzuma, T., McFarlane, W., Suzuki, S. and Sykes, A. G. Reactivity of pseudoazurin from *Achromobacter cycloclastes* with inorganic redox partners and related NMR and electrochemical studies. *Inorg. Chem.* **33,** 3299-3305 (1994).

147. Yanagisawa, S., Sato, K., Kikuchi, M., Kohzuma, T. and Dennison, C. Introduction of a π-π interaction at the active site of a cupredoxin: Characterization of the Met16Phe pseudoazurin mutant. *Biochemistry* **42,** 6853-6862 (2003).

148. Impagliazzo, A. Transient protein interactions: The case of pseudoazurin and nitrite reductase. Ph.D. Thesis, (Leiden University, 2005).

149. Lommen, A. and Canters, G. W. pH-dependent redox activity and fluxionality of the copper site in amicyanin from *Thiobacillus versutus* as studied by 300-MHz and 600-MHz ^{1}H NMR. *J. Biol. Chem.* **265,** 2768-2774 (1990).

150. Zhu, Z. Y., Cunane, L. M., Chen, Z. W., Durley, R. C. E., Mathews, F. S. and Davidson, V. L. Molecular basis for interprotein complex-dependent effects on the redox properties of amicyanin. *Biochemistry* **37,** 17128-17136 (1998).

151. Groeneveld, C. M., Feiters, M. C., Hasnain, S. S., Vanrijn, J., Reedijk, J. and Canters, G. W. The pH and redox-state dependence of the copper site in azurin from *Pseudomonas aeruginosa* as studied by EXAFS. *Biochim. Biophys. Acta* **873,** 214-227 (1986).

152. Hunt, A. H., Toypalmer, A., Assamunt, N., Cavanagh, J., Blake, R. C. and Dyson, H. J. Nuclear Magnetic Resonance ^{15}N and ^{1}H resonance assignments and global fold of rusticyanin - Insights into the ligation and acid stability of the blue copper site. *J. Mol. Biol.* **244,** 370-384 (1994).

153. Jeuken, L. J. C., Ubbink, M., Bitter, J. H., van Vliet, P., Meyer-Klaucke, W. and Canters, G. W. The structural role of the copper-coordinating and surface-exposed histidine residue in the blue copper protein azurin. *J. Mol. Biol.* **299,** 737-755 (2000).

154. Guss, J. M., Harrowell, P. R., Murata, M., Norris, V. A. and Freeman, H. C. Crystal-structure analyses of reduced (CuI) poplar plastocyanin at 6 pH values. *J. Mol. Biol.* **192,** 361-387 (1986).

155. Lommen, A., Canters, G. W. and Vanbeeumen, J. A ^{1}H NMR study on the blue copper protein amicyanin from *Thiobacillus versutus* - Resonance identifications, structural rearrangements and determination of the electron self-exchange rate-constant. *Eur. J. Biochem.* **176,** 213-223 (1988).

156. Vakoufari, E., Wilson, K. S. and Petratos, K. The crystal-structures of reduced pseudoazurin from *Alcaligenes faecalis*-S-6 at 2 pH values. *FEBS Lett.* **347,** 203-206 (1994).

157. Guss, J. M., Harrowell, P. R., Murata, M., Norris, V. A. and Freeman, H. C. Crystal-structure analyses of reduced (CuI) poplar plastocyanin at 6 pH values. *J. Mol. Biol.* **192,** 361-387 (1986).

158. Armstrong, F. A., Hill, H. A. O., Oliver, B. N. and Whitford, D. Direct electrochemistry of the photosynthetic blue copper protein plastocyanin - Electrostatic promotion of rapid charge-transfer at an edge-oriented pyrolytic-graphite electrode. *J. Am. Chem. Soc.* **107,** 1473-1476 (1985).

159. Kramer, D. M., Sacksteder, C. A. and Cruz, J. A. How acidic is the lumen? *Photosynth. Res.* **60,** 151-163 (1999).

160. Yanagisawa, S. and Dennison, C. Loop-contraction mutagenesis of type 1 copper sites. *J. Am. Chem. Soc.* **126,** 15711-15719 (2004).

161. Battistuzzi, G., Borsari, M., Canters, G. W., Di Rocco, G., de Waal, E., Arendsen, Y., Leonardi, A., Ranieri, A. and Sola, M. Ligand loop effects on the free energy change of redox and pH-dependent equilibria in cupredoxins probed on amicyanin variants. *Biochemistry* **44,** 9944-9949 (2005).

162. Li, C., Yanagisawa, S., Martins, B. M., Messerschmidt, A., Banfield, M. J. and Dennison, C. Basic requirements for a metal-binding site in a protein: The influence of loop shortening on the cupredoxin azurin. *Proc. Natl. Acad. Sci. U. S. A* **103,** 7258-7263 (2006).

163. Machczynski, M. C., Gray, H. B. and Richards, J. H. An outer-sphere hydrogen-bond network constrains copper coordination in blue proteins. *J. Inorg. Biochem.* **88,** 375-380 (2002).

164. Battistuzzi, G., Borsari, M., Loschi, L. and Sola, M. Redox thermodynamics, acid-base equilibria and salt-induced effects for the cucumber basic protein. General implications for blue-copper proteins. *J. Biol. Inorg. Chem* **2,** 350-359 (1997).

165. Picard, V., Ersdalbadju, E., Lu, A. Q. and Bock, S. C. A rapid and efficient one-tube PCR-based mutagenesis technique using Pfu DNA-polymerase. *Nucl. Acids Res.* **22,** 2587-2591 (1994).

166. Ubbink, M., Lian, L. Y., Modi, S., Evans, P. A. and Bendall, D. S. Analysis of the ^{1}H NMR chemical shifts of Cu(I)-, Cu(II)- and Cd-substituted pea plastocyanin - Metal-dependent differences in the hydrogen-bond network around the copper site. *Eur. J. Biochem.* **242,** 132-147 (1996).

167. Campbell, I. D., Dobson, C. M., Williams, R. J. P. and Wright, P. E. Pulse methods for simplification of protein NMR-spectra. *FEBS Lett.* **57,** 96-99 (1975).

168. Clubb, R. T., Thanabal, V. and Wagner, G. A constant-time three-dimensional triple-resonance pulse scheme to correlate intraresidue ^{1}H^{N}, ^{15}N, and ^{13}C' chemical shifts in ^{15}N-^{13}C-labeled proteins. *J. Magn. Reson.* **97,** 213-217 (1992).

169. Wittekind, M. and Mueller, L. HNCACB, A high-sensitivity 3D NMR experiment to correlate amide-proton and nitrogen resonances with the alpha-carbon and beta-carbon resonances in proteins. *J. Magn. Reson. ser. B* **101,** 201-205 (1993).

170. Kay, L. E., Xu, G. Y. and Yamazaki, T. Enhanced-sensitivity triple-resonance spectroscopy with minimal H$_2$O satuaration. *J. Magn. Reson. ser. A* **109,** 129-133 (1994).

171. Muhandiram, D. R. and Kay, L. E. Gradient-enhanced triple-resonance 3-dimensional NMR experiments with improved sensitivity. *J. Magn. Reson. ser. B* **103,** 203-216 (1994).

172. Blomberg, F., Maurer, W. and Ruterjans, H. Nuclear magnetic resonance investigation of ^{15}N-labeled histidine in aqueous solution. *J. Am. Chem. Soc.* **99,** 8149-8159 (1977).

173. Laskowski, R. A., Macarthur, M. W., Moss, D. S. and Thornton, J. M. Procheck - A program to check the stereochemical quality of protein structures. *J. Appl. Crystallog.* **26,** 283-291 (1993).

174. Navarro, J. A., Lowe, C. E., Amons, R., Kohzuma, T., Canters, G. W., De la Rosa, M. A., Ubbink, M. and Hervás, M. Functional characterization of the evolutionarily divergent fern plastocyanin. *Eur. J. Biochem.* **271,** 3449-3456 (2004).

175. Modi, S., He, S. P., Gray, J. C. and Bendall, D. S. The role of surface-exposed Tyr-83 of plastocyanin in electron-transfer from cytochrome *c*. *Biochim. Biophys. Acta* **1101,** 64-68 (1992).

176. Nar, H., Huber, R., Messerschmidt, A., Filippou, A. C., Barth, M., Jaquinod, M., Vandekamp, M. and Canters, G. W. Characterization and crystal structure of zinc azurin, a by-product of heterologous expression in *Escherichia coli* of *Pseudomonas aeruginosa* copper azurin. *Eur. J. Biochem.* **205,** 1123-1129 (1992).

177. Crowley, P. B. Transient protein interactions of photosynthetic redox partners. Ph.D. Thesis, (Leiden University, 2002).

178. Hass, M. A. S., Thuesen, M. H., Christensen, H. E. M. and Led, J. J. Characterization of μs-ms dynamics of proteins using a combined analysis of ^{15}N NMR relaxation and chemical shift: Conformational exchange in plastocyanin induced by histidine protonations. *J. Am. Chem. Soc.* **126,** 753-765 (2004).

179. Guss, J. M., Harrowell, P. R., Murata, M., Norris, V. A. and Freeman, H. C. Crystal-structure analyses of reduced (CuI) poplar plastocyanin at 6 pH values. *J. Mol. Biol.* **192,** 361-387 (1986).

180. Battistuzzi, G., Borsari, M., Loschi, L., Righi, F. and Sola, M. Redox thermodynamics of blue copper proteins. *J. Am. Chem. Soc.* **121,** 501-506 (1999).

181. Jeuken, L. J. C., Camba, R., Armstrong, F. A. and Canters, G. W. The pH-dependent redox inactivation of amicyanin from *Paracoccus versutus* as studied by rapid protein-film voltammetry. *J. Biol. Inorg. Chem* **7,** 94-100 (2002).

182. McLeod, D. D. N., Freeman, H. C., Harvey, I., Lay, P. A. and Bond, A. M. Voltammetry of plastocyanin at a graphite electrode: Effects of structure, charge, and electrolyte. *Inorg. Chem.* **35,** 7156-7165 (1996).

183. Battistuzzi, G., Borsari, M., Canters, G. W., de Waal, E., Leonardi, A., Ranieri, A. and Sola, M. Thermodynamics of the acid transition in blue copper proteins. *Biochemistry* **41,** 14293-14298 (2002).

184. Vagin, A. and Teplyakov, A. MOLREP: an automated program for molecular replacement. *J. Appl. Crystallog.* **30,** 1022-1025 (1997).

185. Inoue, T., Gotowda, M., Sugawara, H., Kohzuma, T., Yoshizaki, F., Sugimura, Y. and Kai, Y. Structure comparison between oxidized and reduced plastocyanin from a fern, *Dryopteris crassirhizoma*. *Biochemistry* **38,** 13853-13861 (1999).

186. Segal, M. G. and Sykes, A. G. Kinetic studies on 1-1 electron-transfer reactions involving blue copper proteins.1. Evidence for an unreactive form of reduced protein (pH less-than 5) and for protein-complex association in reactions of parsley (and spinach) plastocyanin. *J. Am. Chem. Soc.* **100,** 4585-4592 (1978).

187. Guss, J. M., Harrowell, P. R., Murata, M., Norris, V. A. and Freeman, H. C. Crystal-structure analyses of reduced (CuI) poplar plastocyanin at 6 pH values. *J. Mol. Biol.* **192,** 361-387 (1986).

188. Tang, C., Iwahara, J. and Clore, G. M. Visualization of transient encounter complexes in protein-protein association. *Nature* **444,** 383-386 (2006).

189. Garrett, D. S., Seok, Y. J., Peterkofsky, A., Gronenborn, A. M. and Clore, G. M. Solution structure of the 40,000 M-r phosphoryl transfer complex between the N-terminal domain of enzyme I and HPr. *Nat. Struct. Biol.* **6,** 166-173 (1999).

190. Liang, Z. X., Nocek, J. M., Huang, K., Hayes, R. T., Kurnikov, I. V., Beratan, D. N. and Hoffman, B. M. Dynamic docking and electron transfer between Zn-myoglobin and cytochrome b_5. *J. Am. Chem. Soc.* **124,** 6849-6859 (2002).

191. Volkov, A. N., Ferrari, D., Worrall, J. A. R., Bonvin, A. M. J. J. and Ubbink, M. The orientations of cytochrome *c* in the highly dynamic complex with cytochrome b_5 visualized by NMR and docking using HADDOCK. *Protein Sci.* **14,** 799-811 (2005).

192. Sigfridsson, K. Plastocyanin, an electron-transfer protein. *Photosynth. Res.* **57,** 1-28 (1998).

193. Cramer, W. A., Soriano, G. M., Ponomarev, M., Huang, D., Zhang, H., Martinez, S. E. and Smith, J. L. Some new structural aspects and old controversies concerning the cytochrome b_6f complex of oxygenic photosynthesis. *Annu. Rev. Plant Physiol. Plant Mol. Biol.* **47,** 477-508 (1996).

194. Gray, J. C. Cytochrome *f*: Structure, function and biosynthesis. *Photosynth. Res.* **34,** 359-374 (1992).

195. Beoku-Betts, D., Chapman, S. K., Knox, C. V. and Sykes, A. G. Kinetic studies on 1:1 electron-transfer reactions involving blue copper proteins .11. Effects of pH, competitive inhibition, and chromium(III) modification on the reaction of plastocyanin with cytochrome *f*. *Inorg. Chem.* **24,** 1677-1681 (1985).

196. Niwa, S., Ishikawa, H., Nikai, S. and Takabe, T. Electron transfer reactions between cytochrome *f* and plastocyanin from *Brassica Komatsuna*. *J. Biochem.* **88,** 1177-1183 (1980).

197. Takenaka, K. and Takabe, T. Importance of local positive charges on cytochrome *f* for electron transfer to plastocyanin and potassium ferricyanide. *J. Biochem.* **96,** 1813-1821 (1984).

198. Takabe, T. and Ishikawa, H. Kinetic studies on a cross-linked complex between plastocyanin and cytochrome *f*. *J. Biochem.* **105,** 98-102 (1989).

199. Soriano, G. M., Ponamarev, M. V., Tae, G. S. and Cramer, W. A. Effect of the interdomain basic region of cytochrome *f* on its redox reactions *in vivo*. *Biochemistry* **35,** 14590-14598 (1996).

200. Zhou, J. H., Fernández-Velasco, J. G. and Malkin, R. N-terminal mutants of chloroplast cytochrome *f*. Effect on redox reactions and growth in *Chlamydomonas reinhardtii*. *J. Biol. Chem.* **271,** 6225-6232 (1996).

----

201. Navarro, J. A., Myshkin, E., De la Rosa, M. A., Bullerjahn, G. S. and Hervás, M. The unique proline of the *Prochlorothrix hollandica* plastocyanin hydrophobic patch impairs electron transfer to photosystem I. *J. Biol. Chem.* **276,** 37501-37505 (2001).

202. Schlarb, B. G., Wagner, M. J., Vijgenboom, E., Ubbink, M., Bendall, D. S. and Howe, C. J. Expression of plastocyanin and cytochrome *f* of the cyanobacterium *Phormidium laminosum* in *Escherichia coli* and *Paracoccus denitrificans* and the role of leader peptides. *Gene* **234,** 275-283 (1999).

203. Boucher, W. AZARA 2.7. Department of Biochemistry, University of Cambridge. http://www.bio.cam.ac.uk/azara (2002).

204. Helgstrand, M., Kraulis, P., Allard, P. and Hard, T. Ansig for Windows: An interactive computer program for semiautomatic assignment of protein NMR spectra. *J. Biomol. NMR* **18,** 329-336 (2000).

205. Grzesiek, S., Bax, A., Clore, G. M., Gronenborn, A. M., Hu, J. S., Kaufman, J., Palmer, I., Stahl, S. J. and Wingfield, P. T. The solution structure of HIV-1 Nef reveals an unexpected fold and permits delineation of the binding surface for the SH3 domain of Hck tyrosine protein kinase. *Nat. Struct. Biol.* **3,** 340-345 (1996).

206. Guex, N. and Peitsch, M. C. SWISS-MODEL and the Swiss-PdbViewer: An environment for comparative protein modeling. *Electrophoresis* **18,** 2714-2723 (1997).

207. Sali, A. and Blundell, T. L. Comparative protein modeling by satisfaction of spatial restraints. *J. Mol. Biol.* **234,** 779-815 (1993).

208. Schwieters, C. D., Kuszewski, J. J., Tjandra, N. and Clore, G. M. The XPLOR-NIH NMR molecular structure determination package. *J. Magn. Reson.* **160,** 65-73 (2003).

209. Hubbard, S. J. and Thornton, J. M. NACCESS. Department of Biochemistry and Molecular Biology, University College London. http://wolf.bms.umistac.uk/ (1993).

210. Worrall, J. A. R., Kolczak, U., Canters, G. W. and Ubbink, M. Interaction of yeast iso-1-cytochrome *c* with cytochrome *c* peroxidase investigated by [^{15}N, ^{1}H] heteronuclear NMR spectroscopy. *Biochemistry* **40,** 7069-7076 (2001).

211. Crowley, P. B. *Transient protein interactions of photosynthetic redox partners*. Ph.D. Thesis (Leiden University, Leiden, the Netherlands, 2002).

212. Díaz-Moreno, I., Díaz-Quintana, A., Molina-Heredia, F. P., Nieto, P. M., Hansson, Ö., De la Rosa, M. A. and Karlsson, B. G. NMR analysis of the transient complex between membrane photosystem I and soluble cytochrome c_6. *J. Biol. Chem.* **280,** 7925-7931 (2005).

----

213. Molina-Heredia, F. P., Díaz-Quintana, A., Hervás, M., Navarro, J. A. and De la Rosa, M. A. Site-directed mutagenesis of cytochrome *c*6 from *Anabaena* species PCC 7199. Identifcation of surface residues of the hemeprotein involved in Photosystem I reduction. *J. Biol. Chem.* **274,** 33565-33570 (1999).

214. Díaz-Quintana, A., Navarro, J. A., Hervás, M., Molina-Heredia, F. P., De la Cerda, B. and De la Rosa, M. A. A comparative structural and functional analysis of cyanobacterial plastocyanin and cytochrome c_6 as alternative electron donors to Photosystem I - Photosystem I reduction in cyanobacteria. *Photosynth. Res.* **75,** 97-110 (2003).

215. Albarrán, C., Navarro, J. A., Molina-Heredia, F. P., Murdoch, P. S., De la Rosa, M. A. and Hervás, M. Laser flash-induced kinetic analysis of cytochrome *f* oxidation by wild-type and mutant plastocyanin from the cyanobacterium *Nostoc* sp. PCC 7119. *Biochemistry* **44,** 11601-11607 (2005).

216. Hulsker, R., Baranova, M. V., Bullerjahn, G. S. and Ubbink, M. Dynamics in the transient complex of plastocyanin-cytochrome *f* from *Prochlorothrix hollandica*. *J. Am. Chem. Soc.* **130,** 1985-1991 (2008).

217. Hirota, S. and Yamauchi, O. Weak interactions and molecular recognition in systems involving electron transfer proteins. *Chem. Rec.* **1,** 290-299 (2001).

218. Hirota, S. and Yamauchi, O. Interactions in plastocyanin-lysine peptide and related systems. *Eur. J. Inorg. Chem.*17-25 (2002).

219. Hirota, S., Hayamizu, K., Endo, M., Hibino, T., Takabe, T., Kohzuma, T. and Yamauchi, O. Plastocyanin-peptide interactions. Effects of lysine peptides on protein structure and electron-transfer character. *J. Am. Chem. Soc.* **120,** 8177-8183 (1998).

220. Hirota, S., Okumura, H., Arie, S., Tanaka, K., Shionoya, M., Takabe, T., Funasaki, N. and Watanabe, Y. Interaction of plastocyanin with oligopeptides: effect of lysine distribution within the peptide. *J. Inorg. Biochem.* **98,** 849-855 (2004).

221. Hibino, T., Lee, B. H. and Takabe, T. Role of transit peptide sequence of plastocyanin for its expression, processing, and copper-binding activity in *Escherichia coli*. *J. Biochem. (Tokyo)* **116,** 826-832 (1994).

222. Maniatis, T., Fritsch, E. F., and Sambrook, J. Molecular Cloning. A Laboratory Manual, Cold Spring Harbor, New York (1982).

223. Lee, B. H., Hibino, T., Takabe, T., Weisbeek, P. J. and Takabe, T. Site-directed mutagenetic study on the role of negative patches on Silene plastocyanin in the interactions with cytochrome *f* and Photosystem I. *J. Biochem.* **117,** 1209-1217 (1995).

----

224. Hirota, S., Hayamizu, K., Okuno, T., Kishi, M., Iwasaki, H., Kondo, T., Hibino, T., Takabe, T., Kohzuma, T. and Yamauchif, O. Spectroscopic and electrochemical studies on structural change of plastocyanin and its tyrosine 83 mutants induced by interaction with lysine peptides. *Biochemistry* **39,** 6357-6364 (2000).

225. Hirota, S., Endo, M., Hayamizu, K., Tsukazaki, T., Takabe, T., Kohzuma, T. and Yamauchi, O. Interactions of cytochrome *c* and cytochrome *f* with aspartic acid peptides. *J. Am. Chem. Soc.* **121,** 849-855 (1999).

226. Luby-Phelps, K. Cytoarchitecture and physical properties of cytoplasm: volume, viscosity, diffusion, intracellular surface area. *Int. Rev. Cytol.* **192,** 189-221 (2000).

227. Zimmerman, S. B. and Trach, S. O. Estimation of macromolecule concentrations and excluded volume effects for the cytoplasm of *Escherichia coli*. *J. Mol. Biol.* **222,** 599-620 (1991).

228. Minton, A. P. Influence of excluded volume upon macromolecular structure and associations in 'crowded' media. *Curr. Opin. Biotechnol.* **8,** 65-69 (1997).

229. Ellis, R. J. Macromolecular crowding: an important but neglected aspect of the intracellular environment. *Curr. Opin. Struct. Biol.* **11,** 114-119 (2001).

230. Minton, A. P. The influence of macromolecular crowding and macromolecular confinement on biochemical reactions in physiological media. *J. Biol. Chem.* **276,** 10577-10580 (2001).

231. Ellis, R. J. Macromolecular crowding: obvious but underappreciated. *Trends Biochem. Sci.* **26,** 597-604 (2001).

232. Verkman, A. S. Solute and macromolecule diffusion in cellular aqueous compartments. *Trends Biochem. Sci.* **27,** 27-33 (2002).

233. Hall, D. and Minton, A. P. Macromolecular crowding: qualitative and semiquantitative successes, quantitative challenges. *Biochim. Biophys. Acta* **1649,** 127-139 (2003).

234. Banks, D. S. and Fradin, C. Anomalous diffusion of proteins due to molecular crowding. *Biophys. J.* **89,** 2960-2971 (2005).

235. Morar, A. S., Wang, X. and Pielak, G. J. Effects of crowding by mono-, di-, and tetrasaccharides on cytochrome *c*-cytochrome *c* peroxidase binding: comparing experiment to theory. *Biochemistry* **40,** 281-285 (2001).

236. Morar, A. S. and Pielak, G. J. Crowding by trisaccharides and the 2:1 cytochrome *c*-cytochrome *c* peroxidase complex. *Biochemistry* **41,** 547-551 (2002).

----

237. Kozer, N. and Schreiber, G. Effect of crowding on protein-protein association rates: fundamental differences between low and high mass crowding agents. *J. Mol. Biol.* **336,** 763-774 (2004).

238. Schlarb-Ridley, B. G., Mi, H., Teale, W. D., Meyer, V. S., Howe, C. J. and Bendall, D. S. Implications of the effects of viscosity, macromolecular crowding, and temperature for the transient interaction between cytochrome *f* and plastocyanin from the cyanobacterium *Phormidium laminosum. Biochemistry* **44,** 6232-6238 (2005).

239. Zhou, Y. L., Liao, J. M., Chen, J. and Liang, Y. Macromolecular crowding enhances the binding of superoxide dismutase to xanthine oxidase: Implications for protein-protein interactions in intracellular environments. *Int. J. Biochem. Cell B.* **38,** 1986-1994 (2006).

240. Dedmon, M. M., Patel, C. N., Young, G. B. and Pielak, G. J. FlgM gains structure in living cells. *Proc. Natl. Acad. Sci. U. S. A* **99,** 12681-12684 (2002).

241. McNulty, B. C., Young, G. B. and Pielak, G. J. Macromolecular crowding in the *Escherichia coli* periplasm maintains α-synuclein disorder. *J. Mol. Biol.* **355,** 893-897 (2006).

242. Stevens, A., Wang, S. X., Caines, G. H. and Schleich, T. ^{13}C-NMR off-resonance rotating frame spin-lattice relaxation studies of bovine lens γ-crystallin self association: effect of macromolecular crowding. *Biochim. Biophys. Acta* **1246,** 82-90 (1995).

243. Varley, J. P. A., Moehrle, J. J., Manasse, R. S., Bendall, D. S. and Howe, C. J. Characterization of plastocyanin from the cyanobacterium *Phormidium laminosum*: copper-inducible expression and SecA-dependent targeting in *Escherichia coli. Plant Mol. Biol.* **27,** 179-190 (1995).

244. Gill, S. C. and Von Hippel, P. H. Calculation of protein extinction coefficients from amino acid sequence data. *Anal. Biochem.* **182,** 319-326 (1989).

245. Luby-Phelps, K., Castle, P. E., Taylor, D. L. and Lanni, F. Hindered diffusion of inert tracer particles in the cytoplasm of mouse 3T3 cells. *Proc. Natl. Acad. Sci. U. S. A* **84,** 4910-4913 (1987).

246. Homchaudhuri, L., Sarma, N. and Swaminathan, R. Effect of crowding by dextrans and Ficolls on the rate of alkaline phosphatase-catalyzed hydrolysis: a size-dependent investigation. *Biopolymers* **83,** 477-486 (2006).

247. Furukawa, R., Arauzlara, J. L. and Ware, B. R. Self-diffusion and probe diffusion in dilute and semidilute aqueous solutions of dextran. *Macromolecules* **24,** 599-605 (1991).

----

248. Yam, K. L., Anderson, D. K. and Buxbaum, R. E. Diffusion of small solutes in polymer-containing solutions. *Science* **241,** 330-332 (1988).

249. Lavalette, D., Tetreau, C., Tourbez, M. and Blouquit, Y. Microscopic viscosity and rotational diffusion of proteins in a macromolecular environment. *Biophys. J.* **76,** 2744-2751 (1999).

250. Vergara, A., Paduano, L. and Sartorio, R. Mechanism of protein-poly(ethylene glycol) interaction from a diffusive point of view. *Macromolecules* **35,** 1389-1398 (2002).

251. Wenner, J. R. and Bloomfield, V. A. Crowding effects on EcoRV kinetics and binding. *Biophys. J.* **77,** 3234-3241 (1999).

Summary

The biological processes that are the basis of all life forms are mediated largely by protein-protein interactions. The protein complexes involved in these interactions can be categorised by their affinity, which results in a range from static (high affinity) to transient (low affinity) complexes. Electron transfer complexes, which have to combine high turn-over with specificity are typically transient complexes. They achieve their high turn-over rates by high dissociation rate constants, while the association rates are comparable or higher to those found for static protein complexes. Together this results in the weak binding that characterises transient protein complexes.

The transient complexes under investigation in this work are all part of the photosynthetic redox chain, in which electrons are transferred from membrane bound cytochrome f (cyt$f$) to either plastocyanin (Pc) or cytochrome c_6 (cytc_6). The active site of these proteins contains a metal ion, and in the case of the cytochromes a haem, coordinated by several side chains of the protein.

In Chapter II, we study the protonation of a histidine copper ligand in plastocyanin at low pH, which inactivates the protein. This behaviour is observed for all plastocyanins, with one exception. Fern plastocyanin was thought not to protonate, because of the presence of a π-π stacking interaction. With the use of nuclear magnetic resonance (NMR) spectroscopy we were able to show that the particular histidine does show protonation, although at a lower pK_a than expected. Mutations F12L and G36P that were expected to influence this behaviour did in fact not change the pK_a. Curiously, the crystal structure of both the wild type (wt) and G36P fern Pc shows a deprotonated histidine. The apparent discrepancy between crystallographic and NMR data can be explained by the presence of crystal contacts around the histidine. The proximity of the neighbouring asymmetric unit probably favours crystallisation of the deprotonated form. This example shows the advantages of solution state NMR, which can be used for the investigation of proteins and particularly transient protein complexes.

Studies of the Pc - cyt$f$ complex and other transient protein complexes has led to a two-step model for complex formation. According to this model, free proteins associate to

form a dynamic encounter complex, followed by a well-defined state, which is capable of electron transfer. The effect of the mutation of two otherwise conserved residues, located in the hydrophobic patch surrounding the active site of *P. hollandica* Pc is investigated in Chapter III. While the structure of the wt Pc - cyt*f* complex could be determined by docking with NMR restraints, derived from chemical shift perturbations and pseudocontact shifts (PCS), this was not possible for the complex with mutant Pc. From a decrease in size of both the chemical shift perturbations and the PCS it could be concluded that the mutant complex is more dynamic than the wt Pc - cyt*f* complex. The movements in the complex were simulated by creating an ensemble of structures using the wt structure as a starting point. Comparison of the simulated and observed averaged NMR parameters shows that the mutations cause the complex to shift from the well-defined state towards the encounter state. This provides a way to examine the movements and dynamics in the encounter state of a transient protein-protein complex.

A similar approach is used in Chapter IV to study the dynamics in the cytc_6 - cyt*f* complex. The use of paramagnetic relaxation enhancement (PRE) was introduced here, which provides information additional to that from chemical shift perturbations and PCS. For this purpose five separate spin labels were placed on the surface of cyt*f*, causing stronger relaxation of the cytc_6 nuclei in the vicinity of the spin label. When PRE derived restraints from several positions of spin labels are used in docking calculations, converged structures are found, but with different orientations, depending on the combination of PRE data used. Furthermore, the violations for each of these determined structures remain large, suggesting that the complex is dynamic and cannot be described by a single structure. As in Chapter III ensembles of structures were created, which in this case could not decrease the violations of the PRE restraints. This leads to the conclusion that the cytc_6 - cyt*f* complex cannot be described by an evenly distributed ensemble of structures and that the ensemble is most likely characterised by preferred orientations. The use of methods that do not require a starting structure, such as Brownian dynamics, might be more successful in precisely describing the encounter state of this complex.

136

Electrostatic interactions between the proteins forming a complex play an important role in the association and orienting of the proteins. An additional requirement for the formation of a transient complex is that electrostatic interactions should not prevent the fast dissociation of the proteins. For this reason the balance of electrostatics, hydrophobics and other surface properties that characterise the complex interface has been the subject of many studies. In Chapter V, charged peptides are used to study the role of electrostatics in protein-protein association. For this purpose ^{15}N-labelled *S. pratensis* Pc was produced and its backbone amides were assigned. The addition of positively charged tetra-lysine peptide to Pc, which is known to inhibit electron transfer to cyt*f*, causes chemical shift perturbations at the negatively charged patches. Surprisingly, the number of affected residues and the size of the chemical shift perturbations indicate the complex between tetra-lysine and Pc is relatively dynamic. The addition of hydrophobic residues to the peptide does not significantly change the binding of the peptide supporting the idea that surfaces of electron transfer proteins are designed to interact weakly but specifically with their partners.

The dilute solutions in which proteins and protein complexes are often studied are different from the cellular environment in which these proteins normally function. This issue has been addressed by the use of macromolecular crowders, which mimic the presence of large amounts of other macromolecules in high concentrations. In Chapter VI the transient Pc - cyt*f* complex is studied by NMR in the presence of crowders. The use of several crowders was tested on a small globular protein, which revealed that Ficoll70, a highly branched polymer of sucrose, and dextran T70, a synthetic linear polysaccharide interfere least with the NMR experiments. The addition of up to 20% Ficoll70 to the Pc - cyt*f* complex did not result in significant differences of both binding constant or binding map. This supports the idea that high molecular weight crowders such as Ficoll70 are not uniformly distributed in solution and form a 'porous' medium in which relatively small proteins can move as they would in dilute solution. This raises the question whether high molecular weight crowders offer the most appropriate model of the cellular environment.

This work describes the investigation of several aspects of transient protein-protein interactions that are applicable to many other transient complexes. The use of NMR as a

tool of choice for these studies has proven it an invaluable technique that provides insight in rules that govern the world of transient complex formation. New approaches such as PRE and the creation of ensembles of structures will hopefully lead to a full understanding of dynamics and the variety of ways that transient complexes use dynamics to perform their function in the cell.

Nederlandse samenvatting

De biologische processen, die de basis vormen van al het leven, worden voor een groot deel bepaald door eiwitinteracties. De eiwitcomplexen, die betrokken zijn bij deze interacties, kunnen ingedeeld worden naar affiniteit, waarbij we statische (hoge affiniteit) en kortlevende of transient (lage affiniteit) complexen onderscheiden. Complexen die elektronen transporteren, zijn meestal kortlevende complexen, omdat ze een hoge omzetsnelheid moeten combineren met specificiteit. Ze bereiken hun hoge omzetsnelheid door hoge dissociatie constanten, terwijl hun associatie constanten vergelijkbaar of hoger zijn dan die van statische complexen. Samen resulteren zij in de zwakke binding die karakteristiek is voor kortlevende eiwitcomplexen.

De kortlevende complexen die in dit werk worden onderzocht zijn allemaal onderdeel van de fotosynthetische redox keten, waarin elektronen van het membraan gebonden cytochrome f (cyt$f$) naar plastocyanine (Pc) of naar cytochrome c_6 (cytc_6) worden overgedragen. Het katalytische centrum van deze eiwitten bevat een metaal-ion, en in het geval van de cytochromen een haem, die gecoördineerd worden door de zijketens van verschillende aminozuren van het eiwit.

In Hoofdstuk II wordt de protonatie van een histidine koper ligand in plastocyanine bestudeerd bij een lage pH, die het eiwit inactiveert. Met één uitzondering wordt dit bij alle plastocyanines waargenomen, Er werd aangenomen dat Pc's uit varen niet protoneerde door de aanwezigheid van een π-π stacking interactie. Met behulp van kernspinresonantie (NMR) spectroscopie hebben we kunnen aantonen dat de histidine wel protoneert, zij het bij een lagere pK_a dan verwacht. Van de mutaties F12L en G36P werd verwacht dat ze de protonatie zouden beïnvloeden, maar dit bleek niet het geval. Ze veranderen de pK_a niet. Het is opvallend dat in de kristalstructuur van het wild type (wt) en G36P varen Pc de histidine gedeprotoneerd is. Deze schijnbare tegenstelling tussen kristallografische en NMR data kan worden verklaard door kristalcontacten rond de histidine. De nabijheid van de aangrenzende asymmetrische eenheid levert waarschijnlijk een voorkeur op voor de gedeprotoneerde vorm. Dit voorbeeld laat de voordelen zien van onderzoek met kernspinresonantie uitgevoerd op eiwitten en in het bijzonder kortlevende eiwitcomplexen in oplossing.

De bestudering van het Pc - cyt*f* complex en andere kortlevende eiwitcomplexen heeft geleid tot een twee-staps model voor complexvorming. Volgens dit model associëren twee eiwitten om een dynamisch encounter complex te vormen, gevolgd door een goed gedefinieerd complex, dat elektronen kan overdragen. Het effect van de mutatie van twee normaal gesproken geconserveerde residuen in het hydrofobe gedeelte rond het katalytische centrum van *P. hollandica* Pc wordt bestudeerd in Hoofdstuk III. De structuur van het wt Pc - cyt*f* complex kon bepaald worden met behulp van bindingssimulaties op basis van NMR begrenzingen. Die begrenzingen zijn gebaseerd op verstoringen van de chemische verschuivingen en pseudocontact verschuivingen (PCS). Voor het complex met het mutante Pc was structuurbepaling niet mogelijk. Uit de kleinere verstoringen van chemische verschuivingen en PCS werd geconcludeerd dat het mutante complex dynamischer is dan het wt complex. De bewegingen in het complex zijn gesimuleerd door een verzameling van structuren, waarbij het wt complex als uitgangspunt is gebruikt. Uit een vergelijking van de gesimuleerde met de geobserveerde gemiddelde NMR parameters blijkt dat het complex van de goed gedefinieerde staat naar de encounter staat verschuift door de mutaties. Dit levert een manier op om de bewegingen en dynamiek van de encounter staat van kortlevende eiwitcomplexen te bestuderen.

Een vergelijkbare benadering is gebruikt in Hoofdstuk IV om de dynamiek in het cytc_6 - cyt*f* complex te bestuderen. In dit hoofdstuk wordt het gebruik van paramagnetische relaxatieversnelling (PRE) geïntroduceerd, die extra informatie oplevert bovenop de verstoringen van de chemische verschuivingen en PCS. Hiervoor werden vijf verschillende spinlabels op de oppervlakte van cyt*f* geplaatst, die de relaxatie van cytc_6 kernen in de buurt van het spinlabel versnellen. Als NMR begrenzingen gebaseerd op PRE van verschillende spinlabel-posities worden gebruikt in bindingssimulaties, worden geconvergeerde structuren gevonden. Deze structuren hebben echter verschillende oriëntaties, afhankelijk van de combinatie van PRE data. Daarbij blijven de overschrijdingen van de begrenzingen voor elk van de bepaalde structuren groot. Dit suggereert dat het complex dynamisch is en niet beschreven kan worden door een enkele structuur. Net als in Hoofdstuk III hebben we verzamelingen van structuren gecreëerd, die in dit geval niet de overschrijdingen van de PRE begrenzingen konden verminderen.

Daaruit kan geconcludeerd worden dat het cytc_6 - cyt$f$ complex niet beschreven kan worden door een gelijkmatig verdeelde verzameling van structuren en dat de verzameling waarschijnlijk voorkeurs-orientaties heeft. Het gebruik van methoden die geen uitgangsstructuur nodig hebben, zoals Brownian dynamics, zou een preciezere beschrijving van de encounter staat van het complex kunnen opleveren.

Elektrostatische interacties tussen eiwitten in een complex spelen een belangrijke rol in de associatie en oriëntatie van de eiwitten. Een andere vereiste bij de vorming van een kortlevend complex is dat de elektrostatische interacties de snelle dissociatie van de eiwitten niet tegenhouden. Daarom is de balans tussen elektrostatische, hydrofobe en andere oppervlakte-eigenschappen van de bindingsplaatsen in complexen het onderwerp van vele studies. In hoofdstuk V worden geladen peptiden gebruikt om de rol van eletrostatica in eiwitassociatie te onderzoeken. Hiervoor werd ^{15}N-verrijkt *S. pratensis* Pc geproduceerd en werden de hoofdketen amiden toegekend. Bij toevoeging van positief geladen tetra-lysine peptide aan Pc, waarvan bekend is dat dat het elektronen transport naar cyt$f$ inhibeert, worden de chemische verschuivingen van het negatief geladen gedeelten van Pc verstoort. Het is verrassend dat het aantal verstoorde residuen en de grootte van de verstoringen aangeven dat het complex tussen tetra-lysine en Pc relatief dynamisch is. De toevoeging van hydrofobe residuen aan het peptide verandert de binding van het peptide niet significant. Dit ondersteunt het idee dat het oppervlak van elektronen transport eiwitten ontworpen is om een zwakke, maar specifieke interactie met de partners te hebben.

De verdunde oplossingen waarin eiwitten en eiwitcomplexen vaak bestudeerd worden, verschillen van het cellulaire milieu waarin ze normaal gesproken functioneren. Dit verschil kan onderzocht worden door het gebruik van moleculaire crowders, die de aanwezigheid van grote aantallen andere macromoleculen in hoge concentraties nabootsen. In Hoofdstuk VI wordt het Pc - cyt$f$ complex bestudeerd met NMR in de aanwezigheid van crowders. Het gebruik van verschillende crowders werd getest op een klein rond eiwit. Hieruit bleek dat Ficoll70, een sterk vertakte polymeer van sucrose en dextran T70, een synthetische, lineaire polysaccharide de NMR experimenten het minst verstoren. De toevoeging van 20% Ficoll70 aan het Pc - cyt$f$ complex resulteerde niet in

significante veranderingen van de bindingsconstante of bindingsplaatsen. Dit ondersteunt het idee dat crowders met een groot molecuulgewicht zoals Ficoll70 niet gelijkmatig over de oplossing verdeeld zijn, maar een poreus medium vormen. Hierin kunnen relatief kleine eiwitten bewegen zoals in een verdunde oplossing. Men kan zich afvragen of crowders met een groot molecuulgewicht het beste model voor het cellulaire milieu vormen.

Dit werk beschrijft de bestudering van verschillende aspecten van kortlevende eiwitinteracties, die toepasbaar is op vele andere kortlevende eiwitcomplexen. Het gebruik van -bij voorkeur- NMR voor deze studies heeft aangetoond dat het een onmisbare techniek is om inzicht te verkrijgen in de regels die de vorming van kortlevende eiwitcomplexen bepalen. Hopelijk zullen nieuwe ideeën, zoals het gebruik van PRE en het creëren van verzamelingen van structuren, leiden tot volledig begrip van de dynamica en van de vele manieren waarop kortlevende complexen die dynamica gebruiken om hun functie in de cel uit te voeren.

List of publications

Hulsker R., Baranova M.V., Bullerjahn G.S., Ubbink M. Dynamics in the transient complex of plastocyanin-cytochrome f from *Prochlorothrix hollandica*. *J. Am. Chem. Soc*. **130**, 1985-1991 (2008).

Hulsker R., Mery A., Thomassen E.A., Ranieri A., Sola M., Verbeet M.P., Kohzuma T., Ubbink M. Protonation of a histidine copper ligand in fern plastocyanin. *J. Am. Chem. Soc*. **129**, 4423-4429 (2007).

Hirota S., Fujimoto Y., Choi J., Baden N., Katagiri N., Akiyama M., **Hulsker R**., Ubbink M., Okajima T., Takabe T., Funasaki N., Watanabe Y., Terazima M.. Conformational changes during apoplastocyanin folding observed by photocleavable modification and transient grating. *J. Am. Chem. Soc*. **128** , 7551-7558 (2006).

Jansen L.E.T., Belo A.I., **Hulsker R.**, Brouwer J. Transcription elongation factor Spt4 mediates loss of phosphorylated RNA polymerase II transcription in response to DNA damage. *Nucleic Acids Res*. **30**, 3532-3539 (2002).

The structure and dynamics in the complex of *Nostoc* sp. PCC 7119 cytochrome f-cytochrome c_6 (manuscript in preparation).

Curriculum vitae

Rinske Hulsker was born on the 30th of December in Leidschendam. She grew up in Zoetermeer where she received her 'VWO diploma" from the Erasmus College in 1997. That same year she joined the University of Leiden to study Chemistry. She conducted her nine month research project on proteins involved in Transcription Coupled Repair in *S. cerevisiae* under the supervision of Dr. L.E.T. Jansen and Prof. J. Brouwer. In 2001, she left for Switzerland to investigate the chromatin structure of mini chromosomes in *S. cerevisiae* under the supervision of Prof. F. Thoma at the ETH in Zürich. Following this, she earned her Master's degree in Chemistry in 2002 and was awarded the Franchimont prize in 2003.

In 2003, she started as a PhD student in the Metalloproteins (now Protein Chemistry) group at the University of Leiden under the supervision of Dr. M. Ubbink and Prof. G.W. Canters. The research focused mainly on the dynamics of transient protein complexes, which was investigated by NMR spectroscopy. She carried out this work in collaboration with several groups, including that of Prof. T. Kohzuma at Ibaraki University, Mito, Japan, that of Prof. G.S. Bullerjahn at the Bowling Green State University, Ohio and the Structural and Functional Proteomics group at the University of Seville, Spain.

As of March 2008 Rinske is employed as Junior Scientist at ProteoNic BV in Leiden.

Acknowledgements

I am grateful to all collaborators and collegues that have contributed in some way to the work presented in this thesis: Maria Baranova, Prof. George Bullerjahn (Ohio), Dr. Irene Díaz-Moreno, Dr. Fernando Molina-Heredia, Prof. Miguel de la Rosa (Seville), Dr. Antonio Ranieri, Prof. Marco Sola (Modena, Italy), Davide Cavazzini, Prof. Gian Luigi Rossi (Parma, Italy), Prof. Takamitsu Kohzuma and his coworkers (Mito, Japan), Prof. Shun Hirota and his coworkers (Kyoto, Japan), Dr. Ellen Thomassen, Dr. Navraj Pannu, Prof. Jan Pieter Abrahams, Francesco Scarpelli, Dr. Martina Huber, Cees Erkelens, Fons Lefeber, Johan Hollander, Gé van Albada, Paul Hensbergen, Crina Balog, Dr. Alexander Volkov, Annabelle Mery, Dr. Martin Verbeet and Michela Finiguerra (Leiden, the Netherlands).

A special thanks to Fleur Broekman and Clarisse Feltzmann that contributed to the work done in Chapters V and VI and reminded me one should never stop learning.

For teaching, helping and supporting me during my adventures at the labbench and beyond I am grateful to all technicians and secretaries that have been part of the Mettalo protein group, particularly Ellen and Anneloes. I have always been amazed by your skills for organising the lab and keeping it that way.

I would like to thank Jon, Monica and Miguel for their valuable advise, encouragement and support. I have gratefully leaned on your experience in science and life.

To my fellow PhD students who have shared the experience with me, either in Leiden or from further away, I would like to say that your understanding, sense of humour and faith in me were as essential as coffee. To those of you who are still in the process of finishing themselves, I hope I can be as helpful. Let's pay it forward!

To all the girls: thank you for all the fun, loyalty and friendship.

To everyone in Protchem I haven't mentioned yet; thank you for the great food, drinks, laughter and company you offered at parties and laboutings.

Leon, je hebt een speciale plek in mijn hart. Je aanvaring met de wetenschap heeft me geleerd dat er belangrijker dingen in het leven zijn dan promoveren.

Aan iedereen die ik vaak of minder vaak aan de bar tegenkom; met jullie heb ik kunnen ontspannen, relativeren en praten over hele andere dingen dan wetenschap. Daarvoor: Bedankt!

Een woord van dank aan de mensen van Molgen, in het bijzonder Lars, Riekje, Tineke, Hans en Jaap, die mij met veel geduld het enthousiasme voor onderzoek hebben bijgebracht. Dat enthousiasme is de best mogelijke drijfveer voor het doen van een promotie.

Als laatste wil ik mijn moeder en Georg bedanken voor alle onvoorwaardelijke steun en vertrouwen. Georg, zonder jou was dit niet gelukt, laten we er samen van gaan genieten.